PROBABALISTIC AND HAZARD ANALYSIS FOR PORE PRESSURE INCREASE IN SOILS DUE TO SEISMIC LOADING

Jean-Lou Chameau

The John A. Blume
Earthquake Engineering Center
Dept. of Civil Engineering
Stanford University
Stanford, CA 94305

A Report on a Research Project
Supported by the
National Science Foundation
Grant Numbers
ENV77-17834 and PFR-80-07083
and the
United States Geological Survey
Grant Number 18380

May 1981

INTENTIONALLY BLANK

ACKNOWLEDGEMENTS

My deepest thanks to my advisor, Professor Wayne Clough, for his encouragement, guidance and patience during the preparation of this dissertation and, most of all, for stimulating my interest in the field of geotechnical engineering.

I would like to express my gratitude to Professor Haresh Shah for his continuing interest in this research and for many helpful discussions.

I am thankful to Professor Edward Kavazanjian for offering valuable suggestions and reviewing the manuscript.

Above all I want to thank Professor Clough, Shah and Kavazanjian for being very good friends.

I wish to express my gratitude:

to Christian Mac Mortgat for being the best friend you can hope for, and making me believe that a Belgian can cook.

to my very good friends, Tarik Hadj Hamou and Jean Benoit, for many valuable suggestions, especially about beer and hamburgers.

to Bob Bachus for his help and friendship, and not smoking cigar before 2 p.m.

to all my friends and colleagues in the geotechnical department and in the Blume Center.

Financial support was provided by the National Science Foundation Grant ENV-17834 and the United States Geological Survey, contract No. USGS 18380.

My deepest gratitude to my parents and to my brother for their encouragement, faith and patience.

A Annie, pour tout.

TABLE OF CONTENTS

LIST OF TABLES

LIST OF FIGURES

Chapter I

INTRODUCTION

The build-up of excess pore pressures in a layer of saturated cohesionless soil during an earthquake can lead to ground movements which damage structures and cause loss of life. This response is due to the application of cyclic shear stresses, which are generated primarily by the upward propagation of shear waves in the soil deposit. As a consequence of the applied cyclic stresses, the structure of the undrained cohesionless soil tends to become more compact, and this results in a transfer of stress to the pore water and a reduction in effective stress. If the sand is loose the pore pressure may increase rapidly to a value equal to the confining pressure and the soil layer will undergo large deformations. If the sand is dense, it may exhibit a zero effective stress condition at the end of a given cycle, but during subsequent cycles the soil will tend to dilate, the pore pressure will drop, and the soil may develop enough resistance to withstand the applied stress. The shear strain associated with this dilation will correspond to a limited degree of deformation. The extreme case of pore pressure increase up to the zero effective stress condition is often called liquefaction, and enormous damages have been attributed to this phenomenon. There are hundreds of recent cases of ground failures and damages to structures due to liquefaction during Earthquakes in China, Japan, Yugoslavia, Chile, Central America and in the United States. The

greatest damages occurred in Niigata, Japan, during the 1964 earthquake, where many structures settled more than 3 feet and suffered up to 80 degrees of tilting, and in Valdez, during the 1964 Alaskan earthqake, where extensive flow slides washed entire sections of the waterfront into the sea.

Following these two events, pioneering research was devoted to the study of pore pressure increase in cohesionless soils due to cyclic loading. This led to the development of laboratory testing procedures which could measure pore pressures in samples during cyclic loading. By the late 1960's and early 1970's simplified procedures were developed to assess the potential for complete liquefaction on a yes-no basis for homogeneous soils. Subsequently, work was undertaken to extend the early developments. These efforts followed along two lines. The first, which has, and still is, receiving the largest share of attention, was directed at developing a deterministic method to predict the actual level of pore pressures in homogeneous and nonhomogeneous soil deposits. In this way the possibility of either complete or only partial liquefaction could be assessed. At present (1980), several methods are available for this purpose although none are yet accepted as applicable to general conditions. The second line of research undertaken in the early 1970's was to establish a probabilistic framework for liquefaction assessment. Relatively little work has been done in this area and that which has been done is oriented towards the problem of complete liquefaction. This dissertation is an attempt to combine these two lines of research in a methodology which casts the phenomenon of pore pressure build-up into a probabilistic and hazard analysis framework. Its two

main objectives are to develop a complete description of the pore pressure build-up in order to differentiate between total and partial liquefaction, and to provide a probabilistic framework in order to incorporate geotechnical, seismological and analytical uncertainties, and to measure the hazard associated with pore pressure build-up and liquefaction. A last aspect of this work is to distinguish between liquefaction and damage, and to propose a methodology to assess the real damage, if any, to the soil and soil supported structures. The following examples will demonstrate why new studies and in particular the present one are needed in this field.

Recently the author has been involved in the assessment of the liquefaction potential of two sites; The first one was located in Bedjaia, Algeria, where the construction of one of the largest refinery in the world was planned by the Algerian government; The second one was in Union City, East of the San Francisco Bay, where a major land development project was under consideration. In both cases the seismicity of the areas and the soil conditions were such that the behavior of the sites under earthquake loading was of concern. The soil and seismicity data were of fair quality and state-of-the-art methods of analysis were used in the studies. Results were presented in a conventional format: For several earthquakes of different magnitudes and characteristics, the liquefaction potential was noted to range from very high to very low. For example, the potential for liquefaction of the Union City site was considered very high during an earthquake of Richter magnitude 7 occurring close to the site on the Hayward fault, and very

low for the same event occuring at large distance from the site; it was also high for a major event of magnitude 8+ on the San Andreas fault. Most importantly, these types of results in both cases did not fulfill the needs of the owners. They were interested in much more specific answers such as:

- Expected damage to their structures during any earthquake, whatever the potential for liquefaction is.

- Measure of the risk involved for the specified life time of the structures and the given seismic environment.

- Comparison of expected damage and risk between alternative sites and construction methods.

These examples show that attention needs to be devoted to more than just liquefaction potential. It is also very important to know: (1) The damage potential associated with pore pressure build-up; and, (2) How this information can be realistically expressed by the engineer. It is not enough to be able to say that the liquefaction potential is very high or very low.

In order to help the decision maker choose between alternatives , the likelihood of a certain consequence occurring should be cast within the context of a probabilistic framework. This quantifies the uncertainties of the problem, the relative frequency of occurrences of seismic events, and and how good our knowledge of the phenomenon is.

A long term research project has been undertaken at Stanford to attack this problem. The proposed work involves developing the following:

- Procedures to evaluate the likelihood of pore pressure build-up during an earthquake.

- Methods to assess the probability that a given pore pressure builld-up will cause ground deformation and damages to supported structures.

- An approach to evaluate the potential for economic loss due to the effects of an earthquake; this would incorporate means of assessing the mitigating effects of alternative site improvement techniques.

The present dissertation represents the first step towards the achievement of this program and it concentrates on the following points:

- Document and investigate the behavior of cohesionless soils under cyclic loading

- Develop a probabilistic pore pressure generation model using laboratory data

- Incorporate uncertainties in soil parameters, laboratory data, and earthquake loading parameters

- Develop a probabilistic pore pressure generation model using effective stress soil models and a probabilistic definition of the seismic loading.

This work is primarily concerned with the evaluation of the likelihood of pore pressure build-up during an earthquake, but it also proposes a hazard and risk analysis methodology, which will open way the continuation of this research. The results of the research program are expected to improve the analysis of pore pressure build-up in soils due to seismic loading, to allow assessment of the technical and economical damage which results, and to demonstrate the value of application of probability concepts in this field.

Chapter II

REVIEW OF METHODS FOR PORE PRESSURE DEVELOPMENT AND LIQUEFACTION EVALUATION

2.1 INTRODUCTION

The behavior of cohesionless soil under earthquake loading has been subjected to extensive research studies in the past fifteen years. Numerous studies and a comprehensive literature exist in the fields of cyclic testing, soil parameters definition, soil modeling and dynamic analysis. Liquefaction analysis methods have been proposed to assess quantitatively or qualitatively the liquefaction potential at a site. Soil behavior models and computer programs have been developed to study the development of pore pressure in cohesionless soil under cyclic loading.

In this chapter, a critical review of the testing techniques and of the most significant methods of analysis of the behavior of cohesionless soils under earthquake loading is presented. A distinction is made between the methods which assess the potential for complete liquefaction and the methods which predict the actual level of pore pressure up to complete liquefaction.

2.2 DEFINITION OF LIQUEFACTION

Different terminologies for liquefaction have been used in the past. The latest definitions (Seed,1979) are as follows:

- Liquefaction: a condition where a soil will undergo continued deformation at a low constant residual stress or with low residual resistance, due to build-up and maintenance of high pore pressure, which reduce the effective confining pressure to a very low value.

- Peak cyclic pore pressure ratio of 100%: a condition where during the course of cyclic stress applications, the residual pore water pressure on completion of any full stress cycle becomes equal to the applied confining pressure.

- Peak cyclic pore pressure ratio of 100% with limited strain potential, also called cyclic mobility (Castro,1975):a condition in which cyclic pore pressure ratio of 100% and subsequent cyclic stress applications cause limited strains.

The cause of cyclic mobility or liquefaction in sands is the build-up of excess hydrostatic pore pressure due to the application of cyclic shear stresses. The shear stresses are generated primarily by the upward propagation of shear waves in a soil deposit. A soil element is subjected to a series of cyclic stress conditions as shown in figure 2.1.a. As a consequence of the applied cyclic stresses, the structure of

the undrained soil tends to become more compact, and this results in a transfer of stress to the pore water and a reduction in effective stress. If the sand is loose, the pore pressure will increase rapidly to a value equal to the confining pressure (peak cyclic pore pressure ratio of 100%) and the soil layer may undergo large deformations. This extreme case of zero effective stress condition and large deformations corresponds to Seed's definition of liquefaction.

2.3 TESTING TECHNIQUES

Cyclic load triaxial compression tests, simple shear tests and torsional shear tests have been introduced to simulate the stress condition illustrated in figure 2.1.a.

2.3.1 Cyclic simple shear tests

The simple shear test tries to provide the closest representation of field conditions: the soil sample is first consolidated under anisotropic stress conditions and is then subjected to alternating horizontal and vertical shear stresses. In principle, this reproduces correctly the loading conditions shown in figure 2.1.a. Unfortunately there are inherent difficulties which limit the accurate simulation of field conditions in this test. For example, there is a development of non-uniform shear strains in the specimen due to stress concentrations at the corners. This means that the actual stress conditions the sample is subjected to are not known. To minimize stress concentration effects, researchers in the past few years have used long and shallow test

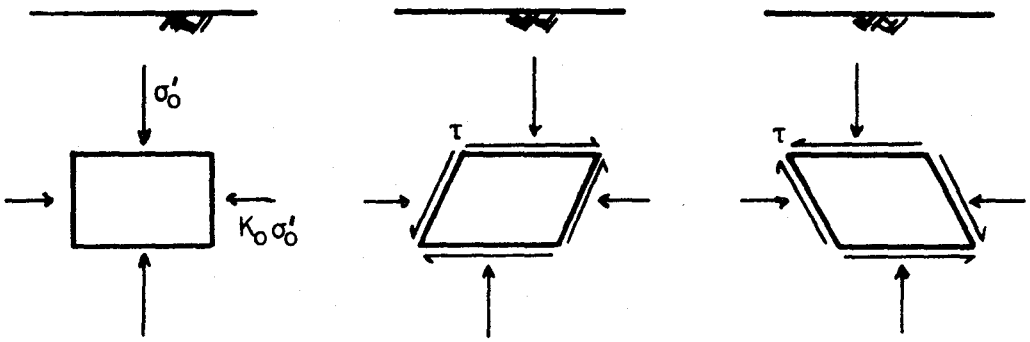

Initial Stresses Cyclic Load Sequence

Figure 2.1.a Idealized Stress Conditions

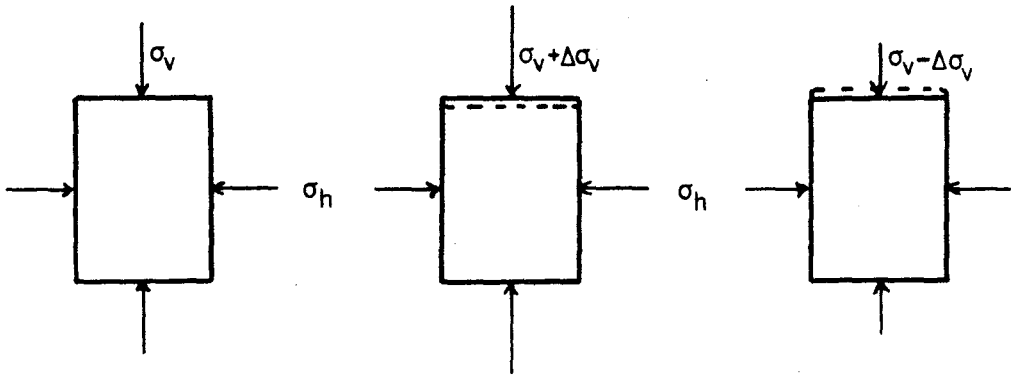

$\sigma_v = \sigma_h$

Figure 2.1.b Triaxial Stress Conditions

samples in simple shear devices or on a shaking table. The most comprehensive investigation of this type is that conducted by DeAlba et al. (1976) on a shaking table.

Samples of Monterey No 0 sand were tested at different relative densities. Typical results for tests at relative densities of 54, 68, 82 and 90 percent are shown in figures 2.2 and 2.3. As may be seen from the curves in figure 2.3, at relative densities less than 40% the application of cyclic stress ratios sufficiently high to cause a zero effective stress state will also cause extremely high and probably unlimited strains in the soil. For relative densities greater than 45%, the application of stress ratios and numbers of cycles sufficient to cause a zero effective stress state results only in a limited amount of shear strain.

2.3.2 Cyclic torsional simple shear tests

The torsional simple shear device has been developed to overcome the previously mentioned difficulties associated with the simple shear device. Castro (1969) first suggested that rotational type testing might be the best way to reproduce liquefaction in the laboratory; Ishihara and Yasuda (1973,1975) studied liquefaction in hollow cylinder torsion under irregular excitation; In 1974 Ishibashi and Sherif proposed their torsional simple shear device and gave comparative results between simple shear tests and torsional simple shear tests; Cho, Rizzo and Humphries (1976) compared the behavior of saturated sand under cyclic axial loading and cyclic torsional shearing.

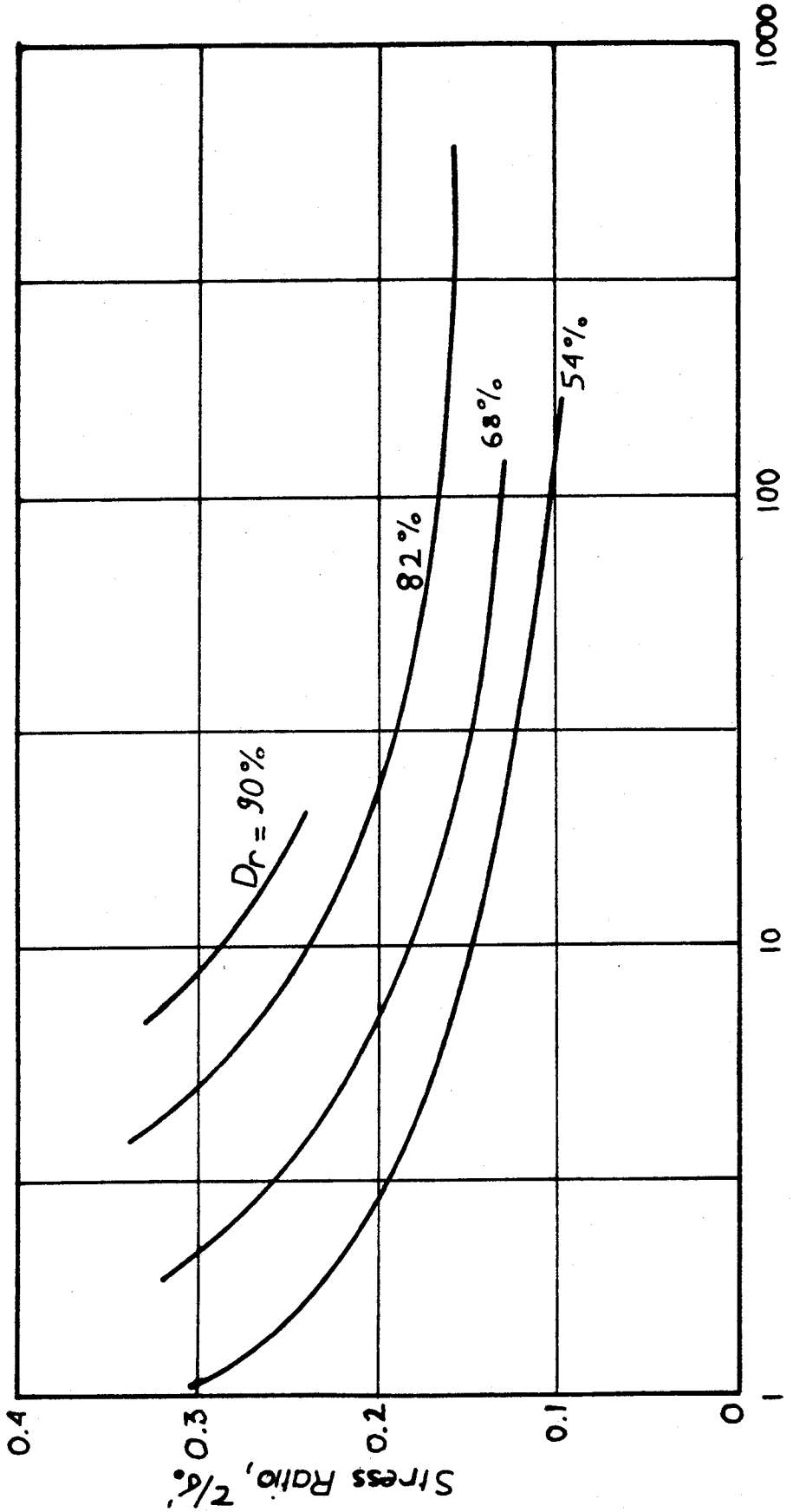

Figure 2.2 Cyclic Strength Curves (after De Alba, 1976)

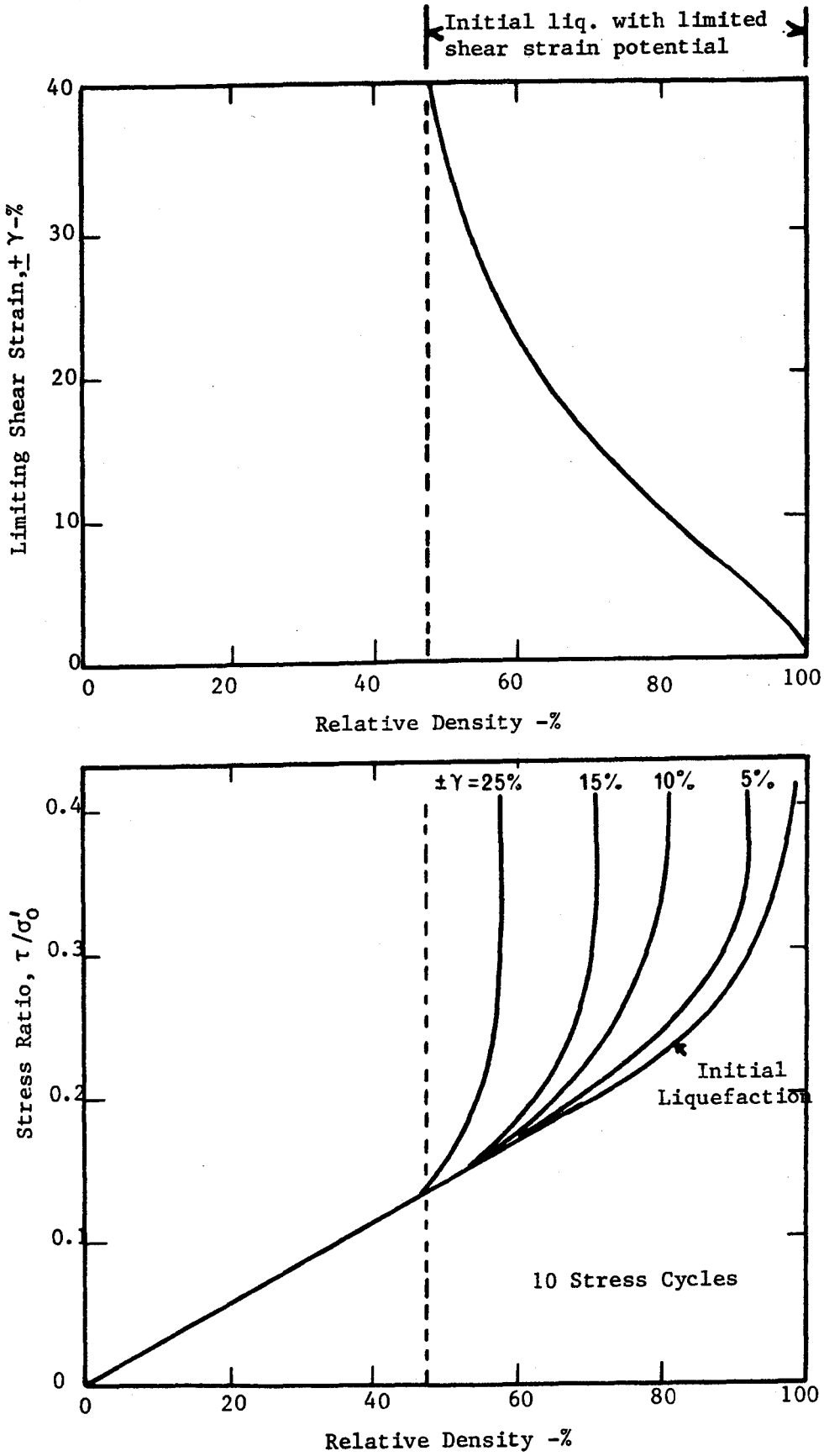

Figure 2.3 Limiting shear strains (after De Alba, 1976)

The sample in a torsional simple shear device has a "donut-like" shape (Ishibashi and Sherif, 1974), with the ratio of the outside diameter to the inside diameter being equal to the ratio of the outside height to the inside height; This ratio is in general equal to 2. The sample can be confined under either isotropic or anisotropic stress conditions. During the test, the shear stress is independently applied on the top of the sample. It is easy to show that the octahedral normal stress remains unchanged during the test and that the equality between the diameters ratio and the heights ratio insures uniform shear strains throughout the sample.

Like the conventional simple shear device, the torsional device closely simulates the in-situ stress-strain conditions during earthquakes, but it also has distinct advantages: (1) It is possible to apply vertical and horizontal stress independently and thus to know exactly the degree of confinment; and, (2) Uniform shear strains and stresses are imposed throughout the sample, making the experimental results more reliable. Some disadvantages have also to be mentioned: (1) Due to the shape of the sample, the sample preparation is relatively complex and it is difficult to achieve uniform characteristics throughout the sample; and, (2) The surfaces at the top and bottom of the specimen have to be rough enough to fully mobilize shear stresses at both ends of the soil sample. This has been found important and difficult to achieve. Ishibashi and Sherif (1974) used steel fins cast into the porous stones which stick into the soil sample. At present this test has the disadvantage of a new test, the devices are not standardized, and the number of experimental results is very limited.

It seems to have a potential for future experiments, because it overcomes some of the difficulties of the simple shear test, and it is easier to perform than a shaking table test.

2.3.3 Cyclic triaxial compression tests

The cyclic loading triaxial compression test was developed by Seed and Lee (1966) to provide an alternative to complicated simple shear test equipment. In this test the cylindrical soil specimen is first consolidated and saturated under isotropic condition, and then subjected to a constant amplitude periodic axial load inducing a stress reversal from compression to extension as shown in figure 2.1.b. This test has been standardized (Silver, 1976) and its simplicity makes it widely used, but it has several limitations:

(1) It does not reproduce the correct initial stress conditions for normally consolidated soil because it must be performed with an initially isotropic pressure condition, coefficient of lateral earth pressure K_0=1. (2) There is a 90 degrees rotation of the direction of the major principal stress during the two halves of the loading cycle; and, (3) Stress concentrations occur at the cap and base of the test specimen.

The results of the test are expressed in terms of the ratio of the maximum shear stress to the ambient pressure, $\Delta\sigma_a/2\sigma'_3$, where $\Delta\sigma_a$ is the amplitude of the periodic axial load and σ'_3 the initial confining pressure; This ratio is related to the ratio of the shear stress on the horizontal plane to the initial effective overburden pressure (τ/σ'_0) in simple shear by (Seed and Peacock, 1971):

$$(\tau/\sigma'_0)_{simple\ shear} = C_r(\Delta\sigma_a/2\sigma'_3)_{triaxial} \qquad (2.1)$$

Recommended values of C_r are listed in Table 2.1.

The next section will show how simple shear and triaxial test results can be used together with analytical models to assess the liquefaction potential at a given site.

2.4 REVIEW OF EMPIRICAL AND THEORETICAL ANALYSES FOR LIQUEFACTION

Various procedures for predicting the liquefaction potential of saturated soil deposits have been proposed; Several of these methods have been primarily developed by Professor Seed and his co-workers, but other investigators have also made important contributions to this field.

2.4.1 Empirical approaches to liquefaction analysis

These methods are based on the comparison of sites where liquefaction has or has not occurred during past earthquakes. The liquefaction potential is usually assessed qualitatively and correlated with an in-situ soil property.

A typical example is the Japanese rule of thumb that liquefaction is not a problem if the blow count from a standard penetration test exceeds twice the depth of the sample, measured in meters (Ohsaki, 1970). Other examples are described in the following paragraphs.

(a) Kishida (1969)

Source	Equations	C_r for $K_o = 0.4$	C_r for $K_o = 0.5$
Finn et al.	$C_r = (1 + K_o)/2$	0.70	1.0
Seed and Peacock	Varies	0.55-0.70	1.0
Castro	$C_r = 2(1 + 2K_o)/3$ 3	0.69	1.15

Table 2.1 Values for C_r (after Seed, 1979)

This criterion (figure 2.4) is based on observations from Japanese earthquakes and Standard Penetration Test results, and is valid for intensities ranging from VII to IX on the MMI scale and for soils with relative density less than 75%. The "possibility" of liquefaction at a given depth is qualitatively related to the standard penetration resistance and the effective overburden pressure.

(b) Castro (1975)

In this criterion the liquefaction potential is a function of the effective shear stress induced by the earthquake and the corrected standard penetration resistance (figure 2.5). The effective shear stress is taken as 0.7 the maximum shear stress.

(c) Seed (1976)

The latest version of this criterion is presented in figure 2.6; It incorporates the results of several studies performed by Seed and Peacock (1971), Seed, Mori and Chan (1975), DeAlba, Seed and Chan (1976). This is similar to the Castro (1975) approach, but supplemented by additional site studies and large scale testing. The magnitude of the earthquake is included in the criterion (figure 2.6). In figure 2.6 a line is drawn for a magnitude 8 1/4 earthquake separating the diagram into two regions. Any combination of penetration resistance and cyclic shear stress ratio which lies in the region above the line represents circumstances where liquefaction has occurred in model tests and field cases. No liquefaction has been observed for cases below that line. Two

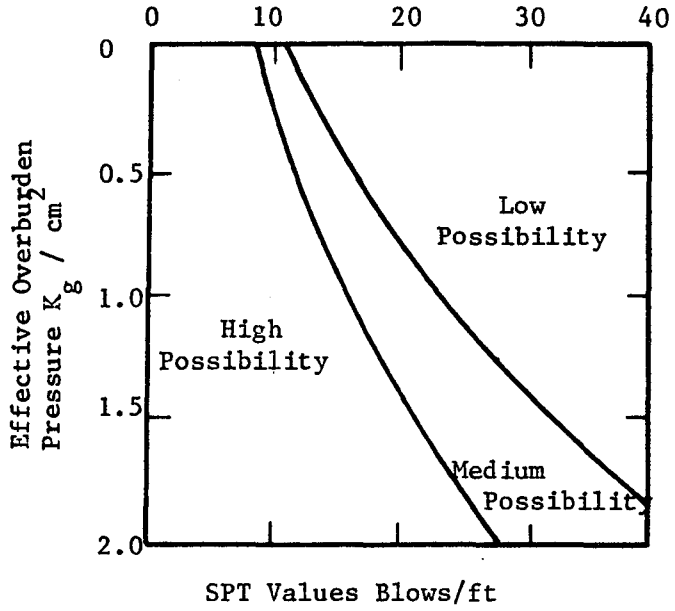

Figure 2.4 Criterion for Liquefaction
(after Kishida, 1969)
for : MMI = VII - IX
D_r = 75 %
C_u < 10
D_{50} < 2 mm

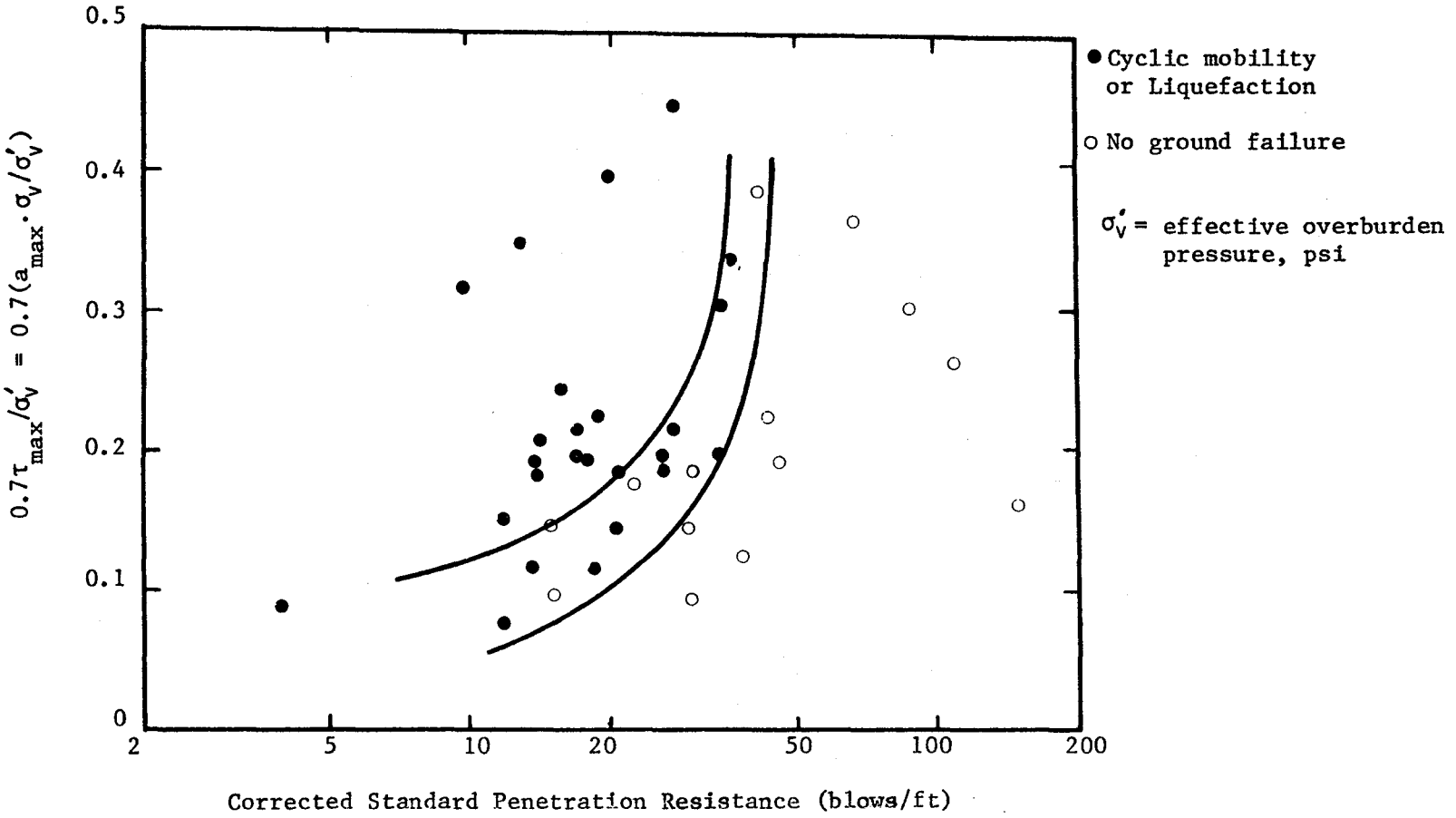

Figure 2.5 Criterion for Liquefaction (after Castro, 1975)

other lines are drawn for magnitudes 7 1/2 and 6. Also given at the top of figure 2.6 is a plot of potential shear strains which can accompany a liquefaction event.

2.4.2 Theoretical analysis of liquefaction

Three of the most significant theoretical studies of liquefaction will be presented: The Seed and Idriss (1971) simplified procedure which was the first to provide a theoretical assessment of liquefaction potential and is the most widely used in practice; the Christian and Swiger (1975) analysis of SPT results which addressed the problem of uncertainty in the liquefaction criteria; and, the Yegian and Whitman (1978) work which further developed Christian's study and defined a probability of liquefaction.

(a) Seed and Idriss simplified procedure (1971)

This method makes a comparison of the shear stress induced by the earthquake to the shear stress to cause liquefaction. The maximum shear stress induced by the earthquake, τ_{max}, is considered proportional to the peak ground surface acceleration and to the total overburden pressure:

$$\tau_{max} = r_d \gamma H a_{max}/g \qquad (2.2)$$

where γ is the total unit weight of the soil, H the depth of interest, g the acceleration of gravity, a_{max} the maximum ground surface

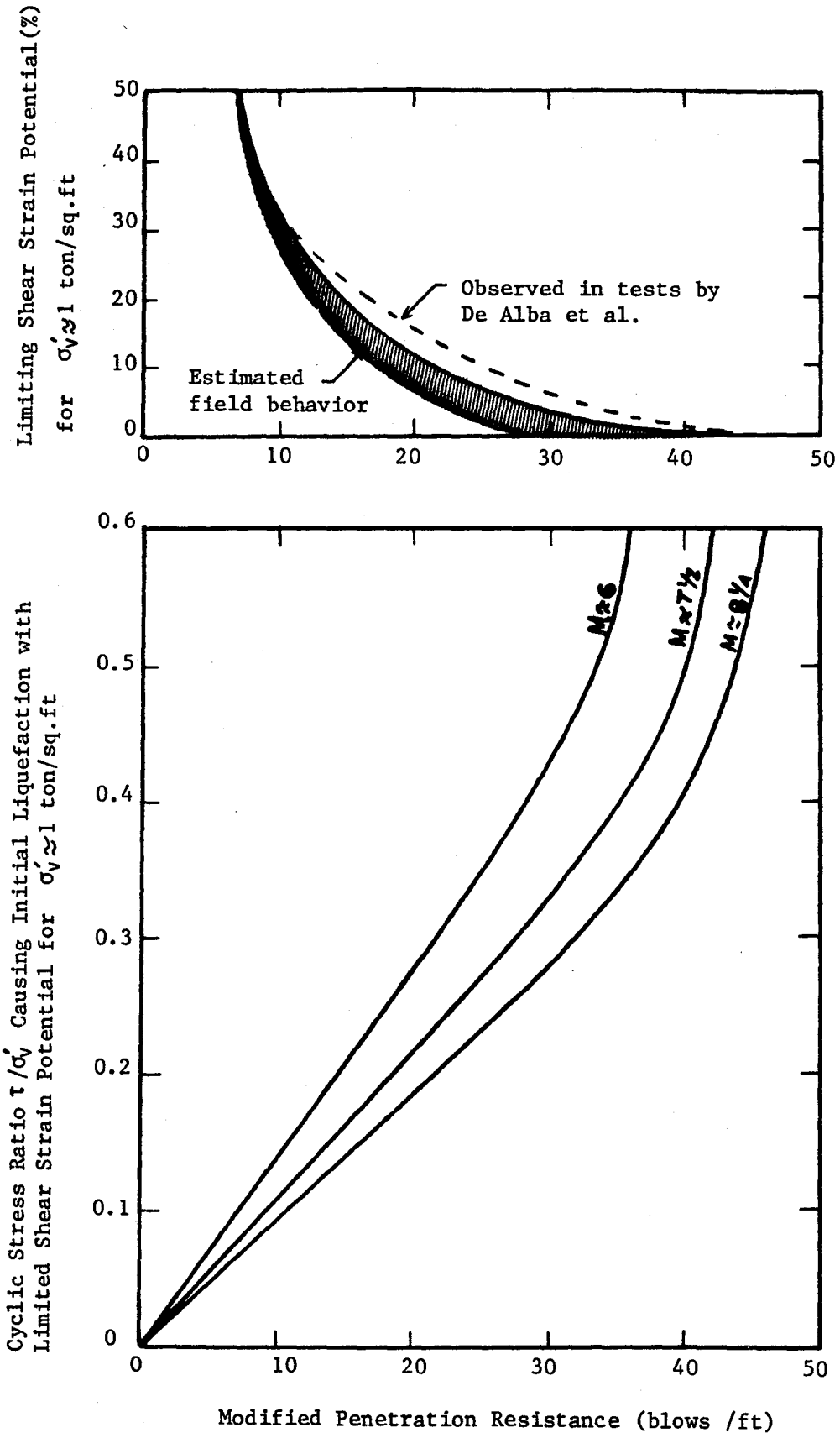

Figure 2.6 Correlation Between Field Liquefaction Behavior of Sands for Level Ground Conditions and Penetration Resistance (after Seed et al.)

acceleration in g-units, and r_d a stress reduction factor (figure 2.7) which accounts for the flexibility of the soil mass (r_d=1 for a perfectly rigid body). The maximum shear stress, τ_{max}, is converted to an average cyclic shear stress τ_{av}:

$$\tau_{av} = 0.65\ \tau_{max} \qquad (2.3)$$

The stress conversion factor 0.65 is associated with the following numbers of equivalent cycles (N_{eq}) of ground motion:

Magnitude	N_{eq}
7	10
7.5	20
8	30

An alternative method to equation 2.3 for computing the shear stress induced by the earthquake is to perform a dynamic analysis using the program SHAKE (Schnabel and al., 1972). This program performs the dynamic analysis of horizontally layered soil deposits by using a total stress approach with strain compatible modulus and damping ratio. The shear stress time history obtained at a given depth can be converted to an number of equivalent uniform cycles (N_{eq}) at an average stress τ_{av}(=.65τ_{max}) using the conversion method developed by Lee and Chan (1972).

The cyclic shear resistance to liquefaction can be assessed from laboratory tests or from a standard relation given by Seed and Idriss (1971):

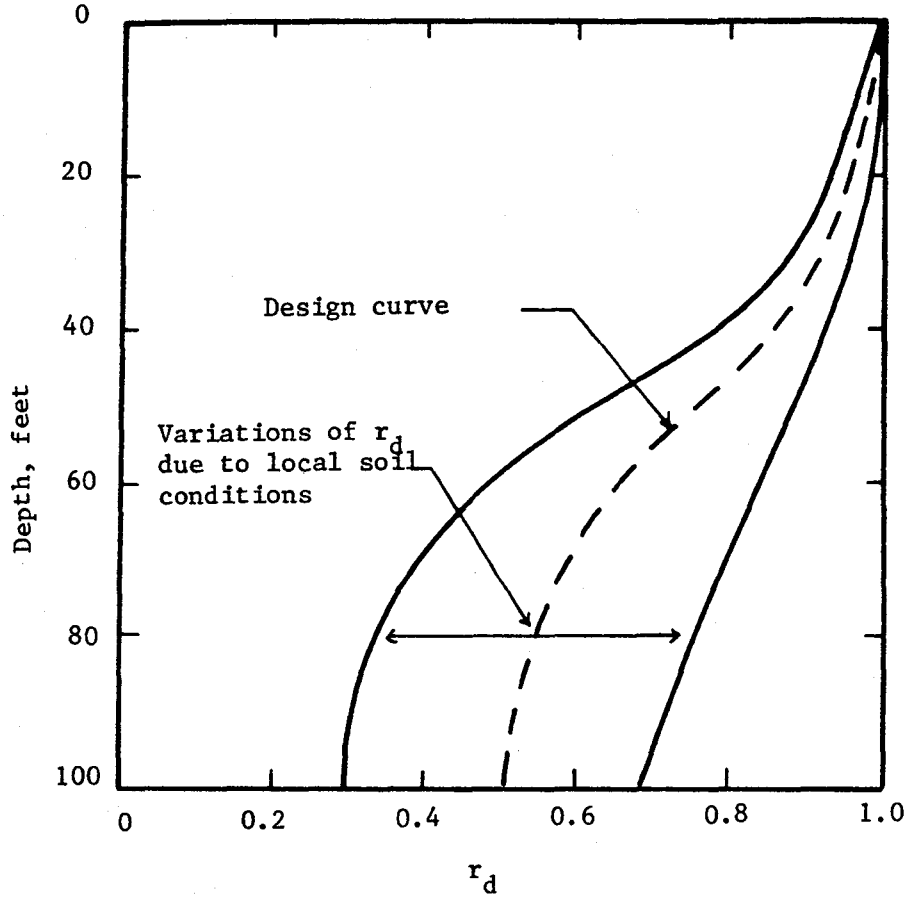

Figure 2.7 Stress Attenuation Factor with Depth (after Seed and Idriss, 1971)

- from simple shear tests

The resistance τ_r is the stress to cause liquefaction in N_{eq} cycles measured in this type of test. It is recommended that this value be multiplied by a correction factor of about 0.9, to account for the effects of multidirectional shaking (Pyke, Chan, and Seed, 1974).

- from cyclic triaxial tests

$$\tau_r = \sigma'_0 \, C_r \, (\Delta\sigma_a/2\sigma'_3)_{triaxial} \qquad (2.4)$$

C_r is a factor ranging from 0.5 to 0.65 depending upon the relative density of the soil (see section 2.3.2).

- standard relation

The resistance is assumed to be proportional to the effective overburden pressure σ'_0 and to the relative density of the soil, D_r:

$$\tau_r = (\Delta\sigma_a/2\sigma'_3)_{50} \, C_r \frac{D_r}{50} \, \sigma'_0 \qquad (2.5)$$

$(\Delta\sigma_a/2\sigma'_3)_{50}$ is the stress ratio causing liquefaction at a relative density of 50% and can be estimated as a function of the mean grain size from average curves proposed by Seed and Idriss (figure 2.8).

The comparison between the cyclic shear stresses caused by an earthquake and the corresponding cyclic shear resistance indicates the

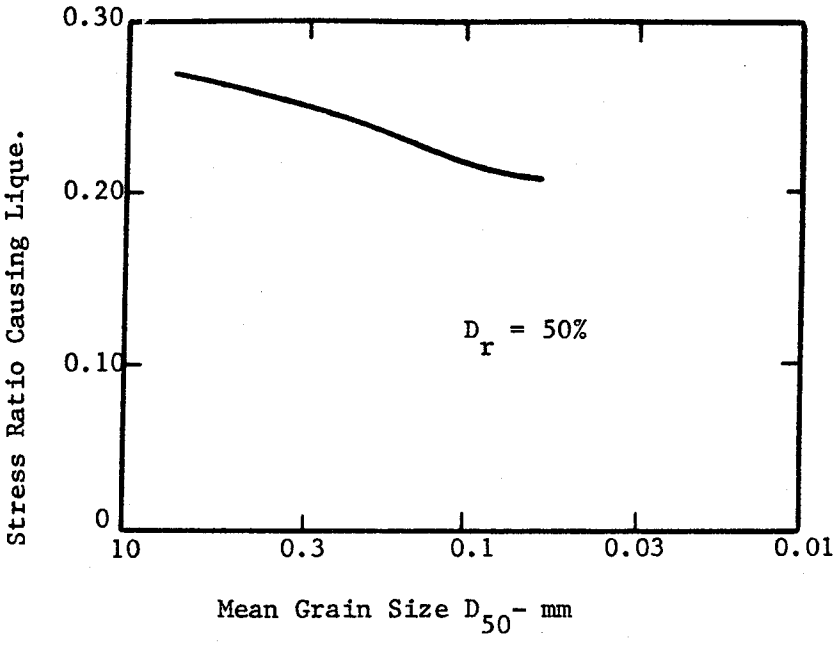

Figure 2.8.a Stress Ratio Causing Liquefaction vs. D_{50} for N_{eq} = 10 (after Seed, 1971)

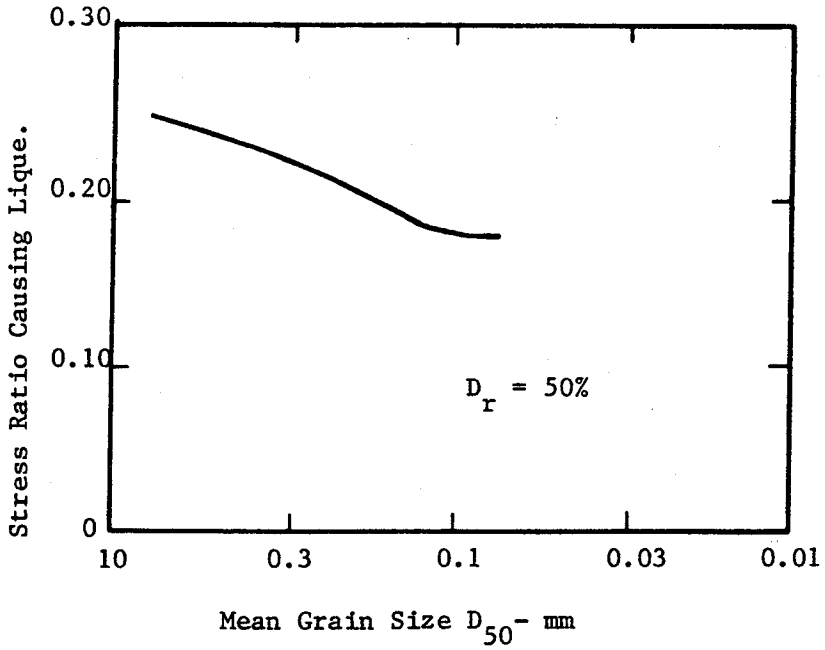

Figure 2.8.b Stress Ratio Causing Liquefaction vs. D_{50} for N_{eq} = 30 (after Seed, 1971)

liquefaction susceptibility of a sand deposit during that particular earthquake: if the induced stresses are greater than the resistance, liquefaction is presumed to occur.

This simplified procedure is convenient to apply but it has several shortcomings, in particular: (1) A stress conversion factor other than 0.65 would be associated with different N_{eq} values and might give answers which are not consistent with the results obtained with a conversion factor of 0.65.; (2) The number of equivalent cycles concept is based on the assumption of linear accumulation of pore pressure which is not verified for most cohesionless soils (see chapter 3); (3) Liquefaction can be indicated when there is no shear strain potential; (4) The information regarding the coefficient C_r is very limited and (5) The cyclic curves shown in figure 2.8 are based on a limited number of laboratory tests and do not include the large uncertainties involved with cyclic triaxial testing. With these limitations being understood, this method has been and still is a very useful tool for liquefaction assessment.

(b) Christian and Swiger (1975)

This analysis was based on the same data as Seed's criterion discussed in section 2.4.1 but used a statistical approach to determine whether a site is likely to liquefy under a given earthquake. Standard penetration resistance values were transformed to relative densities using the Gibbs and Holtz relationship and the data were separated into cases of liquefaction and no liquefaction. For each set of data the

authors found that the relative density and the peak acceleration were lognormally distributed, and using the technique of discriminant analysis they developed the curves given in figure 2.9 according to which a particular soil could be determined to be liquefiable or non liquefiable. The numbers on the curves indicate the probability that such a determination would be in error. It should be recognized that these probabilities are not the probabilities of liquefaction, but a measure of confidence in the location of a line separating liquefiable from non liquefiable sites.

(c) Yegian and Whitman (1978)

These authors developed a criterion which yields the likelihood of liquefaction given a certain level of earthquake shaking.This model is based on the field data previously used by Seed and Christian.To interpret the data a parameter S_c is employed, having the form:

$$S_c = H \exp(0.5M)/(D+16)\sigma'_v \qquad (2.6)$$

in which M is the Richter magnitude, D the hypocentral distance, H is the depth of interest and σ'_v the vertical effective stress at the same point. This parameter is plotted versus corrected SPT values for all the historical cases of liquefaction and of no liquefaction (figure 2.10).

The method of "least square of misclassified points" is then used to define the boundary line between liquefaction and no liquefaction (line S_c in figure 2.10). Until this point this study is very similar to

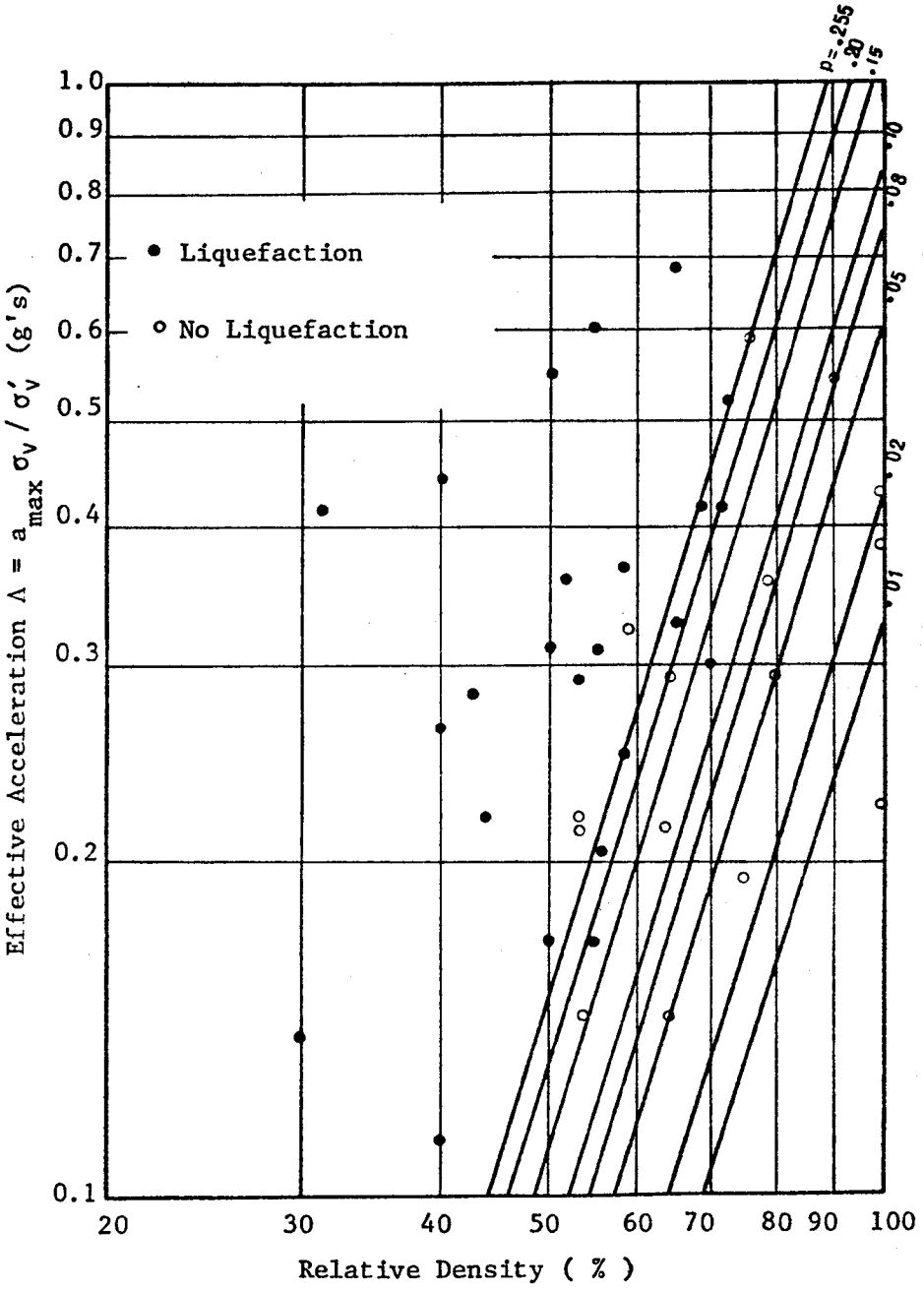

Figure 2.9 Discriminant Criterion for Liquefaction
(after Christian and Swiger, 1975)

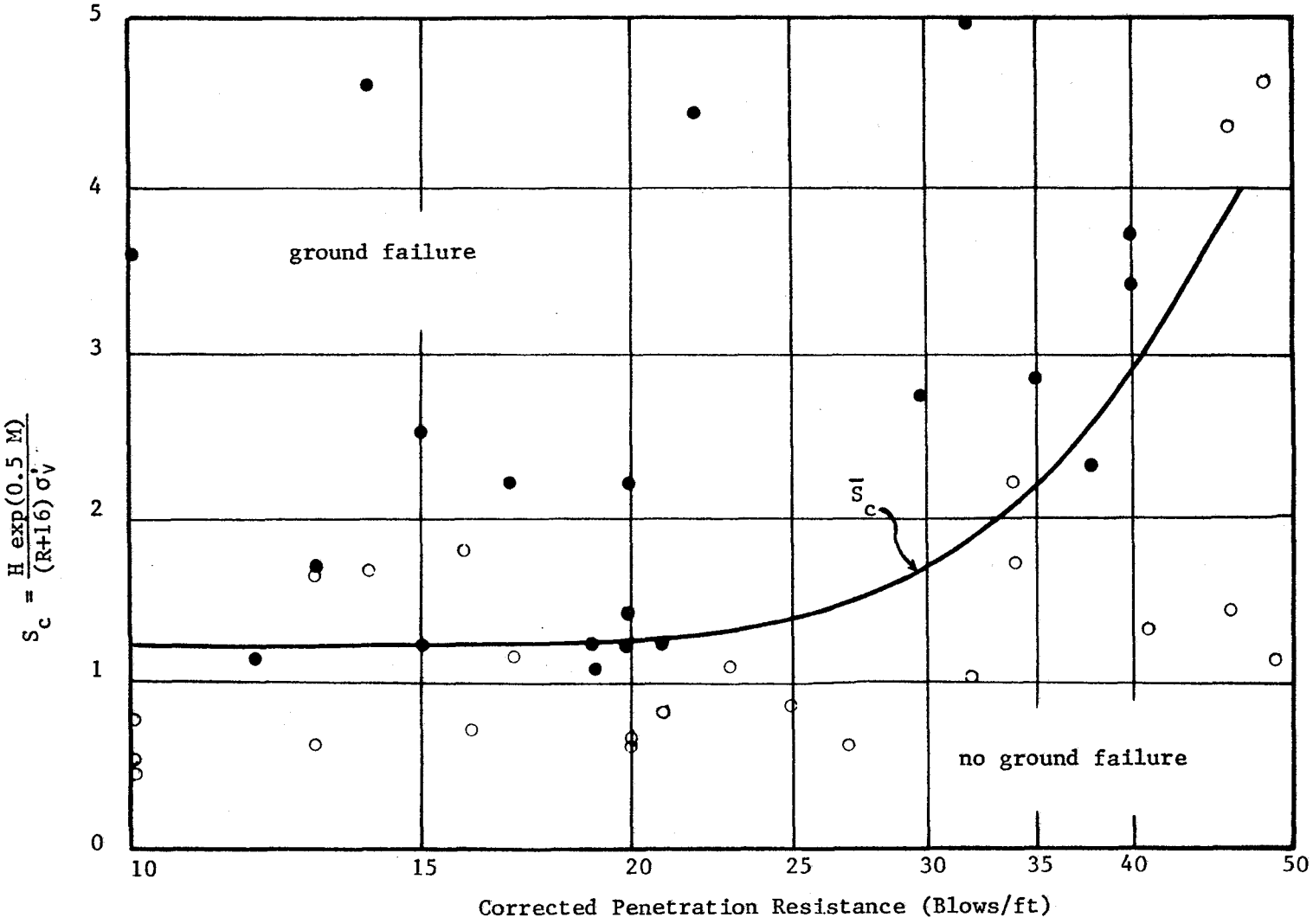

Figure 2.10 Average Strength Parameter $\bar{S}_c$ (after Yegian, 1978)

Christian's work, but it goes one step further to obtain the probability of liquefaction. A liquefaction potential index is defined as the ratio of the shear stress caused by an earthquake shaking to the resistance of the sand to such shaking, and since the parameter S_c is proportional to the shear stress causing liquefaction, the average liquefaction potential index is:

$$LPI = \frac{\exp(0.5M)\ H}{(D+16)\ \sigma'_v\ S_c} \tag{2.7}$$

The conditional probability of liquefaction given an earthquake of magnitude M occurring at a distance D from the site is

$$P[L/M,D] = P[LPI \geq 1.0/M,D] \tag{2.8}$$

Yegian assumed that LPI was lognormally distributed and obtained the necessary statistical parameters to solve equations 2.7 and 2.8. Finally, he conducted an integrated hazard analysis to determine the ground liquefaction potential at a site for a given seismic environment:

$$P[L] = \sum_{M,D} P[L/M,D] \cdot P[M,D] \tag{2.9}$$

The hazard methodology used the notion of uniform circular earthquake source area and had been developed earlier by Cornell (1968), and Cornell and Merz (1975). In summary, this analysis provided an in-depth study of the uncertainties involved with historical cases and integrated those uncertainties to obtain the probability of liquefaction.

2.5 MODELS FOR PORE PRESSURE BUILD-UP AND LIQUEFACTION ANALYSIS

In the past ten years, several models have been proposed to predict the actual level of pore pressure build-up in homogeneous and nonhomogeneous soil deposits. In this way the possibility of either complete or only partial liquefaction could be assessed. Several of the models have been incorporated in computer programs which perform the time domain dynamic response analysis of soil deposits up to the point of liquefaction. These models and programs have several common features: (1) The shear stresses are evaluated using the one-dimensional wave propagation theory; (2) The soil profile is idealized to consist of horizontal layers of soil deposits extending to base-rock; and, (3) The shear stresses are assumed to be caused by waves vertically propagating from the base-rock. The dynamic responses obtained from these models depend on the level of simplifying assumptions made in :

- the representation of stress-strain relations

- the pore pressure generation models

- the numerical integration methods

The most significant of the methods and their fundamental characteristics will be briefly discussed in the next sections.

(a) Liou, Streeter and Richart (1975) model : program CHARSOIL

This program performs non-linear analyses. The shear deformation curve is represented by a Ramberg-Osgood curve for initial loading; the unloading and reloading curves are determined by the Masing criterion. The stress-strain relation for soil skeleton is given by:

$$\sigma'_v = M_c \, \varepsilon_v \qquad (2.10)$$

in which σ'_v is the vertical effective stress, ε_v the vertical or volumetric strain and M_c the constrained modulus. The theory of elasticity is assumed to be valid, thus:

$$M_c = 4/3 \; G + B \qquad (2.11)$$

with G being the shear modulus, and B the bulk modulus of the soil skeleton. As noted by Finn (1977) these assumptions present a basic inconsistency in the sense that the theory of elasticity is assumed to be valid (equation 2.11) while at the same time the shear modulus G is made strain dependent. The program CHARSOIL solves the equations of motion using this soil model. The numerical model is constituted by coupled shear wave and pressure wave motions. The time histories of pore pressure, vertical strain and shear strain can be obtained for the entire deposit.

(b) Finn, Lee and Martin (1977) model : program DESRA

This is the most comprehensive pore pressure model. The initial stress-strain curve is given by an hyperbolic relation; unloading and reloading curves are determined by the Masing criterion. The increase

in pore pressure during each time interval is computed using volume change and rebound modulus characteristics as :

$$\Delta u = E_r \, \Delta \varepsilon_v \qquad (2.12)$$

with Δu the increase in pore pressure, E_r the one-dimensional rebound modulus and $\Delta \varepsilon_v$ the volumetric strain increment. Finn, Lee and Martin have shown that under simple shear conditions, the volumetric strain increment is a function of the cyclic shear strain γ and of the total accumulated volumetric strain ε_v:

$$\Delta \varepsilon_v = C_1(\gamma - C_2 \varepsilon_v) + \frac{C_3 \varepsilon_v^2}{(\gamma + C_4 \varepsilon_v)} \qquad (2.13)$$

in which C_1, C_2, C_3 and C_4 are experimental constants. This model was incorporated into a method of dynamic effective stress response analysis for level ground excited by vertically propagating shear waves. The numerical integration was performed using Newmark's unconditionally stable integration operator. The model and the computer program have been thoroughly tested by Finn and his co-workers and appear to offer a good prediction capability. A problem for its implementation is that it requires very good data on shear moduli and volume changes. Obtaining these data for a specific liquefaction potential investigation would only be economically feasible for a very large construction project. Otherwise they would have to be obtained from available results for standard sands which have been tested extensively.

(c) Bazant and Krizek endochronic formulation of strains (1976):

This formulation provides an alternative description of volume change data to equation 2.13 and can be used in conjunction with Martin and Finn model to predict pore pressure. The advantage of this method relates to the simplicity of the mathematical formulation; the volumetric strain can be expressed as a function of a single variable, a damage parameter K, which is a scalar variable whose increments depend on deformation increments. At present, this model has not been thoroughly tested and few data on the necessary parameters to do so are available.

(d) Stress Path Models :

The first stress path model was proposed by Ishihara and al. (1975) and was modified by Ghaboussi and Dikmen (1978). The original Ishihara model was derived from an extensive investigation of the behavior of sand under triaxial test conditions and it made the following assumptions:(1) The excess pore pressures are generated by plastic deformations only and occur whenever the loading path penetrates the current yield surface; (2) The yield surfaces are represented by straight lines which are also considered to be lines of constant shear strain; (3) The stress path during plastic deformation is of a simple geometrical shape, circle or parabola; (4) The stress path deviates from this shape only when it approaches the failure line; and, (5) The unloading phases are assumed to be purely elastic with no change in pore pressure.Given these assumptions the model can be used to predict increases in pore pressures for a given irregular loading sequence. It is very simple to use but it has limitations: (1) There are sands for

which yield surfaces cannot be represented by straight lines; (2) The assumption that there is no change in pore pressure during unloading is not supported by cyclic simple shear test data; and, (3) The assumption that yield surfaces are lines of constant shear strain imply the occurrence of "elastic traps" during strain controlled cyclic loading test. Ghaboussi (1978) slightly modified this model to reduce the effects of "elastic traps" and incorporated this pore pressure model into a dynamic response analysis program, LASS-II. However, the limitations of the stress path methods are still inherent to this latest model.

(e) Other models :

Several other models have been recently developed and in particular two models which follow along the line of Finn's volumetric strain model: Zienkiewicz (1978) has incorporated the volumetric strain model into an elasto-plastic method of dynamic effective stress analysis, and Sherif and Ishibashi (1980) proposed a simple model which relates the increment of residual pore water pressure to a stress and pore pressure function, and a stress intensity function. This last model is based on torsional simple shear test data, similar to Finn's test data, but the state variable is the pore pressure instead of the volumetric strain, which makes the mathematical formulation more convenient.

2.6 SUMMARY

Cyclic testing techniques exist which simulate the stress condition induced by earthquake loading. The early tests were cyclic loading triaxial compression tests but their limitations led to the development of cyclic simple shear tests which provide the closest representation of field conditions. The latest versions of these tests include the use of long and shallow samples in simple shear devices and the use of thin samples on shaking table.

Several methods have been developed to assess the potential for complete liquefaction. The first empirical approaches were based on the comparison of sites where liquefaction has or has not occurred during past earthquakes and they correlated the liquefaction potential to an in-situ soil property such as the standard penetration resistance. Subsequently methods were proposed to provide a theoretical assessment of the potential for liquefaction. Seed's simplified procedure, which makes a comparison of the shear stress induced by the earthquake to the shear stress to cause liquefaction, is the most significant of these methods. In the past few years, work has been undertaken to study the uncertainties involved in historical and empirical data and to establish a probabilistic framework for liquefaction assessment.

In the past ten years, several models have been proposed to extend the early theoretical developments and to predict the actual level of pore pressure in homogeneous and nonhomogeneous soil deposits. The most comprehensive model is Finn's volumetric strain model, which relates the increase in pore pressure to the volume change and rebound modulus

characteristics of the soil. Several of these pore pressure models have been incorporated in computer programs which perform the time domain dynamic response analysis of soil deposits up to the point of liquefaction.

This review shows that the research efforts, from the early 70's to present, followed along two lines. One line of approach was to develop analytical methods which deterministically assess the possibility of either complete or only partial liquefaction. The other was to establish a probabilistic framework for complete liquefaction assessment. Relatively little work has been done in the second area and there is presently no methodology available to combine these two lines of research. The following chapters attempt to do so. In chapter 3, the accumulation of pore pressure in cohesionless soils is analyzed from both the experimental and theoretical standpoints. Chapter 4 presents the derivation of a probabilistic pore pressure model using laboratory data. Chapter 5 describes practical applications of the probabilistic pore pressure model. Chapter 6 demonstrates that the development of pore pressure can also be probabilistically defined using effective stress models. Finally chapters 7 and 8 propose a hazard and risk analysis methodology for pore pressure build-up in soils and make recommendations for future research.

Chapter III

ACCUMULATION OF PORE PRESSURE IN COHESIONLESS SOILS

3.1 INTRODUCTION

An important mode of failure of a material or a structure under cyclic loading is that of fatigue. Failure by fatigue is the result of cumulative damage caused by the repeated applications of loading and unloading cycles. The liquefaction of cohesionless soils under seismic loading is a fatigue failure which results from cumulative damage, namely, the increase in pore water pressure.

The exact nature of fatigue failures has not been fully understood for most materials, and to a large extent our sources of information are experimental data obtained from deterministic uniform loading conditions. When the loading amplitude is not constant, assumptions have to be made to express the effects of an applied irregular cyclic load in terms of the results of uniform loading tests. The most widely used assumptions were proposed independently by Palmgren (1924) and Miner (1945). The Palmgren-Miner theory postulates that the accumulation of fatigue damage is linear. This approach is currently applied to sand materials subjected to undrained cyclic loading. Triaxial and simple shear test data are used to define their characteristics of pore pressure build-up under uniform cyclic loading, and a method has been developed to express an irregular load sequence in terms of an number of

equivalent uniform cycles, N_{eq} (Lee and Chan, 1972, Seed, Idriss, Makdisi and Banerjee, 1975). This method can be shown to be equivalent to the rule of linear accumulation of damage.

One of the objectives of this dissertation is to develop a probabilistic pore pressure generation model using laboratory data. To do this, it was necessary to have a clear understanding and a correct description of the increase in pore pressure during uniform loading cyclic tests. This requires an assessment of the applicability of the Palmgren-Miner rule to the pore pressure build-up phenomenon, and accordingly a study of the development of pore pressure under irregular loading.

3.2 LINEAR ACCUMULATION OF DAMAGE

Poncelet (1839) was the first to study the strength of materials under repeated loading, and to introduce the term "fatigue". Following his early considerations, experiments were conducted by the Institution of Mechanical Engineers in London (1848) and by Wohler (1860) on beams and rolling stock components. These results showed that the ultimate stress in repeated loading was a considerably reduced value of the ultimate stress in static loading, and they introduced the classical "Stress-Number of Cycles" curve to express the results from repeated load tests (figure 3.1.b). These results were followed by numerous experiments and studies on all kinds of materials and mechanical components. All these experiments used repeated loads of uniform intensity, and it is not until Palmgren (1924) and Miner (1945) that a

method was proposed to extrapolate the effects of cyclic loading from regular to irregular load sequences. The Palmgren-Miner's rule states that:

> - The energy applied during any stress cycle has an accumulative damaging effect on the material; the effect is function of the energy level of the particular cycle and assumed independent of when in time history the stress pulse is applied.

This rule of linear accumulation of damage is described in figure 3.1. An irregular load sequence is synthesized in n cycles, the stress amplitude of the ith cycle being τ_i (figure 3.1.a). If the absolute values of the positive and negative peaks of the ith cycle are not equal, the stress amplitude τ_i is taken as the average of these two absolute values. A cyclic strength curve is developed from laboratory testing using uniform cyclic stresses (figure 3.1.b). The cyclic strength curve relates the number of cycles to reach failure to the cyclic stress intensity. The definition of failure depends upon the material and structure being tested. From the cyclic strength curve, the number of uniform cycles to cause failure at stress level τ_i is N_{if}. Consequently the damage caused by any cycle at stress level τ_i is (figure 3.1.c):

$$D_i = 1/N_{if} \qquad (3.1)$$

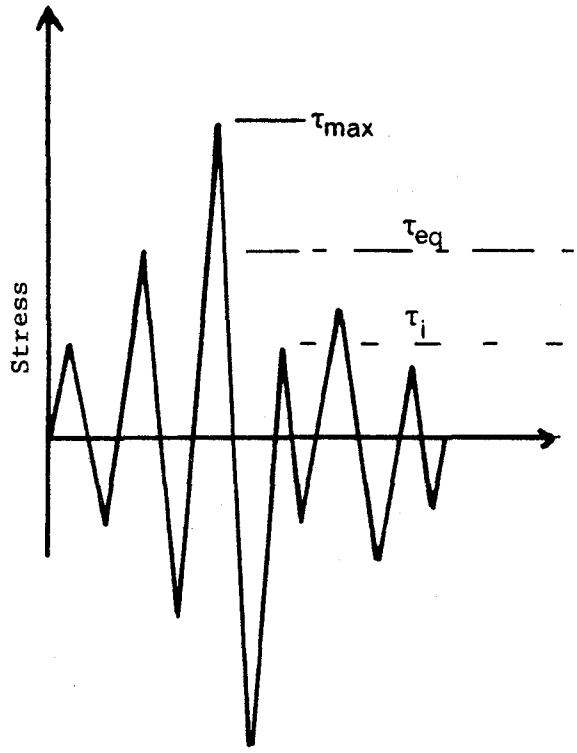

Figure 3.1.a Stress Time History

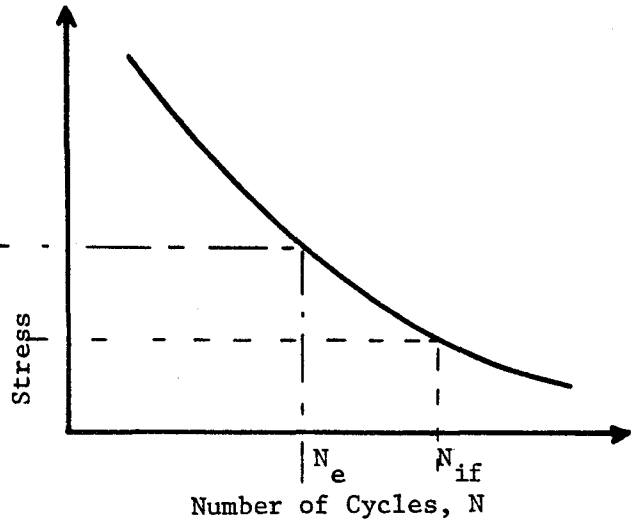

Figure 3.1.b Cyclic Strength Curve

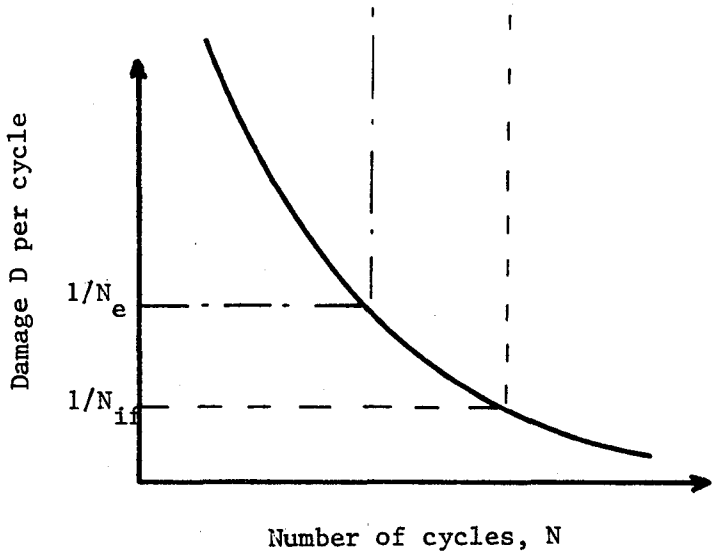

Figure 3.1.c Damage Relation

Figure 3.1 Linear Accumulation of Damage

Given the assumption of independence between cycles of the Palmgren-Miner theory, the total cumulative damage due to the irregular time history is:

$$D = \sum_{i=1}^{n} 1/N_{if} \tag{3.2}$$

Failure occurs when the damage D is equal or greater than unity. The number of equivalent uniform cycles concept is directly derived from the cumulative damage approach. A reference stress τ_{eq} is chosen as a percentage F of the maximum stress τ_{max} of the irregular time history. The number of equivalent uniform cycles N_{eq} is the number of cycles with stress amplitude τ_{eq} which would cause the same amount of damage as the irregular stress history. Based on the cumulative damage approach, N_{eq} cycles with amplitude τ_{eq} cause a damage D evaluated as:

$$D = N_{eq}/N_e \tag{3.3}$$

where $1/N_e$ is the damage caused by one cycle with amplitude $\tau_{eq}(=F\tau_{max})$. The equality of equations 3.2 and 3.3 gives:

$$N_{eq} = N_e \sum_{i=1}^{n} (1/N_{if}) \tag{3.4}$$

This equation can be conveniently used to convert any irregular stress history to a regular stress sequence. By selecting a new value F of the ratio between the reference stress and the maximum stress, a different number of equivalent cycles is determined.

3.3 PALMGREN-MINER RULE AND PORE PRESSURE BUILD-UP

The number of equivalent uniform cycles concept has been described in several papers including Ishihara and Yasuda (1973), Lee and Chan (1972) and Seed and al (1975). And even if it was not explicitly stated, all these papers were using the Palmgren-Miner assumptions. As an example, the latest of these papers assumes that " a given number of cycles at any stress level can be expressed as being equivalent to some other number of cycles at one of the other stress levels ", the equivalence being defined by a cyclic strength curve.

The application of the Palmgren-Miner rule to pore pressure build-up and liquefaction involves some specific characteristics and assumptions:

- The cyclic strength curves are defined from the results of cyclic triaxial tests, simple shear tests and shaking table tests.

- The failure criterion is usually the zero effective stress state, or some level of cyclic shear strain.

- These cyclic strength curves are expressed as the stress ratio to cause failure τ/σ'_0 versus the number of cycles to reach failure N_1, where τ is the shear stress and σ'_0 the initial effective confining pressure.

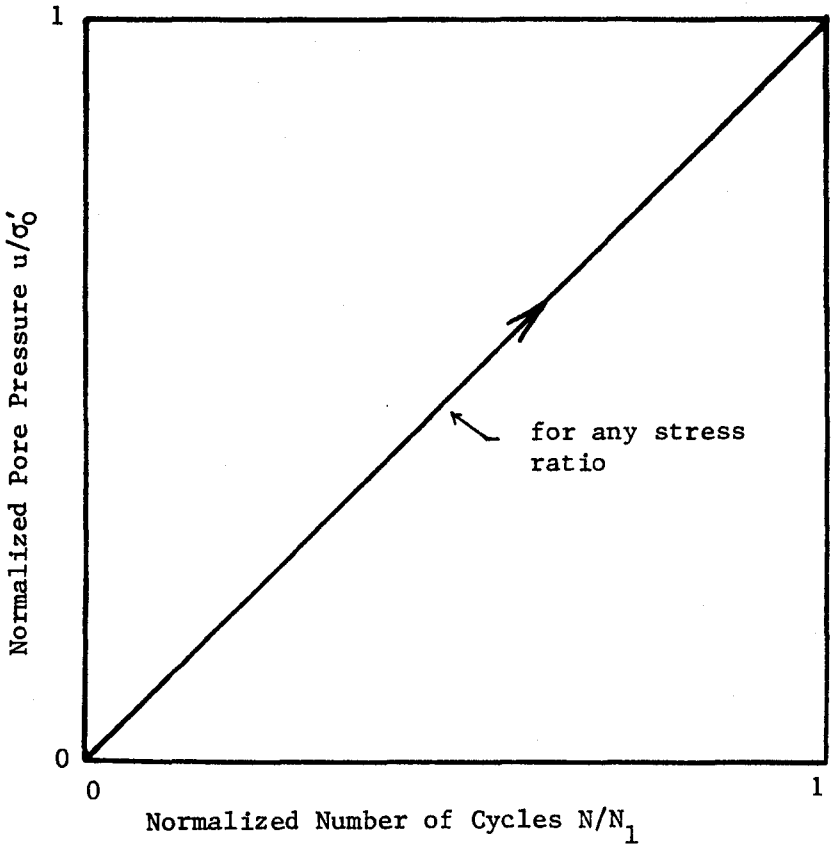

Figure 3.2 Linear Accumulation of Pore Pressure

- The stress conversion factor F is generally taken as .65, and the reference stress is called the effective stress. The ratio .65 is equal to the average value of one cycle of a sine wave.

The assumption of linear accumulation of damage in pore pressure analysis implies that linear development of pore pressure should occur in both uniform cyclic tests results and under random loading. The implied linear behavior in uniform cyclic tests is best described by the use of a normalized pore pressure curve which relates the pore pressure ratio u/σ'_0 obtained at the end of cycle N to the normalized number of cycles N/N_1. The assumption of linear accumulation of pore pressure is expressed by a straight line in the $(u/\sigma'_0, N/N_1)$ plot (figure 3.2), independent of the applied stress ratio τ/σ'_0. This is directly related to the assumption that "the damaging effect is independent of when in time history the stress pulse is applied", which implies that each cycle of a uniform load sequence has the same damaging effect (equations 3.1 and 3.2). The next section will demonstrate that this assumption is not justified.

3.4 OBSERVED ACCUMULATION OF PORE PRESSURE IN CYCLIC TESTS

In order to compare the theoretical behavior described in the previous section to observed behavior, the results of uniform loading cyclic simple shear tests and triaxial tests are given in figures 3.3 to 3.5. In figure 3.3 several pore pressure generation curves are

presented which were deduced from the results obtained by DeAlba and al (1976) during the undrained cyclic testing of Monterey sand on a shaking table. These curves are for a relative density of 54% and stress ratios ranging from 0.10 to 0.18. The corresponding cyclic strength curve is given in figure 2.2. Similar results are presented in figures 3.4 and 3.5 for uniform loading cyclic triaxial tests. These tests were performed on dune sand from San Francisco waterfront fills (Clough and Chameau, 1979). Cyclic strength curves and pore pressure generation curves from these tests are shown for relative densities of 40% and 50%. In both triaxial and simple shear tests it is apparent that the data do not plot on the 45 degree angle line in the $(u/\sigma'_0, N/N_1)$ graph. The observed pore pressure generation curves are non-linear and depend on the amplitude of the applied uniform shear stress τ/σ'_0. These curves present similar trends: there is a sharp rise in pore pressure for N/N_1 less than 0.2 to 0.3, followed by an almost linear behavior up to N/N_1 equal to 0.7 to 0.8, and finally an other sharp rise in pore pressure which leads to the zero effective stress state and large deformations. This observed behavior implies that the damaging effect of a stress cycle depends on when in time it occurs:

$$\Delta u_N = f(\tau, u)_{N-1} \qquad (3.5)$$

Equation 3.5 expresses that Δu , the increase in pore pressure at cycle N, is a function of τ the shear stress applied at cycle N and of u_{N-1} the accumulated pore pressure at the end of cycle N-1. The Palmgren-Miner's rule would consider Δu to be a unique function of τ .

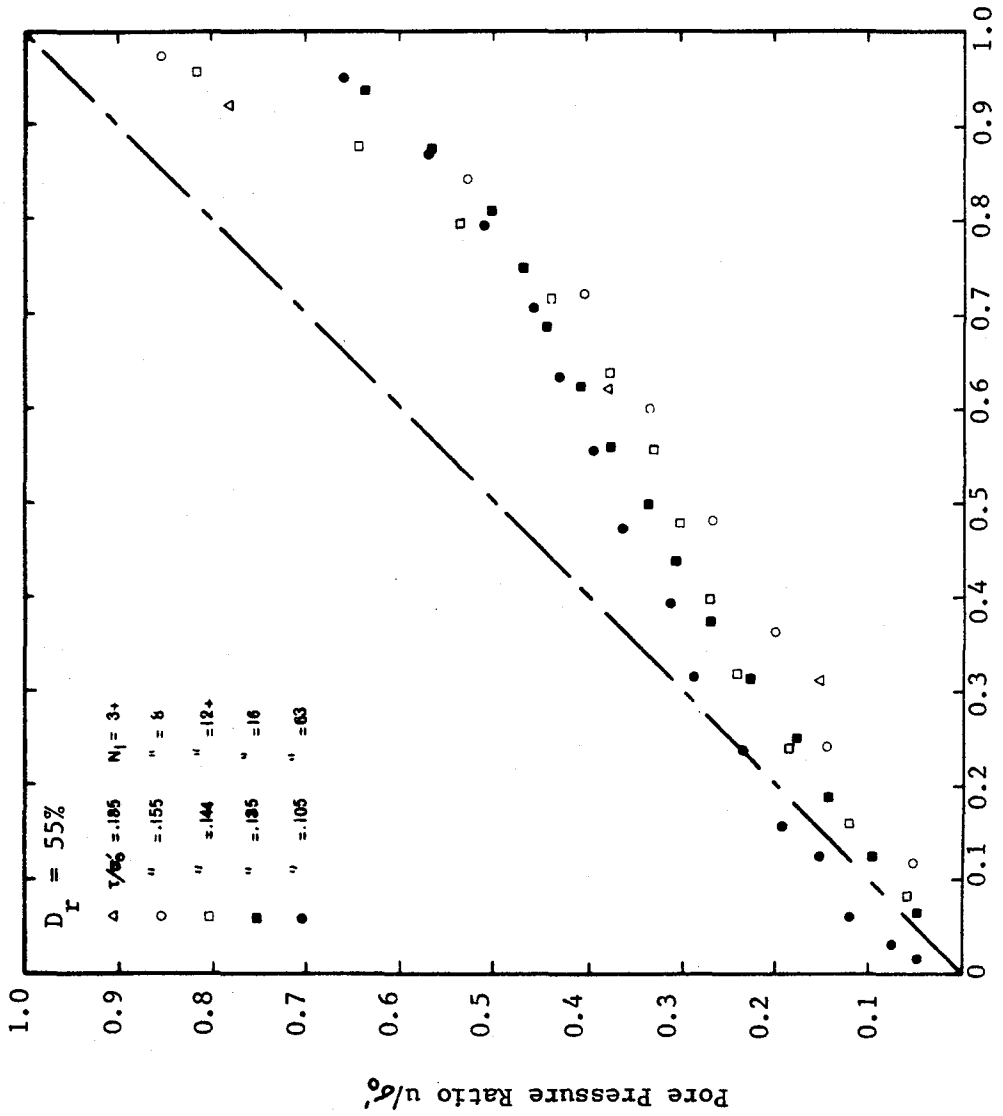

Figure 3.3 Pore Pressure Generation Curves from Shaking Table Tests (after De Alba, 1976)

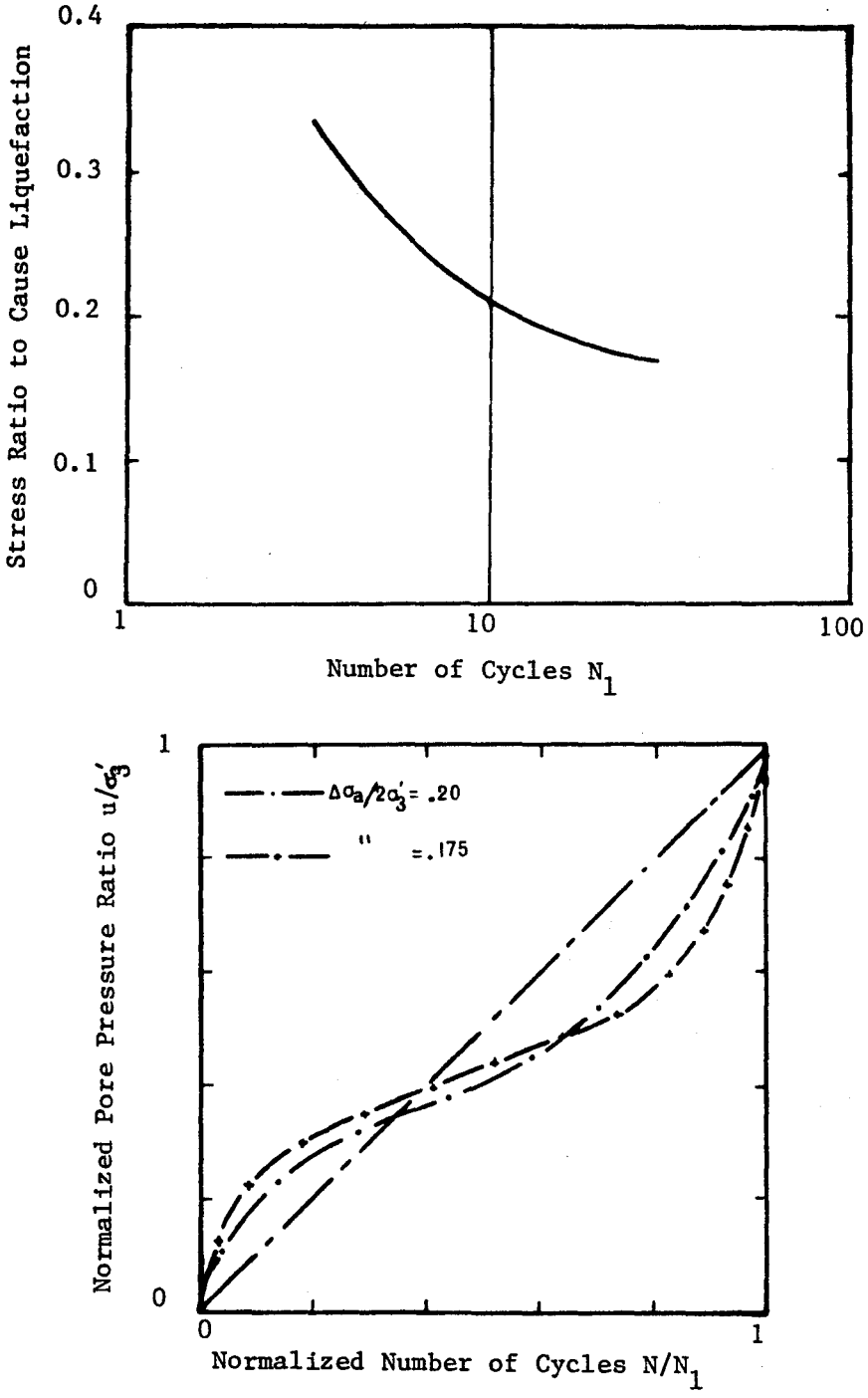

Figure 3.4 Results of Triaxial Cyclic Tests on Dune Sand
(D_r = 40%)

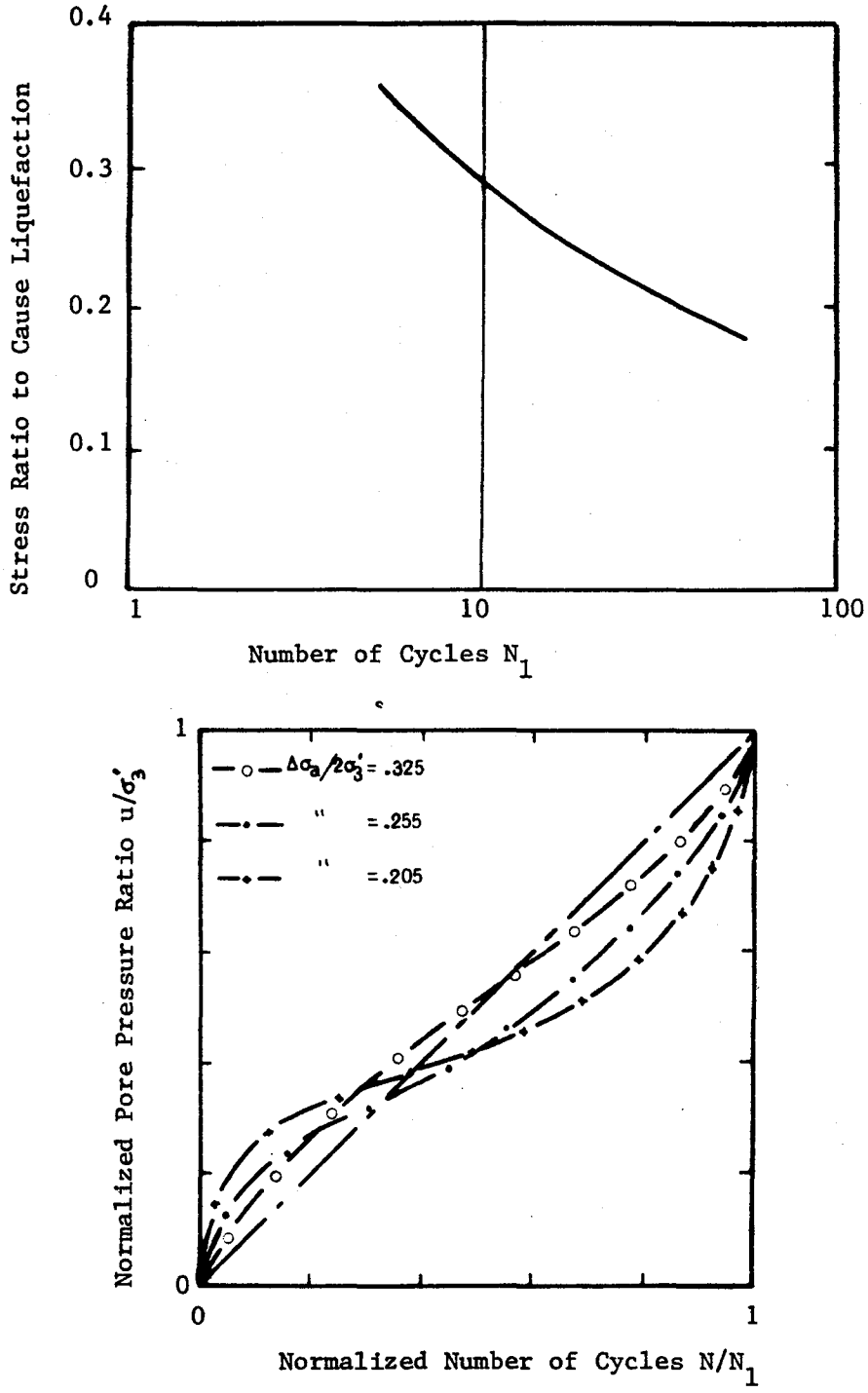

Figure 3.5 Results of Triaxial Cyclic Tests on Dune Sand
(D_r = 50%)

3.5 ACCUMULATION OF PORE PRESSURE DURING NON-UNIFORM LOADING

Due to experimental difficulties, very few investigations have been conducted which used irregular loading sequences. The most significant study was performed by Ishihara and Yasuda (1975) in torsional simple shear testing. Their results indicated that the major damaging effects were caused by the largest stress cycles and that small stress cycles can have disproportionately large damaging effects if they follow a stress cycle high enough to cause a large increase in pore pressure. In order to supplement this lack of experimental data, effective stress pore pressure development models will now be used to study the increase in pore pressure during non-uniform loading and to compare the results to those predicted by the linear accumulation of damage method.

3.5.1 Effective stress model

In chapter 2 several models have been reviewed which attempt to solve the problem of pore pressure build-up in soil deposits due to earthquake loading. Among those was the volumetric strain model proposed by Finn, Lee and Martin (1977) which at present is the most comprehensive method to describe the development of pore pressure under simple shear conditions. This model has been used in this dissertation, and a description of its main characteristics follows. This description is based on the papers by Finn, Lee and Martin (1977) and Finn (1979):

(a) Generation of pore-water pressure:

Consider a cubic element of unit volume and porosity n_p under a vertical effective stress σ'_0. In a drained simple shear test, a cycle of shear strain γ is applied and causes a volumetric compaction $\Delta\varepsilon_v$ due to grain slip. In an undrained test having the same shear strain amplitude, the slip deformation must transfer some of the vertical stress previously carried by intergranular forces to the more incompressible water. The reduction in effective stress results in the release of recoverable volumetric strain $\Delta\varepsilon_{vr}$. For volumetric compatibility the change in volume of voids has to be equal to the net change in volume of the sand structure. The change in volume of voids is $\Delta u n_p / K_w$, where Δu is the increase in pore pressure for the cycle and K_w the bulk modulus of water. The net change in volume of the sand stucture is equal to $\Delta\varepsilon_v$, less the recoverable $\Delta\varepsilon_{vr}$, which is equal to $\Delta u / E_r$, where E_r is the one-dimensional rebound modulus of sand at an effective stress σ'_v. The volume equality gives:

$$\frac{\Delta u \, n_p}{K_w} = \Delta\varepsilon_v - \frac{\Delta u}{E_r} \tag{3.6}$$

If the water is assumed incompressible ($K_w >> E_r$), then equation 3.6 simplifies to:

$$\Delta u = E_r \, \Delta\varepsilon_v \tag{3.7}$$

This is the fundamental equation of Finn's model and it explains why it is called a volumetric strain model. The volumetric strain increment $\Delta\varepsilon_v$ has been shown experimentally to be a function of the total accumulated volumetric strain ε_v and the amplitude of the shear strain cycle γ:

$$\Delta\varepsilon_v = C_1(\gamma - C_2\varepsilon_v) + \frac{C_3\varepsilon_v^2}{\gamma + C_4\varepsilon_v} \qquad (3.8)$$

in which C_1, C_2, C_3 and C_4 are experimental constants that depend on the sand type and relative density. Note that other functional relationships, including Bazant's endochronic relation (section 2.5.c), can be used to relate $\Delta\varepsilon_v$ to ε_v and γ. The rebound modulus may be obtained from a series of one-dimensional unloading tests. It was expressed by Finn as:

$$E_r = \frac{(\sigma'_v)^{1-m}}{mk_2(\sigma'_{v0})^{n-m}} \qquad (3.9)$$

in which σ'_{v0} is the initial value of the vertical effective stress and k_2, m and n are experimental constants for a given sand.

The development of pore pressure can be described by equations 3.7 to 3.9 if the shear strain γ is known.

(b) Constitutive relations

During an earthquake an element of sand is subjected to an irregular loading sequence consisting of intervals of loading, unloading and reloading. This model assumes that up to the point of the first reversal in loading, the response of the sand follows an hyperbolic stress-strain relationship described by :

$$\tau = \frac{G_{mo}\gamma}{1 + (G_{mo}/\tau_{mo})\gamma} = f(\gamma) \qquad (3.10)$$

in which τ is the shear stress amplitude, G_{mo} the initial maximum tangent modulus, and τ_{mo} the maximum shear stress that can be applied to the sand without failure. The initial loading curve $f(\gamma)$ is called the skeleton or backbone curve. During subsequent unloading or reloading from a reversal point (γ_r, τ_r) the stress-strain curve is assumed to be:

$$\frac{\tau - \tau_r}{2} = f\left[\frac{\gamma - \gamma_r}{2}\right] \qquad (3.11)$$

This type of response is referred to as Masing behavior (after Masing, 1926).

The complete stress-strain response of undrained saturated sands is completely described by equations 3.7 to 3.11. The model takes also into account the hardening which occurs in simple shear due to grain slip. The necessary equations to do so are described in Appendix B.

3.5.2 Application of the effective stress model to uniform and non-uniform loading

Given the constitutive relationship and the pore pressure model described in the previous section, the increment of pore-water pressure Δu during a loading cycle with maximum shear stress τ can be computed. The procedure can be computerized in order to obtain the development of pore pressure during uniform and non-uniform loading. The results obtained for uniform loading can be checked against laboratory data in order to assess the validity of the model.

(a) Uniform loading

The author applied the model to predict the development of pore pressure in a sample of crystal silica sand during undrained cyclic simple shear test. The crystal silica sand has been the subject of several investigations under drained and undrained conditions and the parameters necessary to perform the study are available in the literature (Finn, Lee and Martin, 1975). These parameters are listed in table 3.1. The time histories of pore pressure build-up have been calculated for several shear stress ratios at a relative density of 45 percent. Computer results are given in figure 3.6 for three values of shear stress ratios, 0.15,0.125 and 0.10. For each stress ratio the number of cycles to zero effective stress can be obtained and by repeating for a sufficient number of stress ratios an analytical cyclic strength curve can be defined. This analytical curve for the crystal silica sand at a relative density of 45 percent is compared to experimental data in figure 3.7. The very good agreement between analytical and experimental results demonstrates the ability of the model to correctly simulate the behavior of sand during undrained simple shear loading. Similar conclusions were obtained by Finn, Lee and Martin (1975 and 1977). A cyclic strength curve derived for a relative density of 50 percent is given in figure 3.8. It compares well with an experimental curve obtained by Seed and Peacock (1971). In figure 3.9 the pore pressure curves for a relative density of 45 percent have been normalized and the ratio u/σ'_0 is plotted versus the normalized number of cycles N/N_l. These curves are similar to the experimental curves described in section 3.4 and they theoretically confirm that the development of pore pressure during undrained cyclic simple shear loading is highly non-linear.

Relative Density D_r = 45 %

Void Ratio e_o = 0.83

Coefficient of at Rest Lateral Earth Pressure K_o = 0.50

Volumetric Strain Coefficients :

C_1 = 0.80
C_2 = 0.79
C_3 = 0.45
C_4 = 0.73

Rebound Modulus Coefficients :

m = 0.43
n = 0.62
k_2 = 0.0025

Hardening Coefficients (see Appendix B)

H_1 = 0.754
H_2 = 0.406
H_3 = 0.550
H_4 = 0.500

Table 3.1 Parameters Used in the Effective Stress Model for Crystal Silica Sand.

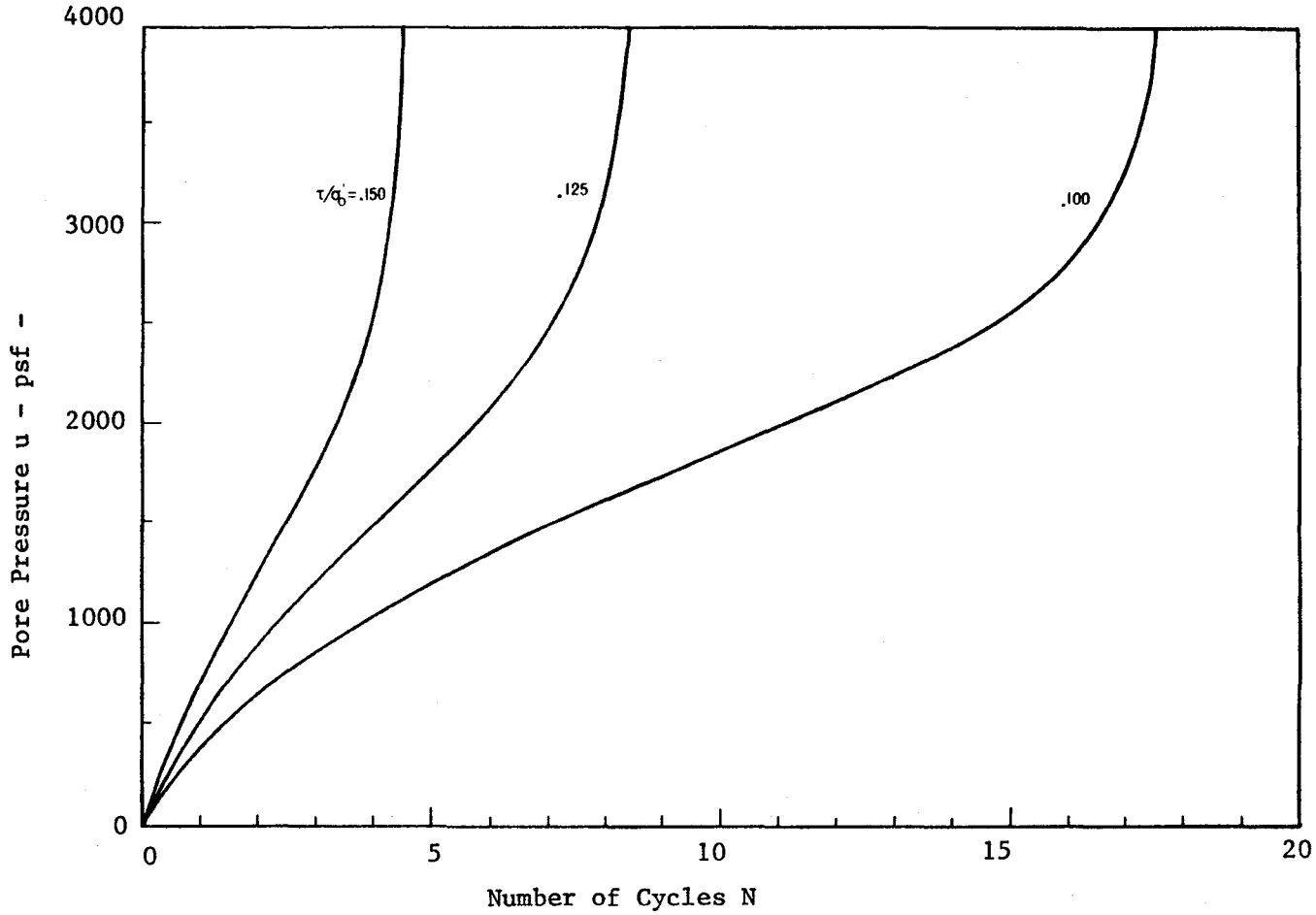

Figure 3.6 Computed Development of Pore Pressure for Stress Ratios of .15, .125 and .10

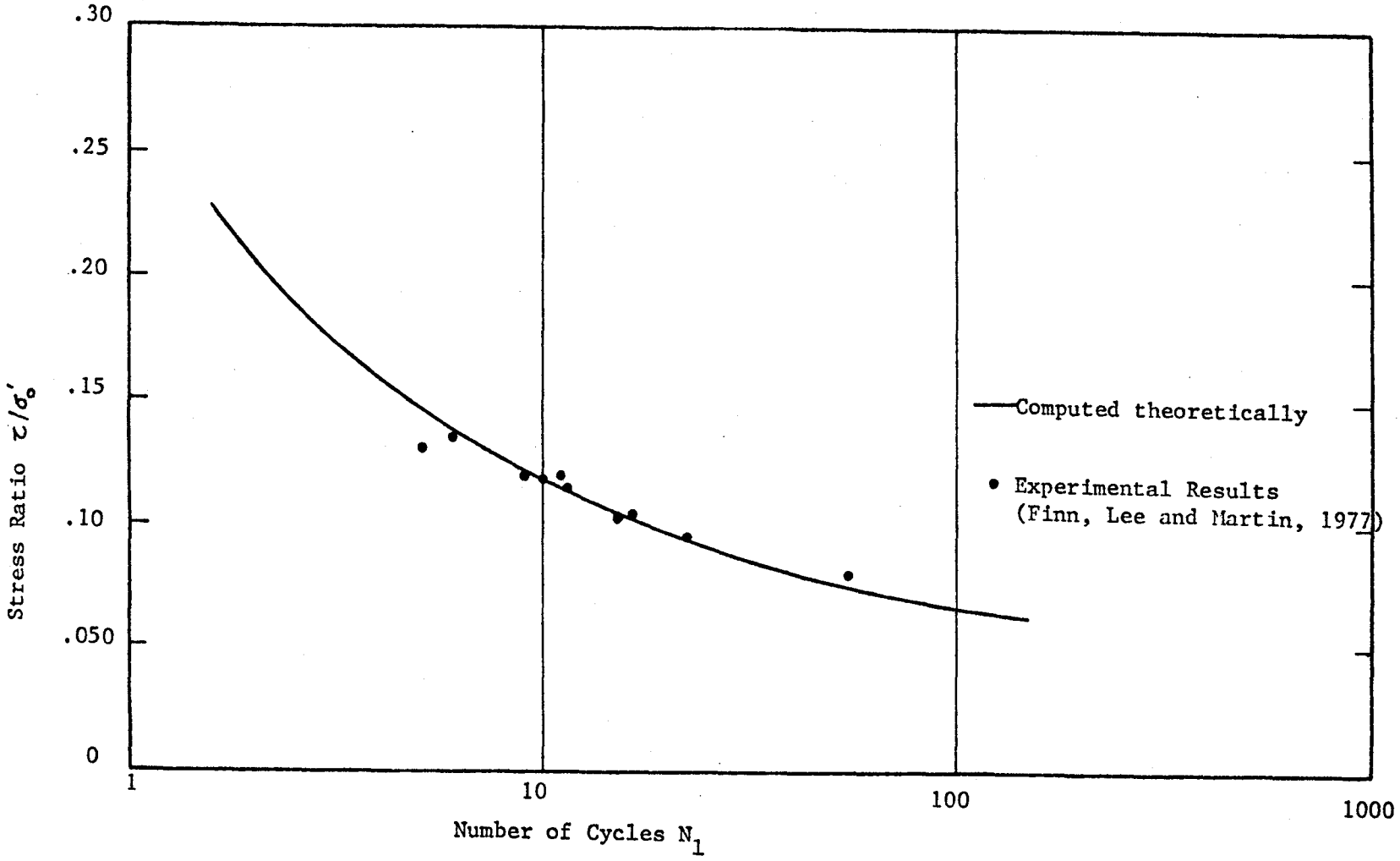

Figure 3.7 Cyclic Strength Curve - Crystal Silica Sand (D_r = 45%)

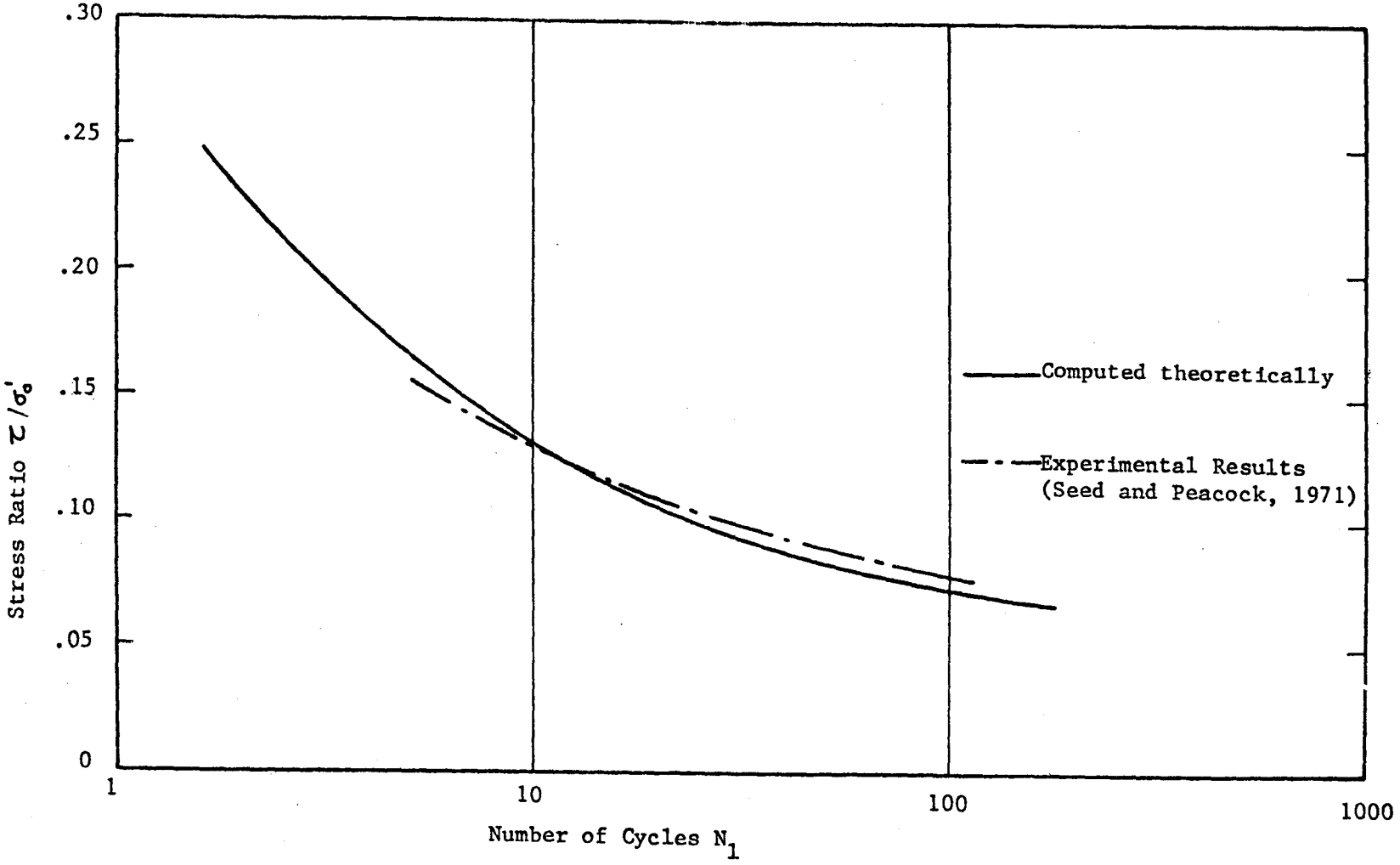

Figure 3.8 Cyclic Strength Curve - Crystal Silica Sand (D_r = 50%)

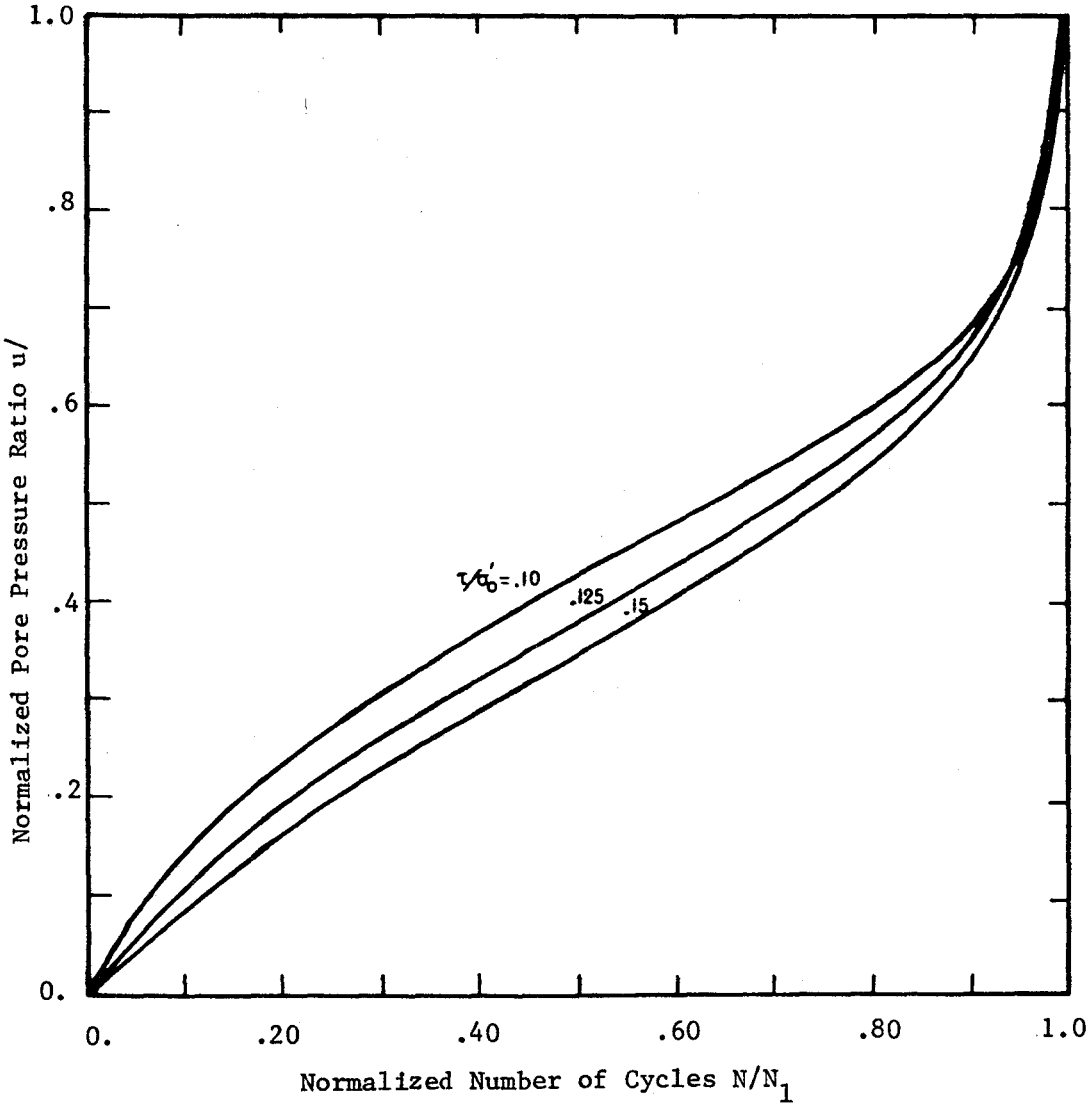

Figure 3.9 Computed Pore Pressure Generation Curves

The increase in pore pressure is dictated by two opposite effects:

- The reduction in rebound modulus as the effective stress decreases, and

- The augmentation of volumetric strain as the shear strain increases.

During the first cycles of the test the rebound modulus is high and consequently the first increments of pore pressure are large. Later the decrease in rebound modulus becomes more important than the augmentation of volumetric strain and the increments of pore pressure are smaller and tend to become constant. This is expressed by the linear portion of the normalized curves. In the last cycles prior to complete liquefaction the increase in shear strain effect is preponderant and the last pore pressure increments are very important. This is demonstrated in a plot of the slope of the normalized pore pressure curve, $du/\sigma'_0 dN$, in which du is the increment of pore pressure at cycle N, versus the normalized number of cycles N/N_l (figure 3.10). Figure 3.10 shows that the slopes are almost constant for N/N_l ranging from 0.2 to 0.8, while they are larger elsewhere.

(b) Non-uniform loading

The pore pressure generation model will now be used to compute the increase in pore pressure during non uniform simple shear loading and to compare it to the prediction given by the linear accumulation of damage

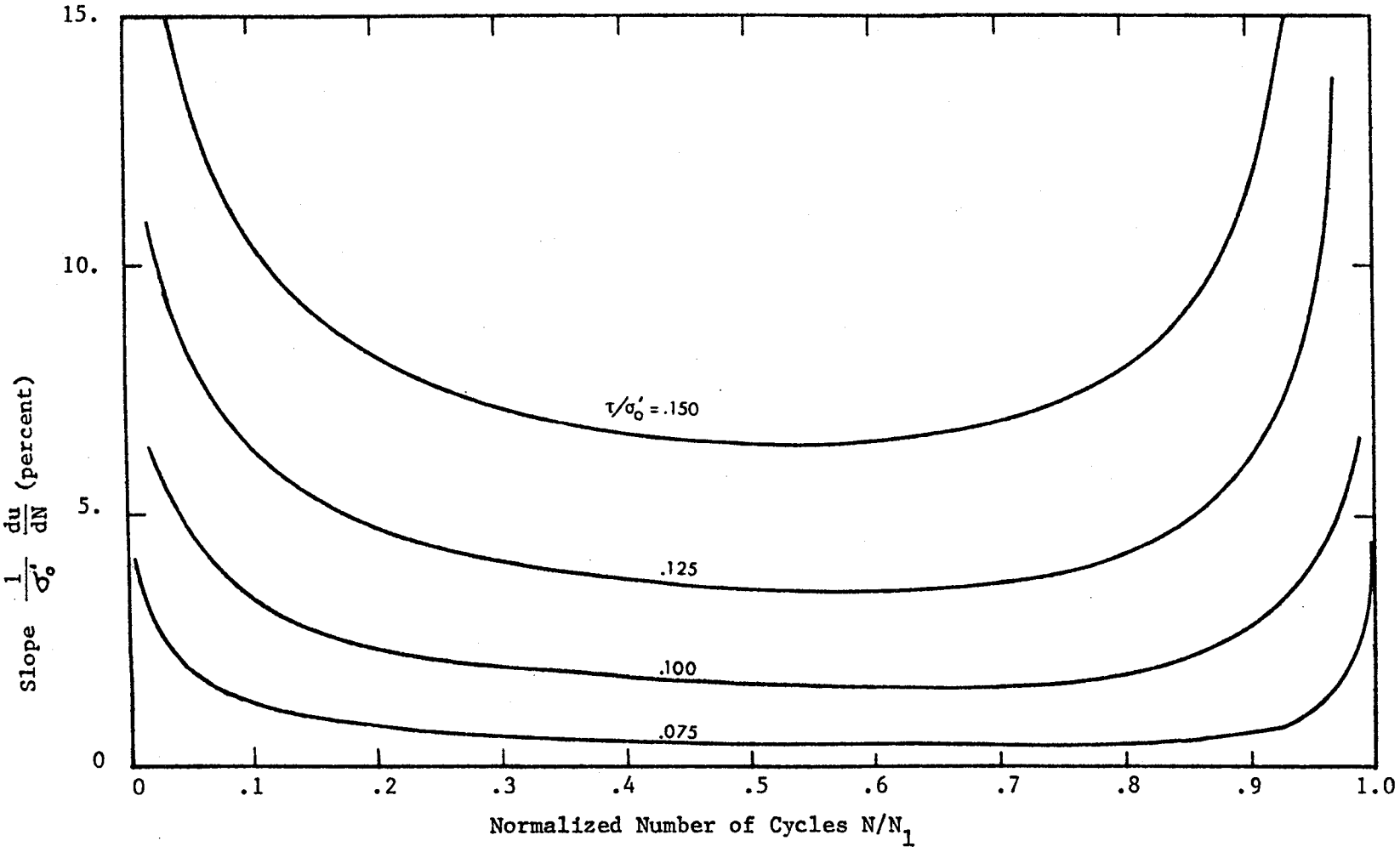

Figure 3.10 Incremental Increase in Pore Pressure

rule. The crystal silica sand at a relative density of 45 percent was analytically subjected to six different sequences of shear stresses. These sequences were made of the same 12 individual cycles, 1 cycle at 600 psf, 4 cycles at 500 psf, 3 cycles at 400 psf and 4 cycles at 300 psf, but the cycles were ordered differently.

Each one of the six sequences is described in table 3.2. If the rule of linear accumulation of pore pressure is applied, the order in which the cycles occur is neglected and the final expected pore pressure ratio is computed from the cyclic strength curve in figure 3.7 and equation 3.2. This computation is detailed in table 3.3 and it yields an accumulated pore pressure ratio of 0.97, which means that any non uniform sequence made from these 12 cycles should come close to the zero effective stress state, but not reach it. The pore pressure development curves which were in fact obtained for the six sequences are plotted in figures 3.11 and 3.12. These results disagree with the linear accumulation of pore pressure rule:

- Three sequences led to the zero effective stress state. Two of those did so in less than 12 cycles, 11 and 10 cycles respectively for sequences 2 and 3.
- The zero effective stress ratio was not reached during sequences 1, 5 and 6. They led to final pore pressure ratios of 0.71, 0.86 and 0.77 respectively, which are much lower than 0.97 predicted by the linear accumulation rule.

Sequence	1	2	3	4	5	6
Cycle 1	300	300	300	300	300	300
" 2	400	400	300	400	300	400
" 3	500	500	300	500	400	600
" 4	600	600	400	6000	600	500
" 5	500	500	400	500	500	400
" 6	500	400	500	400	400	500
" 7	500	300	500	300	500	300
" 8	400	400	500	400	500	400
" 9	400	500	600	500	300	300
" 10	300	400	500	500	500	500
" 11	300	500	400	400	4000	500
" 12	300	300	300	300	300	300
Final Pore Pressure Ratio	.71	1.0 (cycle 12)	1.0 (cycle 10)	1.0 (cycle 11)	.86	.77

Table 3.2 Description of the Non-Uniform Shear Stress Loading Sequences (values are in psf)

Stress Level**	Number of Cycles N	N_1*	N/N_1
.075	4	54	.08
.100	3	17.5	.17
.125	4	8	.50
.150	1	4.5	.22
Accumulated Pore Pressure $=\sum N/N_1$			.97

Table 3.3 Accumulation of Pore Pressure Using the Palgrem-Miner rule

* The N_1 values are the number of cycles to zero effective stress state obtained from figure 3.7

** σ_0' is equal to 4000 psf

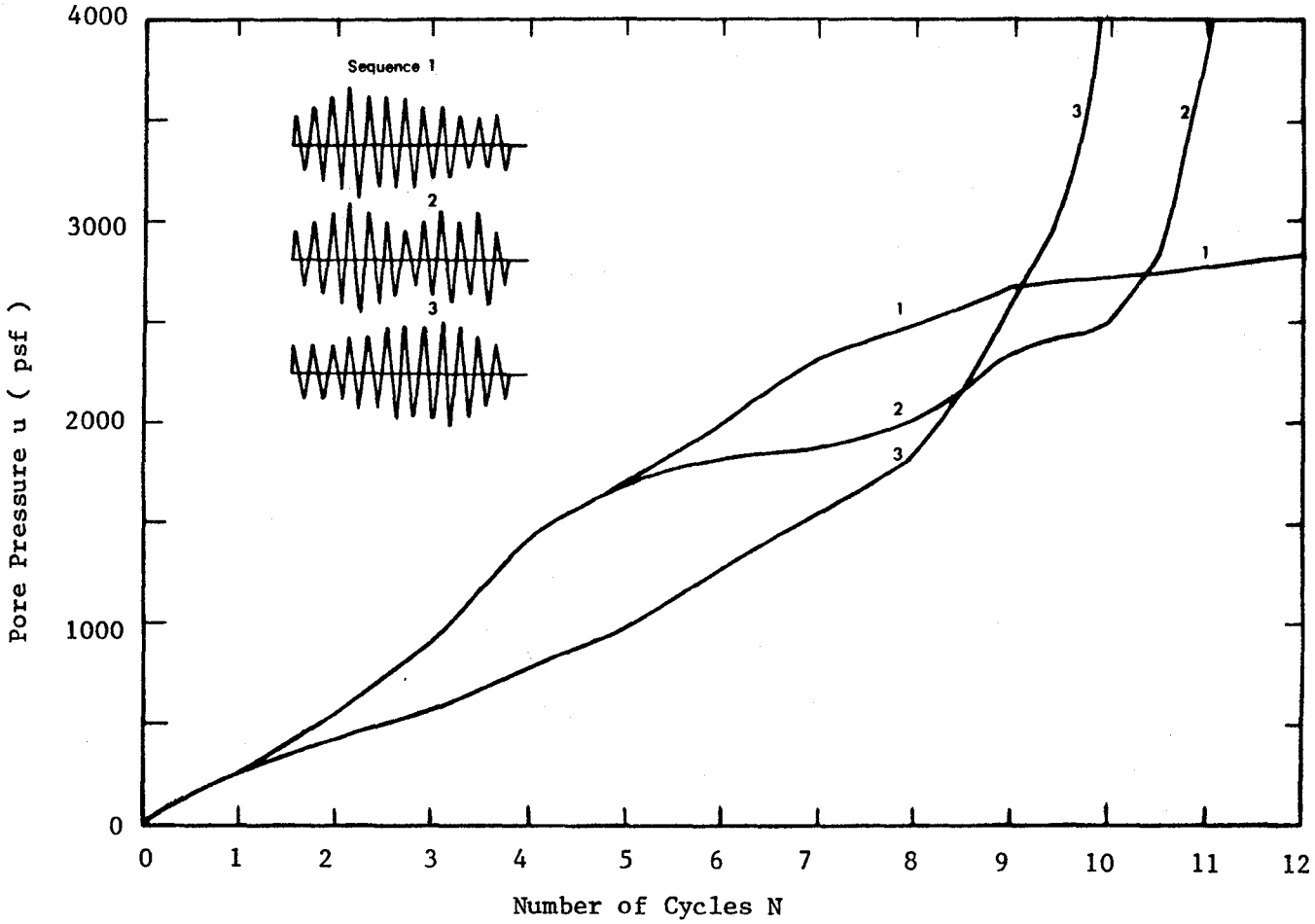

Figure 3.11 Development of Pore Pressure - Non-uniform Sequences 1, 2 and 3

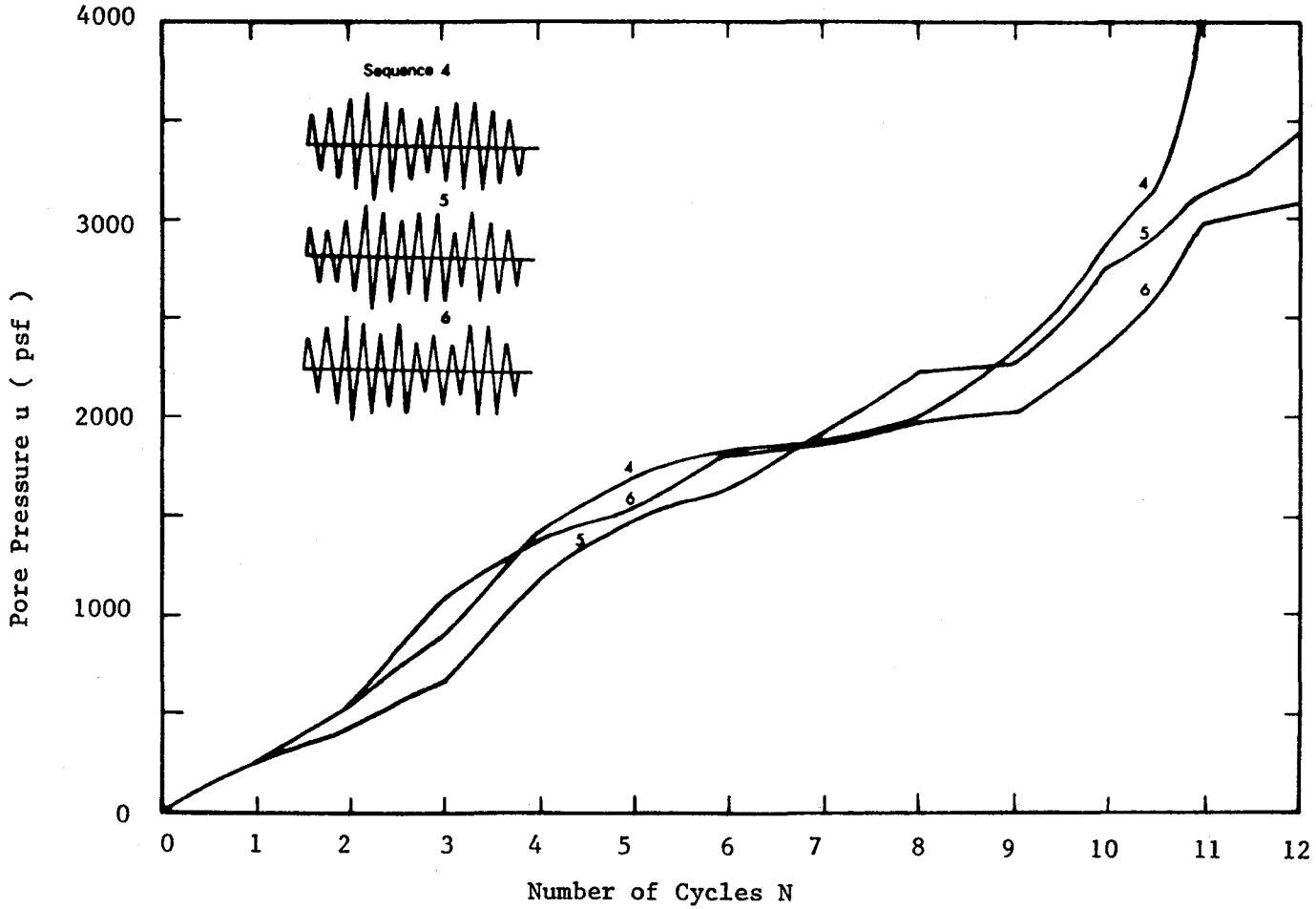

Figure 3.12 Development of Pore Pressure - Non-uniform Sequences 4, 5 and 6

These results indicate that the accumulation of pore pressure is a function of the order in which the stress cycles are applied. A series of small to moderate cycles can loosen the material enough so that the largest peaks will have a disastrous effect (example of sequence 3). Small to moderate cycles following a large peak will have different effects, depending upon the order in which they occur. For instance, sequence 1 leads to a moderate pore pressure ratio while sequences 2 and 4 lead to zero effective stress state. Sequences which occur in "clumps" of low-high-low cycles, such as 2 and 4, appear more damaging than sequences in which cycles are applied in a more erratic order, such as sequences 5 and 6. To further demonstrate that the damaging effect of a stress cycle is function not only of its intensity but also of the accumulated pore pressure, two sequences were studied for which "the pore pressure path" could be easily followed. The sequence 7 is made of the 12 preceeding cycles ranged by increasing size while sequence 8 is the opposite sequence, with the cycles decreasing in intensity. The pore pressure time histories were computed for both sequences and the results are plotted in figure 3.13. Sequence 7 leads to the zero effective stress state, a pore pressure ratio of 1., during the last cycle while at the end of the opposite sequence the pore pressure ratio is only 0.62. Figure 3.14 describes in detail the evolution of the pore pressure paths during these two sequences. In this figure the normalized pore pressure ratio u/σ_0 is plotted versus the number of cycles N, on a logarithmic scale, for uniform loading and stress ratios equal to 0.15, 0.125, 0.10 and .075, corresponding to the four shear stress amplitudes. These curves are directly deduced from the results previously given in

figure 3.6. Using figure 3.14 the time history of pore pressure can be easily followed for sequences 7 and 8. During sequence 7, the first 4 cycles at a stress ratio τ/σ'_0 of 0.075 lead to a pore pressure ratio u/σ'_0 of 0.175. From this pore pressure ratio the 3 cycles at τ/σ'_0 of 0.10 lead to a pore pressure ratio of 0.31. Then the 4 cycles at τ/σ'_0 of 0.125 accumulate pore pressure up to u/σ'_0 equal to 0.62 and finally the last cycle at τ/σ'_0 of 0.15 leads to the zero effective stress state. In the same manner the evolution of pore pressure during sequence 8 is described in figure 3.14, which shows why the final pore pressure ratio is only about 0.62. In sequence 7 the smaller cycles loosen the material enough so that the larger cycles are detrimental, while in sequence 8 the larger cycles lead the pore pressure ratio to about 50% which happens to be in the range of values for which the development of pore pressure is relatively slow for stress ratios of 0.100 and 0.075 (figure 3.6), and as a consequence the final accumulated pore pressure ratio is less than 1..

The comparison of these 8 sequences of non uniform shear stress cycles has shown that:

- A pore pressure ratio of 100% can occur during a loading sequence for which the ratio computed by the linear accumulation rule is less than 1.

- The opposite effect can also occur: the final pore pressure ratio can be much lower than the value predicted by the linear accumulation of pore pressure concept.

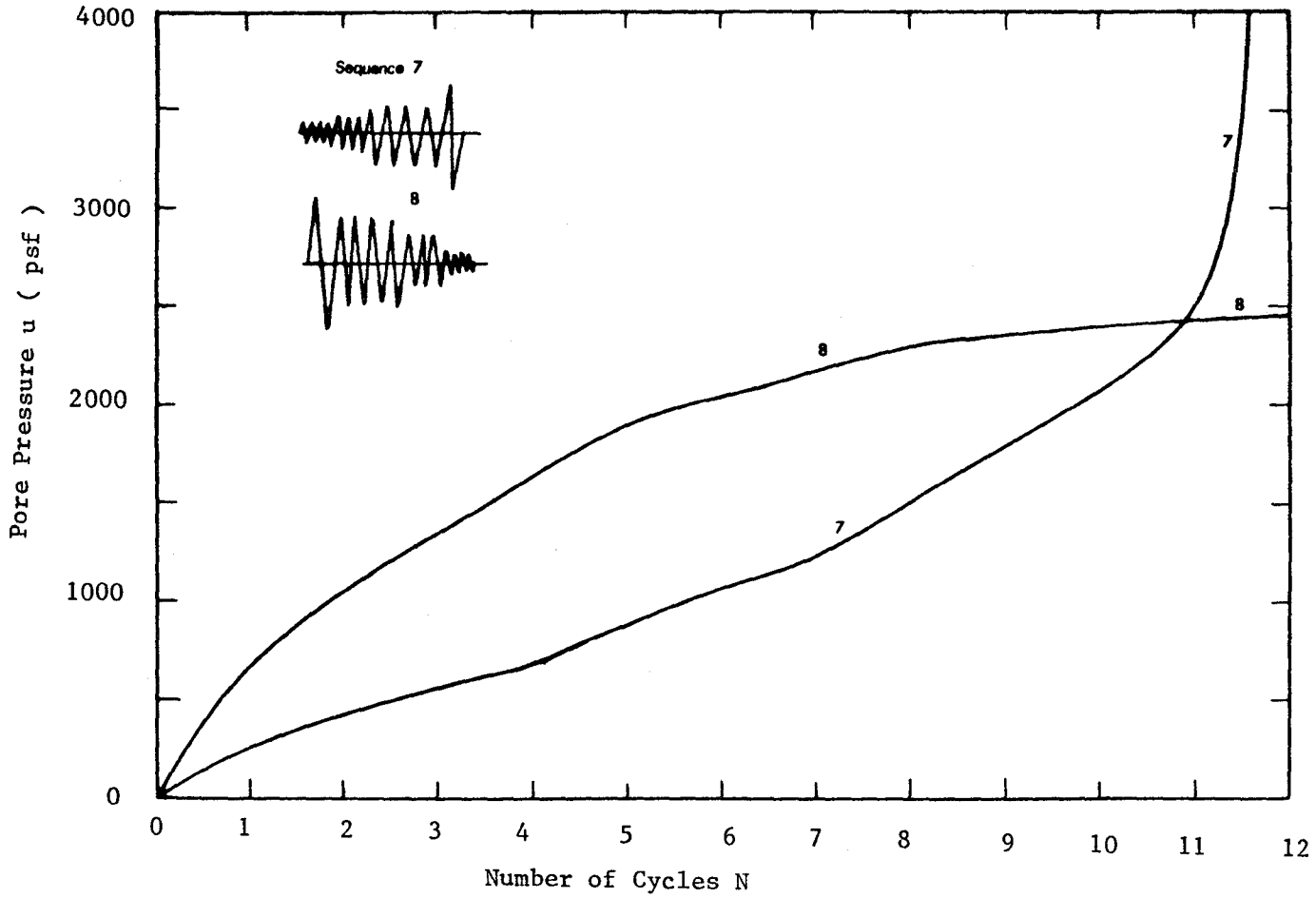

Figure 3.13 Development of Pore Pressure - Non-uniform Sequences 7 and 8

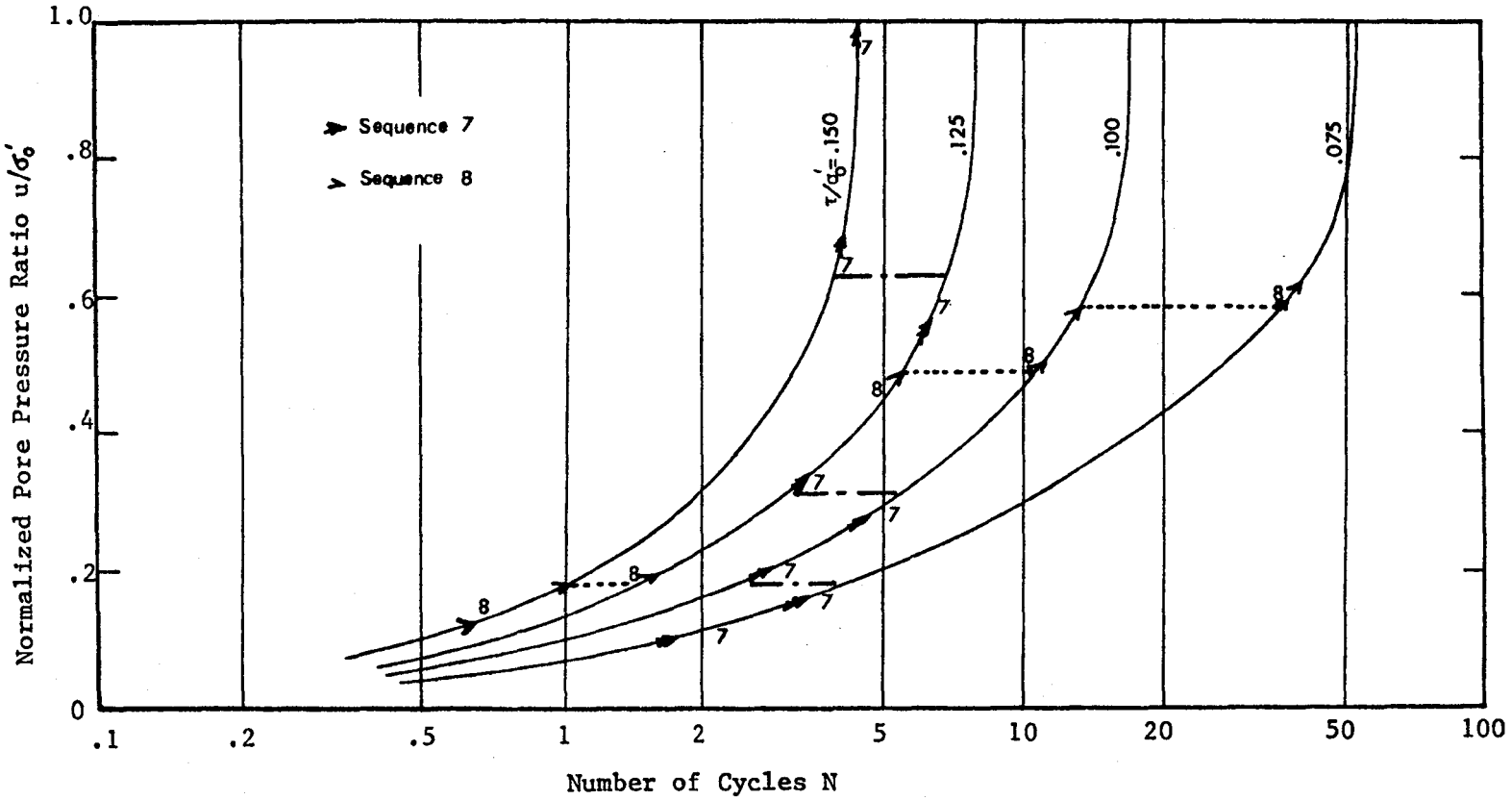

Figure 3.14 Pore Pressure Paths for Sequences 7 and 8

- The effect of a cycle is a function of both its intensity and location in the sequence. It depends on the level of pore pressure previously accumulated. In Appendix C it is demonstrated how this can be taken into account by deriving a "non-linear number of equivalent uniform cycles".

3.6 SUMMARY

The Palmgren-Miner rule of linear accumulation of damage under non-uniform loading has been extensively applied to the study of pore pressure build-up and liquefaction in cohesionless soils. The concept of the equivalent number of uniform cycles of a stress time history can be derived from this rule.

The accumulation of pore pressure in cyclic simple shear and trixial tests does not follow the Palmgren-Miner rule. This is expressed by a plot of the normalized pore pressure ratio u/σ'_0, versus the normalized number of cycles N/N_1 which shows the normalized pore pressure curve to be a non-linear function of the applied stress ratio.

The pore pressure model proposed by Finn, Lee and Martin (1977) can be used to study the increase in pore pressure during uniform and non-uniform loading. For both cases it was demonstrated that the accumulation of pore pressure is non-linear. In the case of non-uniform loading it has been shown that a zero effective stress state can occur during a sequence corresponding to a linear damage less than 1. and that less damage can also occur than predicted by the Palmgren-Miner rule.

The increase of pore pressure during a stress cycle depends on the stress intensity and on the pore pressure accumulated during the previous stress cycles. This is valid for uniform and non-uniform loading and is summarized by:

$$\Delta u_N = f(\tau, u)_{N-1} \qquad \text{(3.5 repeated)}$$

in which Δu_N is the increase in pore pressure at cycle N, τ the shear stress applied at cycle N, and u_{N-1} the pore pressure accumulated at the end of the (N-1)th cycle.

Chapter IV

PROBABILISTIC DEVELOPMENT OF PORE PRESSURE USING EXPERIMENTAL DATA

4.1 INTRODUCTION

The previous chapter presented and discussed in detail the non-linear development of pore pressure in sands during cyclic loading. The analytical studies described in this chapter represent an attempt to develop a probabilistic method to study this non-linear development of pore pressure under random loading. Specifically, the probabilistic model is intended to incorporate and combine the following characteristics of the problem:

- The non-linear development of pore pressure under uniform and non uniform loading. Allowance will be made for the fact that the evolution of the "pore pressure path" is function of both the relative intensities of the stress cycles and their relative positions in the time history.

- The uncertainties in assessing the pore pressure buid-up in a sand from laboratory tests. The uncertainties come from inherent problems in the testing procedures, such as inability of the test equipment to perfectly reproduce the field stress conditions, and difficulty in correctly modeling in-situ parameters, such as relative density, small amount of cementation, etc.

- The uncertainties in shear stress time histories which occur in a soil deposit during an earthquake. The reasons for these uncertainties are varied. They include differences in type of source mechanism, travel path, rate of attenuation, choices for the source strength parameter and the ground-motion parameter, and site characteristics. Stability predictions based upon a unique time history analysis may strongly depend upon the particular time history used in the analysis. Results of general validity require an ensemble of time histories or, better, a probabilistic description of the shear stress time history which globally includes the above uncertainties.

In this chapter, the mathematical formulation of the probabilistic model will be derived and several simplifications of this model will be discussed. The next chapter will describe the application of the model to practical examples.

4.2 BASIC ASSUMPTIONS AND NOTATIONS

4.2.1 Assumptions and input parameters

The pore pressure development characteristics of sand are assumed to be obtainable from laboratory experiments. They are composed of (1) a cyclic strength curve which expresses the number of cycles to zero effective stress N_1 as a function of the applied shear stress ratio τ/σ'_0 (figure 4.1.a), and (2) a set of pore pressure generation curves

which relate the normalized pore pressure ratio u/σ'_0 to the normalized number of cycles N/N_l (figure 4.1.b). These pore pressure generation curves have been described in detail in the preceeding chapter, and it is assumed that there is one curve available for each stress ratio τ/σ'_0 of interest. These data can be best obtained from cyclic simple shear testing, or derived from cyclic triaxial test results. Uncertainties in soil characteristics are taken into account. For a given stress ratio, the number of cycles to zero effective stress is not a unique deterministic value, but is defined by a probability density function around its mean or median value. The nature of these uncertainties are discussed in the next chapter, together with the specific form of the associated probability density function.

The shear stress loading function is assumed not to be a unique time history, but a probability density function, which for each cycle of loading defines the probability that the shear stress amplitude will be greater than or equal to a given value. Common representations of shear stress probability density functions are given in figure 4.1.c.

4.2.2 Notation

In order to simplify the mathematical expressions, the following notation is adopted in this chapter:

(a) The pore pressure ratio u/σ'_0 is called R.

(b) The shear stress ratio τ/σ'_0 is called S.

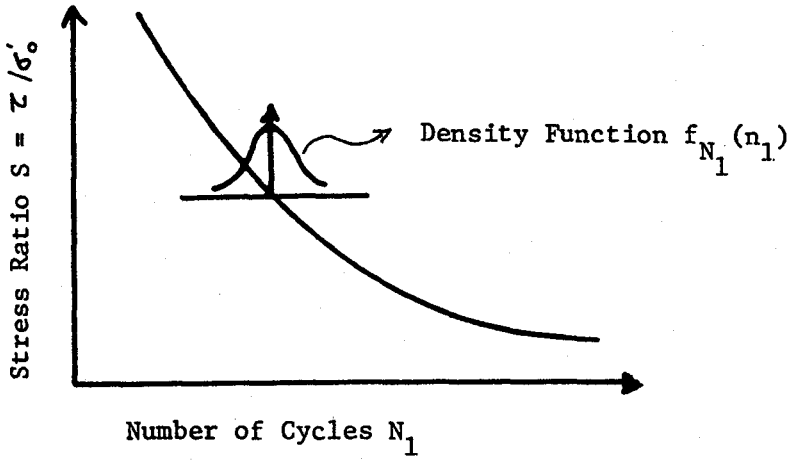

Figure 4.1.a Cyclic Strength Curve

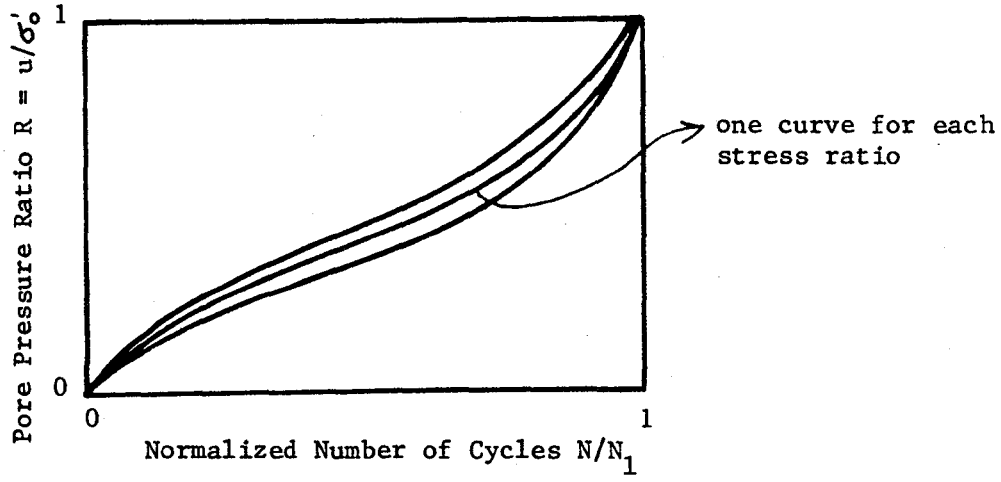

Figure 4.1.b Pore Pressure Generation Curves

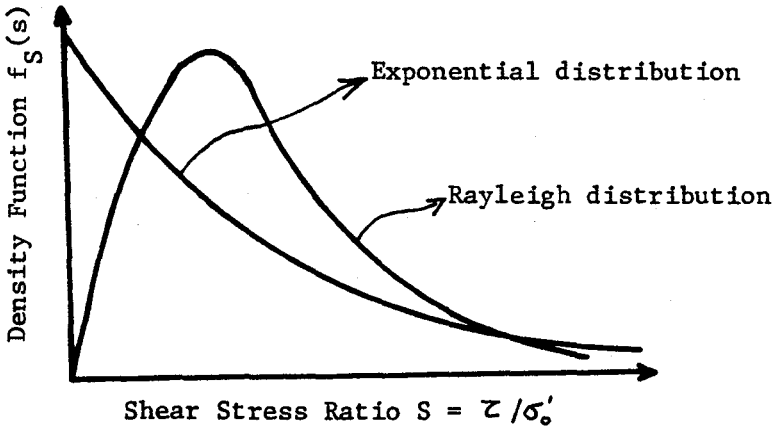

Figure 4.1.c Typical Shear Stress Density Functions

Figure 4.1 Parameters for the Probabilistic Model

(c) The probability density function of the number of cycles to zero effective stress state N_1 is noted $f_{N_1}(n_1)$. In general, this distribution is also function of the shear stress ratio S.

(d) The probability density function of the stress ratio is noted $f_S(s)$. This function can be easily derived from the knowledge of the probability density function of the shear stress. This is shown in the next chapter in which the shear stress is assumed to be Rayleigh or exponentially distributed.

(e) In this analysis the term "cycle" means the interval between two zero-crossings of the shear stress. During each cycle, or interval between zero-crossings, the shear stress amplitude is described by the density function $f_S(s)$.

(f) There is a functional relationship between the pore pressure ratio R, the stress ratio S, and the normalized number of cycles N/N_1, as shown in figure 4.1.b. For mathematical convenience this relationship is expressed as:

$$N/N_1 = f_n(R,S) \qquad (4.1)$$

The index n indicates that all the parameters of the relation are normalized.

(g) P(A) is the probability that the event A occurs.

(h) $P(A/B)$ is the probability that the event A occurs given that event B has occurred.

(i) $f_X(x)$ and $F_X(x)$ are the notations for the probability density function and cumulative distribution function of a random variable X.

The next section will show that, given the probability density functions $f_S(s)$ and $f_{Ne}(n_1)$ and the functional relationship $f_n(R,S)$, a probabilistic model which computes the cumulative distribution of pore pressure can be derived. In chapter 6 the specific forms of the functions f_S, f_R and f_n will be discussed and typical results will be obtained with the probabilistic model.

4.3 GENERAL FORMULATION

In this section the cumulative distribution function of the pore pressure ratio R at the end of the ith cycle of loading is derived. It is shown to be function of the cumulative distribution of pore pressure at the end of the (i-1)th cycle. In order to do so, the first step of the derivation is to obtain this distribution function at the end of the first cycle of loading.

(a) first cycle of loading

To determine the cumulative distribution function of R, first consider the conditional distribution function of R given that the

stress ratio S equals some particular value s; This function equals the probability that the normalized increment $1/N_1$ is less or equal than $f_n(r,s)$. Mathematically this can be written:

$$F_{R|S}(r,s) = P[R \leq r | S=s]$$

$$= P[1/N_1 \leq f_n(r,s)] \qquad (4.2)$$

$$= P[N_1 \geq 1/f_n(r,s)]$$

The right-hand term in equation 4.2 is the probability that N_1 is greater than $1/f_n(r,s)$ at a stress ratio s. It is obtained from the probability density function of N_1, $f_{N_1}(n_1)$:

$$P[N_1 \geq 1/f_n(r,s)] = \int_{1/f_n(r,s)}^{\infty} f(u)du \qquad (4.3)$$

$$= 1 - F_{N_1}[1/f_n(r,s)]$$

where $F_{Nc}(n_1)$ is the cumulative distribution function of the number of cycles to zero effective stress N_1, schematically represented in figure 4.2.

Equations 4.2 and 4.3 lead to:

$$F_{R|S}(r,s) = 1 - F_{N_1}[1/f_n(r,s)] \qquad (4.4)$$

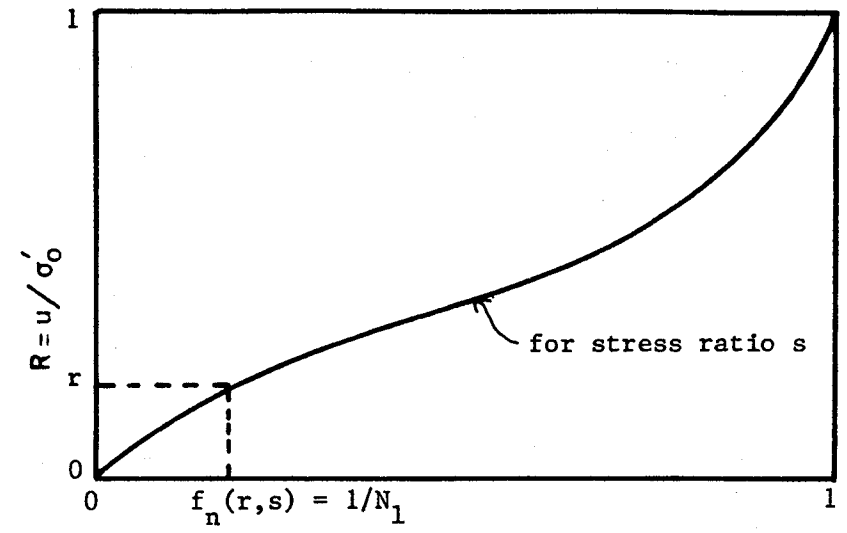

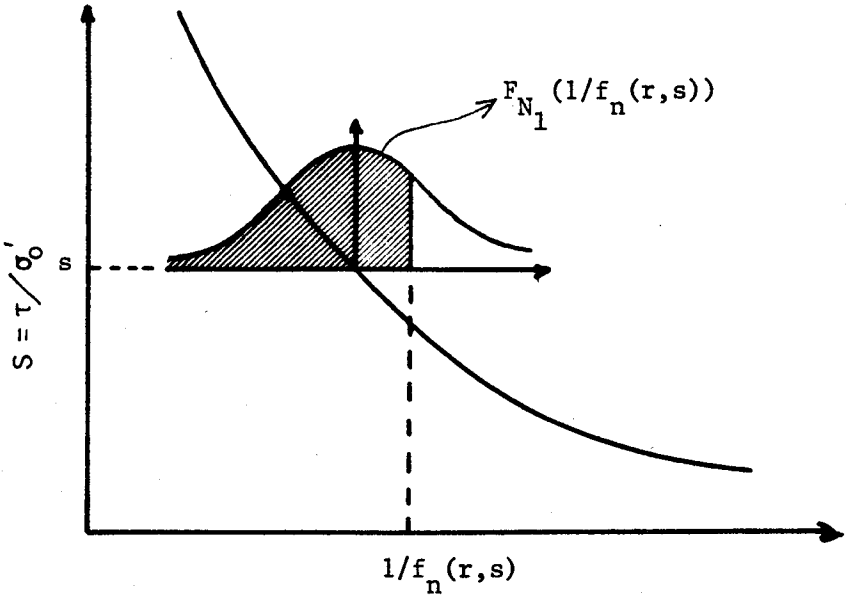

Figure 4.2 Probabilistic Model - First Cycle of Loading

The marginal cumulative distribution of R follows upon integration over all values of s:

$$F_R(r) = \int_0^{\infty} F_{R|S}(r,s) f_S(s) ds \tag{4.5}$$

$$= \int_0^{\infty} \{1 - F_{N_1}[1/f_n(r,s)]\} f_S(s) ds$$

The double integration expressed by equation 4.5 completely describes the cumulative probability distribution function of the pore pressure ratio R for any value r of this ratio between 0 and 1. The probability of exceedance of any pore pressure ratio between 0 and 1 is directly deduced as:

$$P(R \geq r) = 1 - F_R(r) \tag{4.6}$$

The probability density function of R can be obtained by differentiation:

$$f_R(r) = dF_R(r)/dr \tag{4.7}$$

In general the integration 4.5 and the differentiation 4.7 cannot be solved in close form. They have to be performed numerically by computer.

(b) ith cycle of loading

The cumulative distribution $F_R(r)$ and the density function $f_R(r)$ of the pore pressure ratio at the end of the (i-1)th cycle will be used to derive the same functions at the end of cycle i. Similar to the first cycle study, the first step of the derivation is to consider the conditional distribution of R. The complexity is increased because this distribution depends not only on the shear stress ratio R but also on the accumulated pore pressure ratio at the end of cycle (i-1). If this accumulated ratio and the stress ratio have the particular values ξ and s, respectively, then the pore pressure ratio R will be less than r at the end of cycle i if, and only if, the increase in pore pressure is less than $\Delta r = r - \xi$. Δr can be related to the normalized increment $1/N_1$ as (figure 4.3):

$$\frac{1}{N_1} = f_n(r,s) - f_n(\xi,s) \qquad (4.8)$$

For convenience call this difference $\Delta f_n(r,\xi,s)$. With this notation, the conditional distribution function of R, given that the stress ratio S equals some particular value s and given that the accumulated pore pressure ratio at the end of cycle (i-1) equals some particular value ξ, is:

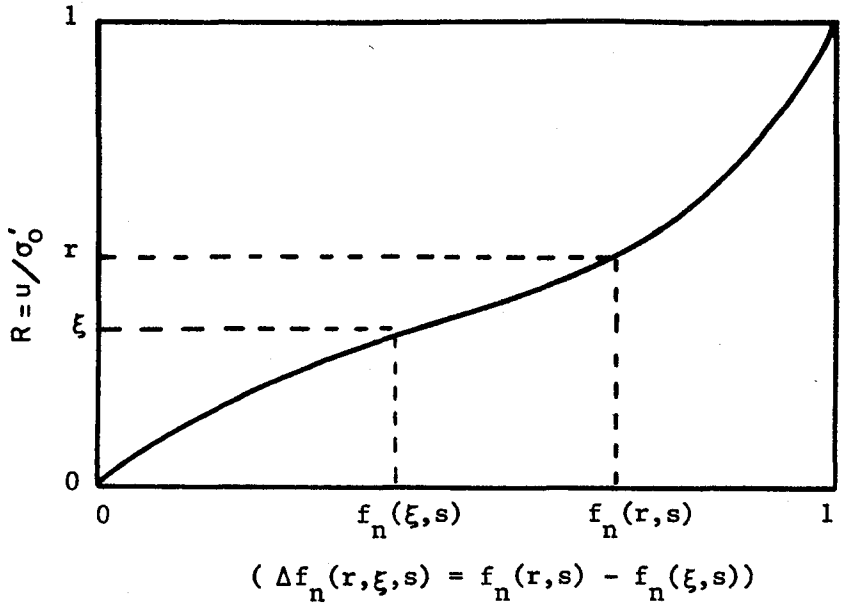

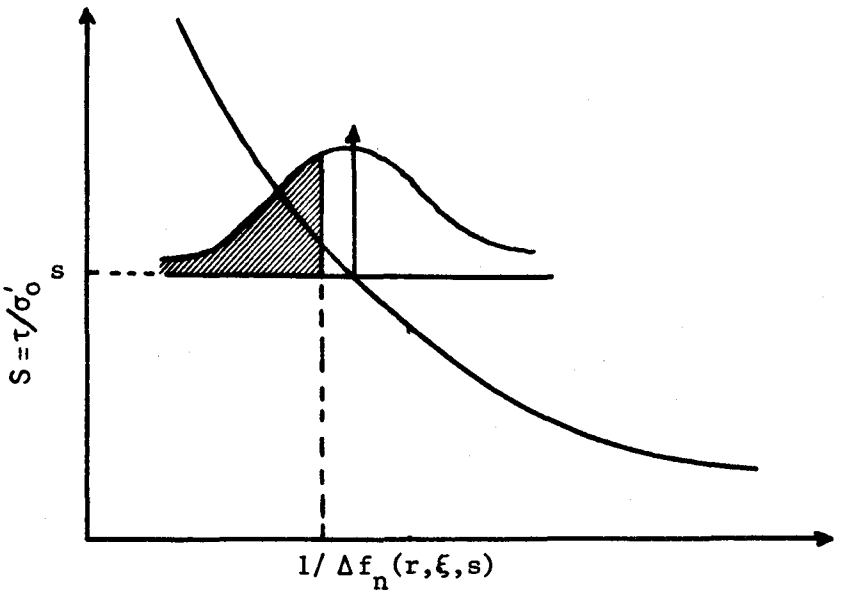

Figure 4.3 Probabilistic Model - i^{th} Cycle of Loading

$$F_{R|\xi|S}(r,\xi,s) = P\left[\frac{1}{N_1} \leq \Delta f_n(r,\xi,s)\right]$$

$$= P\left[N_1 \geq \frac{1}{\Delta f_n(r,\xi,s)}\right]$$

$$= \int_{1/\Delta f_n(r,\xi,s)}^{\infty} f_{N_1}(u)du \tag{4.9}$$

$$= 1-F_{N_1}[1/\Delta f_n(r,\xi,s)]$$

By integrating over all possible values of s, the cumulative distribution of R given that the accumulated pore pressure ratio at the end of cycle (i-1) equals some particular value ξ is :

$$F_{R|\xi}(r,\xi) = \int_0^{\infty} \{1-F_{N_1}[1/\Delta f_n(r,\xi,s)]\}f_S(s)ds \tag{4.10}$$

By the defintion of ξ, its probability density function is the density function of the ratio R at the end of cycle (i-1), and as a consequence the distribution of R follows by integration:

$$F_R^i(r) = \int_0^r F_{R|\xi}(r,\xi)f_R^{i-1}(\xi)d\xi \tag{4.11}$$

where the upper scripts i and i-1 stand for cycle i and cycle i-1.Finally, from 4.10 and 4.11:

$$F^{i}_{R}(r) = \int_0^r \int_0^{\infty} \{1-F_{N_1}[1/\Delta f_n(r,\xi,s)]\} f_S(s) f^{i-1}_{R}(\xi) ds d\xi \qquad (4.12)$$

This expression is a triple integral because the term in $F_{N_1}[\bullet]$ is already an integral which in general is a function of s. If the ratio R is already greater or equal to r at the end of cycle (i-1), the probability that it will be less than r at the end of cycle i is zero, and as a consequence the first integration has upper limit r.

The probability density function of R at the end of cycle i is formally:

$$f^{i}_{R}(r) = dF^{i}_{R}(r)/dr \qquad (4.13)$$

Equations 4.5, 4.7, 4.12 and 4.13 completely describe the "probabilistic evolution" of the pore pressure ratio R. At the end of any cycle i, the probability of exceedance of any pore pressure ratio r between 0 and 1 can be computed:

$$P(R \geq r \text{ at end of cycle } i) = 1 - F^{i}_{R}(r) \qquad (4.14)$$

The probability that R is greater than r is also the probability that the excess pore pressure u is greater than r times σ'_0.

4.4 POSSIBLE SIMPLIFICATIONS

The general expressions derived previously in this chapter include both uncertainties in soil parameters and in the shear stress loading. They also assume that there is one pore pressure generation curve (figure 4.1) for each value of stress ratio S. Two simplifications of the model will be described which will reduce the generality as follows: (1) a unique pore pressure generation curve will be used, and (2) the cyclic strength curve will be considered deterministic, without uncertainty. These simplifications will not be used in the following chapters but they are noteworhty because, even in a simpler form, the proposed probabilistic method has advantages over previous studies: (1) It includes uncertainty in the loading; (2) It incorporates the non-linear development of pore pressure; and, (3) It provides a complete description of pore pressure from zero up to the zero effective stress state.

(a) Unique pore pressure generation curve

Laboratory data are usually available for a few selected stress ratios, and in between those stress ratios, the pore pressure generation curves have to be interpolated. Furthermore, for sand at low densities and in the useful range of stress ratios, the pore pressure generation curves are close to each other (figures 3.3 to 3.5). Hence for most

cases, it would be sufficient to use a limited number of pore pressure generation curves, each of which is assigned a range of shear stress ratios, or to use a unique curve which represent the mean curve of the experimental curves. If a unique curve is used, the function $f_n(r,s)$ is a unique function of r, $f_n(r)$, and equations 4.5 and 4.12 become:

$$F_R(r) = \int_0^{\infty} \{1 - F_{N_1}[1/f_n(r)]\} f_S(s)\,ds \qquad (4.15)$$

and

$$F_r^i(r) = \int_0^{r} \int_0^{\infty} \{1 - F_{N_1}[1/\delta f_n(r,\xi)]\} f_S(s) f_R^{i-1}(\xi)\,ds\,d\xi \qquad (4.16)$$

This simplification greatly reduces the computations, because the term [•] is not a function of the stress ratio anymore. If several pore pressure generation curves are used, equations 4.15 and 4.16 are still valid over a given range of stress ratios.

(b) Deterministic cyclic strength curve

This simplification of the model is introduced for three reasons: (1) it corresponds to an early model proposed by the author to introduce the notion of probabilistic development of pore pressure, (2) it simplifies the mathematical formulation so that one can follow the different steps involved in the computations, (3) it can be used to

compare the deterministic analysis to the analysis in which uncertainty is included.

If there is a unique cyclic strength curve, there is a unique value $S_n = \tau_n/\sigma'_0$ which corresponds to the normalized cycle increment $1/f_n(r)$, (figure 4.4), and as a consequence:

$$P\left[N_1 \geq \frac{1}{f_n(r)} \right] = 1 \qquad \text{if } S < S_n$$

$$= 0. \qquad \text{if } S > S_n \tag{4.17}$$

It follows that for the first cycle:

$$F_R(r) = \int_0^{S_n} f_s(s)ds \tag{4.18}$$

The same remark applies to the following cycles. There is a unique value S_n corresponding to the increment $\Delta f_n(r)$, resulting in:

$$P\left[N_1 \geq \frac{1}{\Delta f_n(r)} \right] = 1.0 \quad \text{if } S < S_{\Delta n}$$

$$= 0.0 \quad \text{if } S > S_{\Delta n} \tag{4.19}$$

and equation 4.12 becomes:

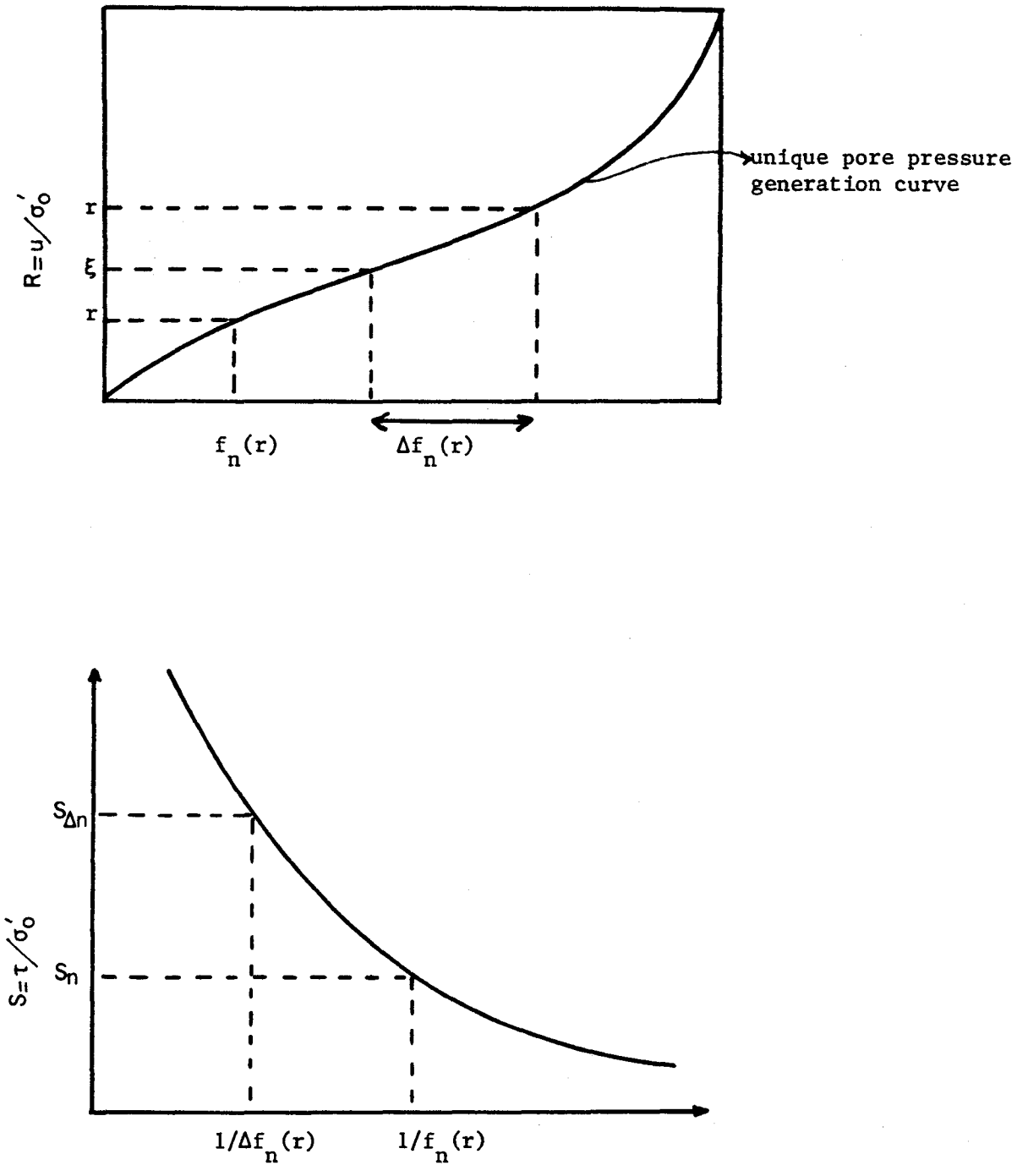

Figure 4.4 Simplified Formulation of the Probabilistic Model

$$F_R^i(r) = \int_0^r \int_0^{S_n} f(s) f^{i-1}(\xi) ds d\xi \qquad (4.20)$$

The steps of the computations described by the preceeding equations are basically the same as in the general method, but their mathematical formulation is more convenient and they can be followed graphically in figure 4.4.

4.5 SUMMARY

A probabilistic model has been proposed to study the development of pore pressure in sands under random loading. It takes into account the non-linear behavior of the "pore pressure path" and incorporates uncertainties in the soil and loading characteristics.

The pore pressure is probabilistically defined by its cumulative distribution function at the end of any cycle of loading. There is sort of a "Markovian" dependence between cycles: the distribution function of the pore pressure at the end of cycle i is deduced from the knowledge of the probability density function of the pore pressure at the end of cycle (i-1).

Two simplified versions of the model have been described. The first one hypothesizes a unique pore pressure curve. The second one considers a unique pore pressure generation curve and a deterministic cyclic strength curve.

Practical applications of the general formulation of the probabilistic model are presented in the next chapter.

Chapter V

APPLICATION OF THE PROBABILISTIC PORE PRESSURE MODEL

5.1 INTRODUCTION

In chapter 4, the development of pore pressure in saturated sands under random loading was probabilistically defined. A probability density function describes the loading shear stress by characterizing the amplitude of each cycle of loading. The cyclic strength curve and pore pressure generation curves used in the analysis can be obtained from laboratory experiments. Uncertainty is included in the cyclic strength curve by considering a probability density function around the mean or the median curve . The model computes the cumulative distribution function of pore pressure at the end of any cycle of loading.

This chapter describes the specific mathematical expressions of the probability density functions and of the laboratory data. It also presents several examples of application which use the results of laboratory experiments discussed in chapter 3. None of the particular assumptions made by the author in this chapter are critical to the model. The derivation performed in chapter 4 is independent of the form of the input functions and parameters. Should any other assumption for these parameters appear more realistic, it could be substituted in the computer formulation of the model.

5.2 EARTHQUAKE MOTION

In seismic resistant design it is important to know the characteristics of the cyclic load reversal of an earthquake ground motion. This is most important in the problem of pore pressure build-up due to the non-linearity of the phenomenon (see chapter 3). Random process models and statistical procedures can be used to estimate the number of peaks and their probability density functions. The Rayleigh and Exponential distributions of load cycles are used in this chapter.

5.2.1 Rayleigh distribution

Earthquake ground motions are representative of the output from a random process, and their description as a stationary process of finite duration is generally considered a fair approximation for the strong motion part of the time history (Vanmarcke, 1976).

Consider the earthquake motion to be a narrow band stationary function having a normal probability density function:

$$f_x(x) = \frac{1}{\sqrt{2\pi}\ \sigma_t} \exp\left(-\frac{x^2}{2\sigma_t^2}\right) \qquad (5.1)$$

where $f_x(x)$ is the density function of the acceleration at time t, and σ_t the standard deviation of the acceleration time history. The statistical distribution of the maxima of x(t) is the distribution of the envelope of the sequential peak values and is given by:

$$f_A(a) = \frac{a}{\sigma_t} \exp\left[-\frac{a^2}{2\sigma_t^2}\right] \qquad 0 \leq a \leq \infty \tag{5.2}$$

where $f_A(a)$ is the probability density function of the peak value of the acceleration time history during any cycle of loading. The mathematical steps involved between equations 5.1 and 5.2 are not specific to earthquake motion and are described in any standard textbook on random vibrations (Lin, 1967, or Newland, 1975).The description of the earthquake motion by a Rayleigh distribution (equation 5.2) requires the knowledge of the standard deviation σ_t, which for the present case of a process with zero mean is equal to the root mean square of acceleration, r_t. A value called the sigma ratio is used to relate the peak ground acceleration PGA, which is the most common parameter to define ground motion, to the root mean square, r_t:

$$\text{sigma ratio} = PGA/r_t \tag{5.3}$$

This ratio has been used recently by other investigators (Lysmer and al., 1975, Donovan and Singh, 1976, Valera and Donovan, 1976, and, Romo-Organista and al., 1979). Values of the sigma ratio for earthquake records range between 3 and 6. For large earthquakes it lies close to the lower part of this range.

Equation 5.2 and a value of the sigma ratio completely define the acceleration density function. Given the surface acceleration x(t), the shear stress time history at a depth H can be closely represented by:

$$\tau(t) = r_d \gamma H x(t) \tag{5.4}$$

where γ is the total unit weight of the soil, r_d the coefficient which accounts for the flexibility of the soil mass (Seed and Idriss, 1971), and g the acceleration of gravity. The root mean square of the shear stress time history r , is :

$$r = r_d \gamma H r_t \tag{5.5}$$

Equations 5.1 and 5.4 imply that the shear stress is a stationary function with a normal probability density function. As a consequence, the probability density function of the amplitude of the shear stress cycle is :

$$f(\tau) = (\tau/r) \exp(-\tau^2/2r^2) \qquad 0 \leq \tau \leq \infty \tag{5.6}$$

The density function of the normalized shear stress S ($=\tau/\sigma'_0$) used in chapter 4 can be related to f (τ) as follows:

$$P(S \leq s) = P(\tau \leq s\sigma'_0)$$

$$= \int_0^{s\sigma'_0} f(\tau)d\tau \tag{5.7}$$

$$= 1 - \exp(-s^2\sigma'^2_0/2r^2)$$

and

$$f_S(s) = \frac{dP(S \leq s)}{ds}$$

$$= \frac{s}{r^2_s} \exp\left(-\frac{s^2}{2r^2_s}\right) \qquad (5.8)$$

This demonstrates that S is Rayleigh-distributed with a root mean square r_s equal to $r\sqrt{\sigma'_0}$.

5.2.2 Exponential distribution

An alternative to the stationary random process theory described previously is to use statistical procedures to estimate the distribution of load cycles from available strong-motion time histories. Various probability functions, such as Beta, Gamma and exponential distributions, can be used to fit the distribution of the amplitudes of acceleration peaks in strong-motion records. The exponential distribution is the simplest one and fits the data reasonably well (Mortgat, 1979). The probability density function for exponential shape is given by :

$$f_A(a) = \lambda \exp(-\lambda a) \qquad (5.9)$$

where $f_A(a)$ is the density function of the amplitude of one cycle of loading and λ is the parameter of the exponential distribution. The root mean square of the distribution is given by:

$$r_a = \left\{ \int_0^{\infty} a^2 f(a) da \right\}^{1/2} \qquad (5.10)$$

$$= \sqrt{2}/\lambda$$

For a given earthquake record the parameter λ is found by making the root mean square of the distribution equal to the root mean square of the peaks r_p:

$$\lambda = \sqrt{2}/r_p \qquad \text{with } r_p = \frac{\sqrt{\sum a_i^2}}{\sqrt{n-1}} \qquad (5.11)$$

where a_i is the individual peak acceleration amplitude and n the total number of peaks.

The ability of equations 5.10 and 5.11 to represent the distribution of peaks in an accelerogram was hypothesized by Mortgat and Shah (1978) and further tested by Zsutty and De Herrera (1979), who proposed a statistical procedure for detecting exponential behavior among peaks and identifying the parameter λ. Typical results are given in table 5.1 for earthquakes of Richter magnitude 5.5 to 7.2. The description of the amplitudes of the load cycles by an exponential distribution presents two advantages. First, it is related to the root mean square of the acceleration which is a relatively stable parameter. Second, it leads to a direct application in seismic hazard analysis by using attenuation laws on the root mean square (Mortgat, 1979).

Location and Year	Magnitude	Site	$1/\lambda$ *	N	PGA *
El Centro, 1940	6.4	Soil	52.8	274	342
Ferndale, 1951	5.8	Soil	21.2	100	110
Taft, 1952	7.2	Soil	26.8	320	176
St. Barbara, 1952	7.2	Soil	17.9	150	129
Hollister, 1961	5.6	Soil	27.5	94	176
El Centro, 1934	6.5	Soil	36.6	196	179
Ferndale, 1938	5.5	Soil	21.0	96	141
Olympia, 1949	7.1	Soil	42.4	286	275
Olympia, 1965	6.5	Soil	30.8	272	194
Parkfield, 1966	5.5	Rock	68.8	70	426
Pacoima, 1971	6.4	Rock	212.0	98	1148
First St., 1971	6.4	Soil	25.8	114	123
Figueroa, 1971	6.4	Soil	27.5	82	147

Table 5.1 Typical $1/\lambda$ Values and Number of Peaks N for Exponential Distribution (after Zsutty and De Herrera, 1979 and 1980)

* $1/\lambda$ and PGA are in cm/sec^2

As is the case with the Rayleigh distribution, it can be shown that if the peaks are exponentially distributed the normalized shear stress $S = \tau/\sigma'_0$ is also exponentially distributed :

$$f_S(s) = \lambda_s \exp(-\lambda_s s) \tag{5.12}$$

with

$$\lambda_s = \sqrt{2}\sigma'_0 / r_d \gamma H r_p \tag{5.13}$$

The term $r_d \gamma H r_p$ in equation 5.13 is the root mean square of the shear stress peak amplitude at a depth H.

Table 5.2 summarizes the characteristics of the Rayleigh and exponential distributions necessary to their application in the probabilistic pore pressure model.

5.3 CYCLIC STRENGTH CURVE

The use of a cyclic strength curve in the probabilistic model necessitates the following : (1) An analytical expression must be fitted to the experimental data; (2) A probability density function around the mean or median cyclic strength curve has to be selected; and, (3) A level of uncertainty has to be assigned to the cyclic strength curve. This section discusses these three developments successively.

	Rayleigh Distribution	Exponential Distribution
Probability Density Function	$f_S(s) = (s/r_s^2).\exp(-s^2/2r_s^2)$	$f_S(s) = \lambda_s.\exp(-\lambda_s s)$
Cumulative Distribution Function	$P(S \leqslant s) = 1.-\exp(-s^2/r_s^2)$	$P(S \leqslant s) = 1.-\exp(-\lambda_s s)$
Parameter of Distribution	$r_s = r_d \gamma H r_t / \sigma_o'$	$\lambda_s = 2\sigma_o'/r_d \gamma H r_p$

Notation :

- s normalized stress
- σ_o' initial effective stress
- γ total unit weight
- H depth
- r_d flexibility coefficient
- r_t root mean square of acceleration time-history
- r_p root mean square of peaks

Table 5.2 Rayleigh and Exponential Distribution for the Normalized Shear Stress

5.3.1 Analytical expression

The shapes of the cyclic strength curves, such as in figures 3.7 and 3.8, suggest the use of a parabola to fit the data :

$$\log N_l = a_0 + a_1 \left(\frac{\tau}{\sigma'_0}\right) + a_2 \left(\frac{\tau}{\sigma'_0}\right)^2 \qquad (5.14)$$

where the constants a_0, a_1 and a_2 are obtained by the least square regression method. A least square parabola is generally biased by the data points in the center of the curve and fails to represent accurately the experimental data at low and high N values. As an alternative to the parabola, the author suggests a piecewise linear representation of the cyclic strength curve :

$$\log N_l = a_0 + a_1(\tau/\sigma'_0) \qquad \tau_{i-1} < \tau \leq \tau_i \qquad (5.15)$$

where the constants a_0 and a_1 can be obtained by regression analysis on the interval τ_{i-1}, τ_i. The interval can be made as small as necessary to correctly represent the experimental data.

5.3.2 Probability density function

Previous statistical studies by Donovan (1971) and Ferrito, Forrest and Wu (1979) suggest that the number of cycles to zero effective stress in cyclic triaxial tests follows a lognormal distribution ($\log N_l$ being normally distributed). Their data were taken from reliable research and commercial testing organizations and point out both the variability of

soils and soil testing procedures performed by competent geotechnical engineers. The results were fairly consistent for all densities and soil types present in the data base. While no such studies are available for simple shear test data , it is reasonable to assume that the number of cycles to zero effective stress in simple shear test also follows a lognormal distribution. This assumption is made in the following examples, but in order to give the maximum generality to the model, the computer program includes the normal and Beta distributions as possible alternatives.

5.3.3 Level of uncertainty

The level of uncertainty to be assigned to the cyclic strength curve can be defined by the standard deviation of the lognormal distribution, $\sigma_{ln\,Nc}$. There are many reasons for the uncertainties in the cyclic strength curves. First, it is difficult to correctly assess in-situ parameters such as relative density, coefficient of at rest earth pressure, amount of cementation etc. Second, the test equipment does not perfectly reproduce the field conditions and experimental techniques may distort the specimen, creating errors in the results. Finally, variations also come from second level parameter effects, such as soil fabric, fines content, sample history etc. In the present work values of $\sigma_{\varepsilon_n Nc}$ will be assigned based upon the studies by Donovan (1971) and Ferrito, Forrest and Wu (1979) and upon the author's subjective judgment. Values of the standard deviation $\sigma_{ln\,Nc}$ ranging between 0.2 and 1.0 can be expected for most soils and site conditions. The author believes that one of the major developments following the present

dissertation will be to perform statistical studies of simple shear test data in order to provide better guidelines for the estimation of σ_{en} Ne

5.4 PORE PRESSURE GENERATION CURVES

The probabilistic model derived in chapter 4 makes allowance for the non-linear development of pore pressure. In order to do so it necessitates a functional relationship between the pore pressure ratio R, the stress ratio S, and the normalized number of cycles N/N_1 (equation 4.1 in Chapter 4):

$$N/N_1 = f_n (R,S)$$

Seed, Martin and Lysmer (1975) proposed an expression of the form :

$$N/N_1 = [\tfrac{1}{2}(1- \cos\pi R)]^{\theta} \qquad (5.16)$$

where θ is a function of the soil properties and stress ratio S. The authors chose a unique curve with $\theta = 0.7$ as an average representation of different soil properties and test conditions. Comparison with actual data shows that this functional shape is not sufficient to obtain a correct fit. For example, in figure 5.1 shaking table test results for Monterey sand at a relative density of 54% and a stress ratio of 0.104 are compared to a set of curves with θ values of 0.7 to 0.4. These data were obtained by DeAlba and al. (1975) and have been presented in detail in chapters 2 and 3. None of these curves can represent correctly the

data and a least square regression value of θ=0.55 is a very poor fit. The functional relationship used by Seed, Martin and Lysmer recognizes the sine wave shape of the pore pressure generation curve for N/N_1 less than 0.3 and greater than 0.7, but is not versatile enough to represent the linear portion in the center of the curve and the large slopes for N/N_1 close to 1.0. In order to do so another functional shape is proposed :

$$R = \left[1 - \frac{2}{\pi}\arcsin\left(1-\frac{N}{N_1}\right)^{1/2\alpha}\right]^{\beta} \qquad (5.17)$$

where α and β are functions of the soil properties and stress ratios and are obtained by regression analysis. The data for a relative density of 54% and a stress ratio of 0.104 are almost perfectly represented by a curve with α=2.00 and β=1.05 (figure 5.2). Table 5.3 gives the results of the regression analysis performed on the shaking table test data for all densities and stress ratios. Typical α and β values range from 0.5 to 2.0 and 1.0 to 2.5, respectively. The parameters α and β are functions of both the relative density and the stress ratio.

For a given relative density, α decreases almost linearly with increasing stress ratios, while β increases hyperbolically . A high potential for pore pressure increase is characterized by a small value of α and a large value of β. This is the case of a sample of low relative density tested at a high stress ratio. Equation 5.16 can be inverted to obtain the functional relationship necessary to the model:

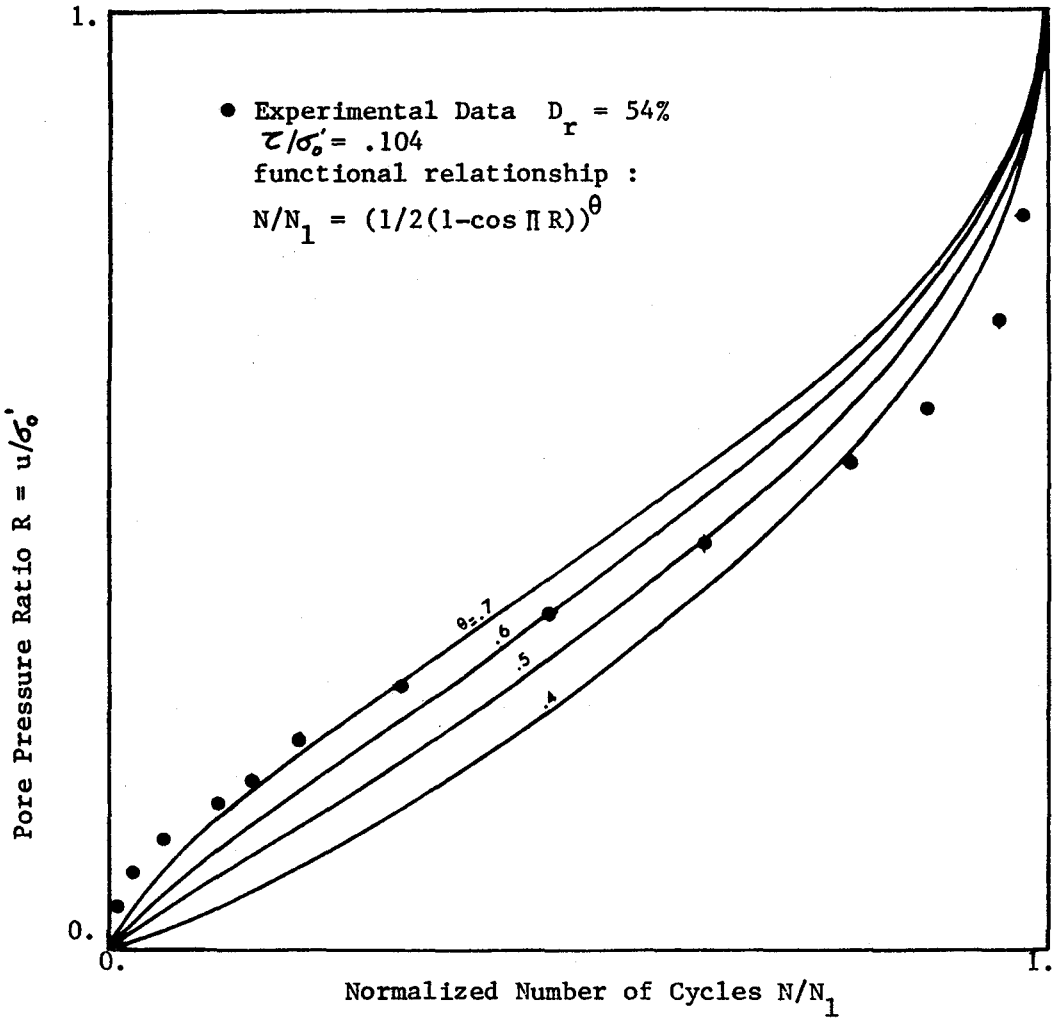

Figure 5.1 Comparison Between Experimental Data and Seed, Martin and Lysmer Relationship for the Pore Pressure Generation Curve

$$N/N_l = 1 - [\sin^{-1}(1-R^{1/\beta})]^{2\alpha} \qquad (5.18)$$

Equations 5.8, 5.12, 5.15 and 5.18 completely describe the mathematical expressions which are required in the probabilistic model derived in chapter 4.

5.5 APPLICATIONS OF THE PROBABILISTIC MODEL

This section describes two series of applications of the probabilistic pore pressure model. The first one considers an hypothetical level ground site and uses available data on Monterey sand and on the exponential distribution of shear stress. The second one demonstrates that, even based on limited data, the model can correctly predict the behavior of several sites during the Niigata earthquake of 1964. These applications show that while the mathematical formulation of the model is cumbersome, the results are fairly simple to analyze and suited to make comparisons between sites and loading conditions.

5.5.1 Hypothetical site

This site does not correspond to a specific location but could represent an actual site, where the soil is a saturated sand similar to Monterey sand and where loading conditions as high as those described in table 5.1 can be expected.

The site conditions and loading characteristics are described in table 5.4. The soil is assumed to consist of sand having the

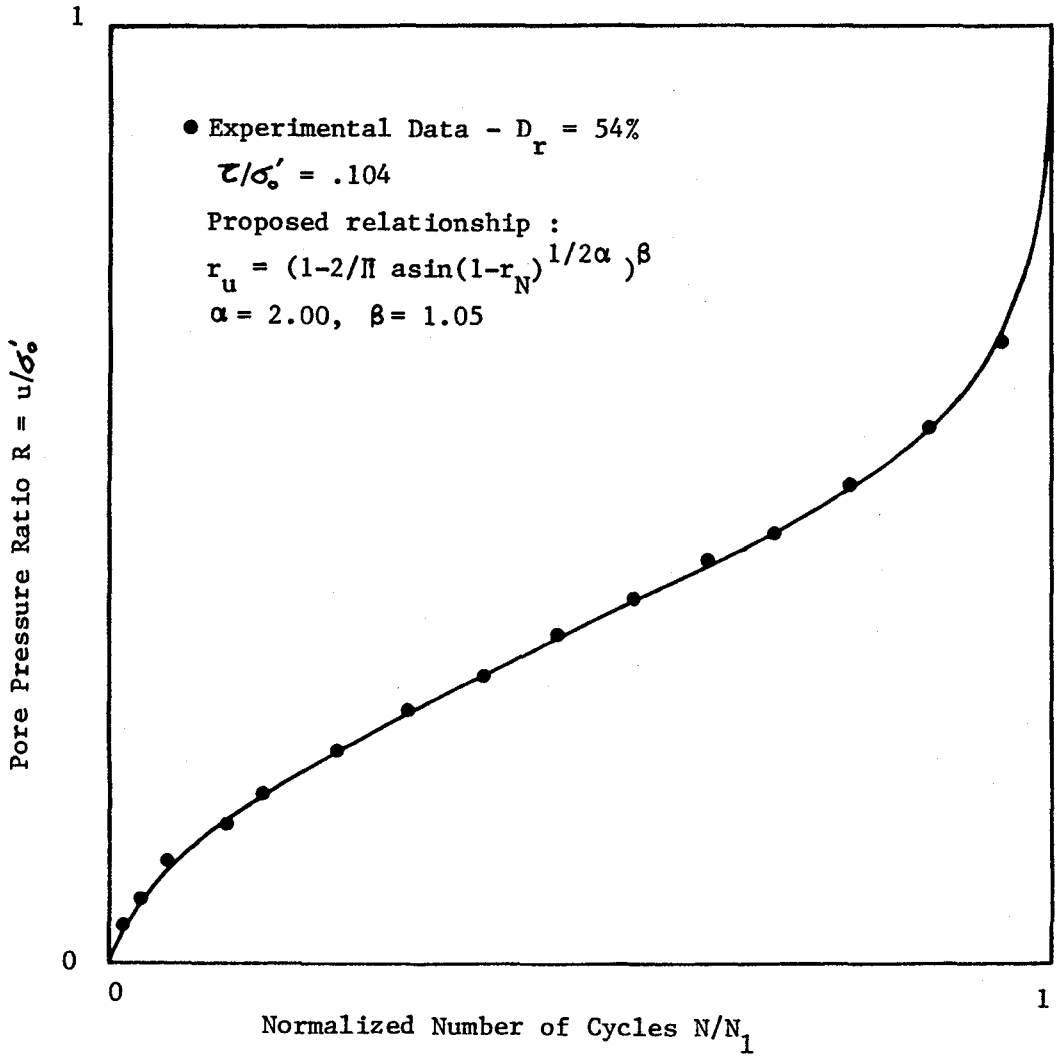

Figure 5.2 Proposed Relationship for the Pore Pressure Generation Curve

Relative Density (Percent)	Stress Ratio τ/σ_o'	α	β
90	.280	0.5	1.55
82	.219	0.7	1.35
82	.188	1.2	1.10
68	.230	0.7	1.90
68	.211	0.8	1.75
68	.171	1.2	1.70
68	.134	1.5	1.15
54	.185	0.7	2.40
54	.155	1.1	1.80
54	.144	1.4	1.35
54	.135	1.6	1.25
54	.104	2.0	1.05

$$R = \left[1. - 2 \arcsin(1-N/N_1)^{1/2\alpha}\right]^{\beta}$$

Table 5.3 α and β Values for Monterey Sand Obtained by Regression Analysis (proposed relationship)

characteristics of Monterey sand, with the water table at a depth of two feet. The pore presure development will be studied at a depth of 25 feet. Two cases are considered, case I with a relative density of 54 percent and case II with a relative density of 68 percent. For each case the two loading conditions are used, and thus the parameter λ takes on two different values.

(a) Case I

For the 54 percent relative density sand, the cyclic strength curve is obtained from shaking table tests as given in figure 2.2. The level of uncertainty in the cyclic strength curve is σ = 0.50. This value is in the medium range of uncertainty values observed by previous investigators (Donovan, 1971, and Ferrito, Forrest, and Wu, 1979). The parameters α and β of the pore pressure generarion curves are given in table 5.3. The parameter $1/\lambda$ of the acceleration density function is equal to 27 cm/sec^2 which corresponds to a root mean square of shear stress r of 110 psf. This value of $1/\lambda$ is close to the values reported in table 5.1 for each of the Taft, Hollister, First St, and Figueroa St earthquake records. Interestingly, these four records have different number of cycles table 5.1), thus making possible to assess the effect of duration on the potential for pore pressure build-up.

Using these data and equations 4.5 and 4.12 the development of pore pressure is probabilistically defined. At the end of any cycle of loading, the probability of exceeding a given level of excess pore pressure is determined using the computer code developed for this work.

Relative Density : 54 and 68 %

Total Unit Weight : 120 pcf

Depth to Water Table : 2 feet

Depth of Interest : 25 feet

Effective Stress : 1565 psf

Total Stress : 3000 psf

Parameter of Exponential Distribution $1/\lambda$: 27 and 53 cm/sec^2

Flexibility Coefficient r_d : .94

Root Mean Square of Shear Stress : 110 and 215 psf

Uncertainty in Cyclic Strength Curve :

σ_{LnN_1} = 0., 0.50, and 1.0

Table 5.4 Parameters for Hypothetical Site, Exponential Distribution of Shear Stress

The results are expressed in figure 5.3 where the probability of exceeding pore pressure ratios of 0.1 to 1.0 is plotted versus the number of cycles of motion. These data show :

- After 50 cycles of loading the probabilities of exceeding pore pressure ratios of 0.1, 0.5 and 1.0 are 0.98, 0.37 and 0.16, respectively.

- After 150 cycles of loading the probabilities of excceding the same pore pressure ratios are 1.0, 0.97 and 0.87, respectively.

Concentrating on the case of pore pressure ratio of 1.0 (liquefaction) and considering that the number of cycles for the Taft, Hollister, First St, and Figueroa St records are 320, 94, 114 and 82 respectively, it is apparent that : The probability of reaching R = 1.0 during an event having characteristics similar to the Taft record is 1.0, while the probability is 0.52, 0.67 and 0.42 for events similar to the three other records, respectively. This clearly illustrates that earthquakes having same PGA or same magnitude will not necessarily lead to the same hazard in terms of pore pressure build-up, and thus that PGA or magnitude are not sufficient to describe site liquefaction potential. When applied to the same soil and loading conditions, the Seed and Idriss simplified procedure predicts liquefaction in all four cases. A probabilistic method is advantageous over conventional methods in that it makes a distinction between a case where liquefaction is certain and cases where it is not 100 percent probable. These cases arise when the

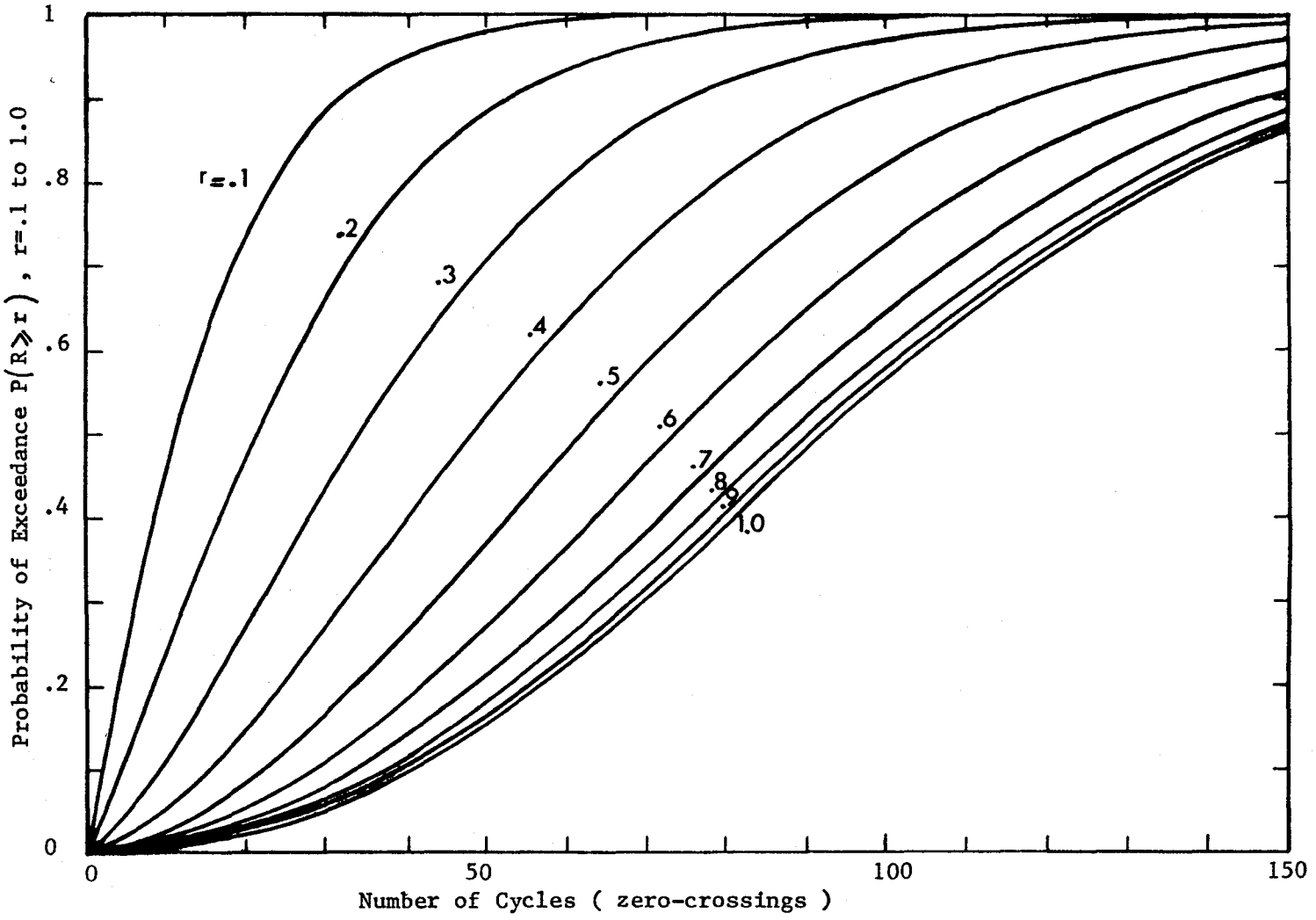

Figure 5.3 Probability Curves - Hypothetical Site - D_r = 54% - $1/\lambda$ = 27 cm/sec^2

resistance of the soil is close to the loading and in the above examples they lead to probabilities of occurrence of 42 to 67 percent.

Comparison of the results for conditions other than liquefaction are also interesting. For all the four earthquake records the probability of exceeding a pore pressure ratio of 0.2 or less is the same, approximatively 1.0. For ratios greater than 0.2 differences in the probabilities begin to develop, with similar findings to those described for R=1.0.

This example of case I demonstrates that the probabilistic model has two important advantages over conventional methods. First, it provides a complete description of pore pressure for any pore pressure ratio. Second, the probability curves reflect the effect of the earthquake duration, showing that for the same PGA, substantially different levels of pore pressure are likely to develop.

(b) Case II

The data for this case are kept the same except that the relative density of the sand is equal to 68 percent, not to 54 percent. The cyclic strength curve used is given in figure 2.2 and the pore pressure generation coefficients α and β in table 5.3. Figure 5.4 presents the computed probability curves for this case. The probabilities of exceedance have been reduced, relative to case I. For example the probability of exceeding R=1.0 and R=0.5 after 150 cycles of loading are 0.18 and 0.52, respectively, as compared to 0.87 and 0.97 in case I. Similarly the probability of exceeding R = 1.0 is less than 5 percent

for events similar to the Hollister, First St and Figueroa St records, as compared to 52, 67, and 42 percent in case I. The 5 percent probability shows that, even if liquefaction is not likely under those conditions, it is still possible for a site to liquefy ,at a probability level of 5 percent. By carrying out the computations up to 320 cycles, the probability of exceeding R = 1.0 for the Taft record is found to be 0.95, while the probability of exceeding R = 0.5 is 1.0. In case I these probabilities were both equal to 1.0. The duration of the Taft record is so long that the probability of liquefaction is close to 1.0 for both relative densities, 54 and 68 percent.

(c) Effect of the level of uncertainty

In order to assess the effect of the uncertainty in the cyclic strength curve, case I is repeated with two additional values of $\sigma_{\epsilon_n Nc}$: (1) $\sigma_{\epsilon_n Nc}$=0., corresponding to a deterministic cyclic strength curve. This assumes perfect agreement between laboratory and field behavior and perfect knowledge of the in-situ relative density; and, (2) $\sigma_{\epsilon_n Nc}$=1.0 which is in the upper values of uncertainty observed by Donovan (1971) and Ferrito and al. (1979). The results are given in figures 5.5 and 5.6 and, in order to facilitate the comparison, figure 5.7 reproduces the probabilistic curves at level R = 1.0 for the three values of the standard deviation $\sigma_{\epsilon_n Nc}$ 0.,0.5 and 1.0. The figure demonstrates the following : (1) If the duration of the loading in number of cycles is such that the probability of exceedance becomes close to 1.0, the effect of soil uncertainty is very limited. Nevertheless the higher the uncertainty is, the faster the probability tends to its limit 1.0; and,

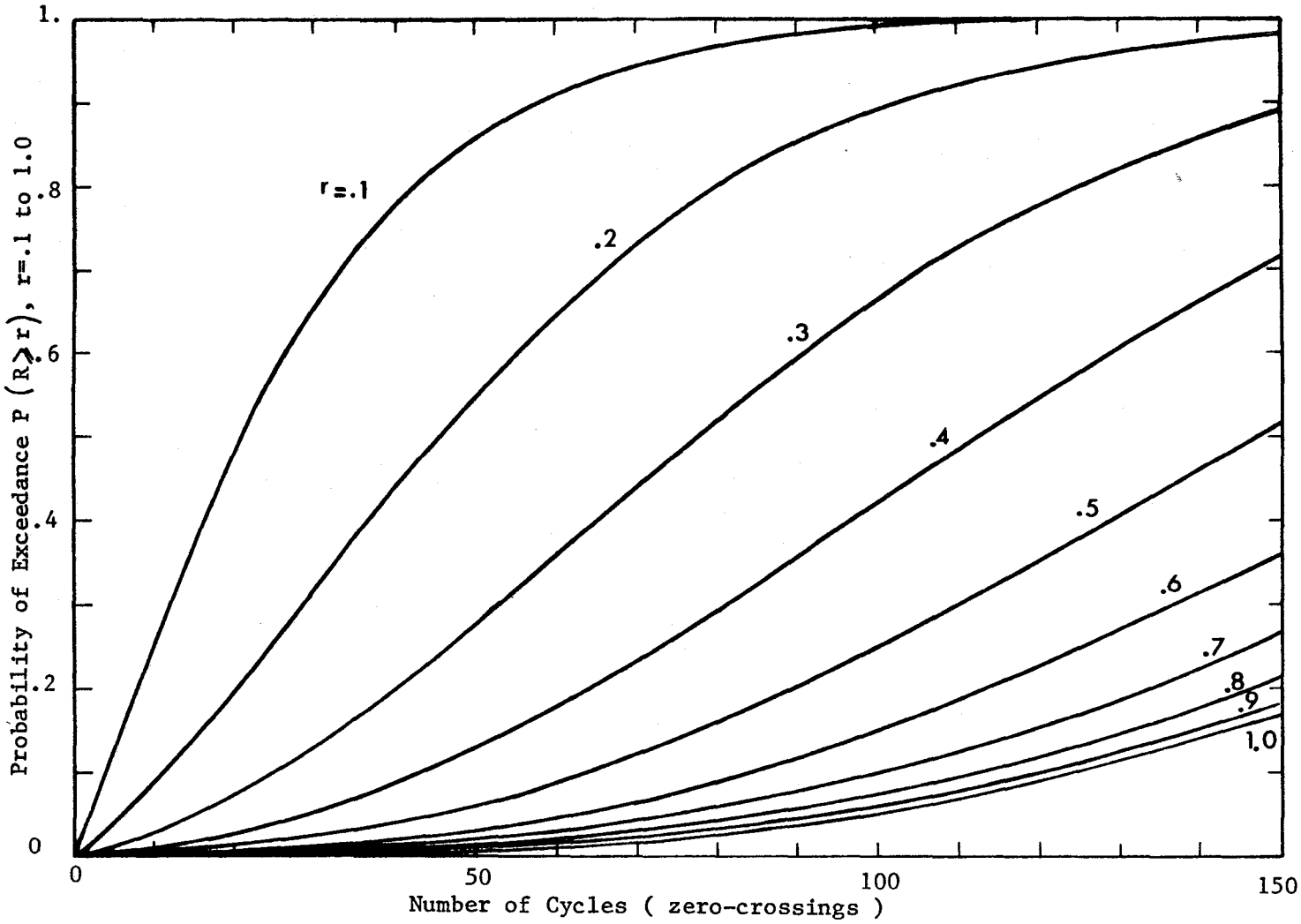

Figure 5.4 Probability Curves - Hypothetical Site - D_r = 68% - $1/\lambda$ = 27 cm/sec^2

(2) The effect of uncertainty becomes more important when the probability of exceedance is less than 0.8. In practical terms this means that soil uncertainty is not important for the Taft record, because the number of cycles is such that the probability of zero effective stress is close to 1.0. On the contrary, for events similar to the Hollister event, the probability of exceeding R = 1.0 jumps from 0.45 to 0.65 when the uncertainty $\sigma_{e_{NL}}$ is increased from 0. to 1.0. The same remarks apply for any other stress ratio such as R = 0.5 in figure 5.8. Several comments can also be made concerning soil uncertainties : (1) In his hazard analysis for liquefaction, Yegian (1978) stated that, for the cases he studied, uncertainties in the resistance against liquefaction were insignificant relative to uncertainties in earthquake induced shaking.

While this is true for complete liquefaction and very high intensity loading, it is not correct for moderate to high intensity loading for which the probability of liquefaction is less than 1.0; (2) The effect of soil uncertainty becomes important for short duration events, which also lead to probability of liquefaction less than 1.0; and, (3) There is a great value in performing statistical analyses of the uncertainties in order to facilitate correct engineering and economic decisions.

(d) Case III

The soil conditions are the same as the conditions of case I with a relative density of the Monterey sand equal to 68 percent. The loading condition is represented by a parameter $1/\lambda$ equal to 53 cm/sec^2. The resulting probabilistic pore pressure curves are given in figure 5.9.

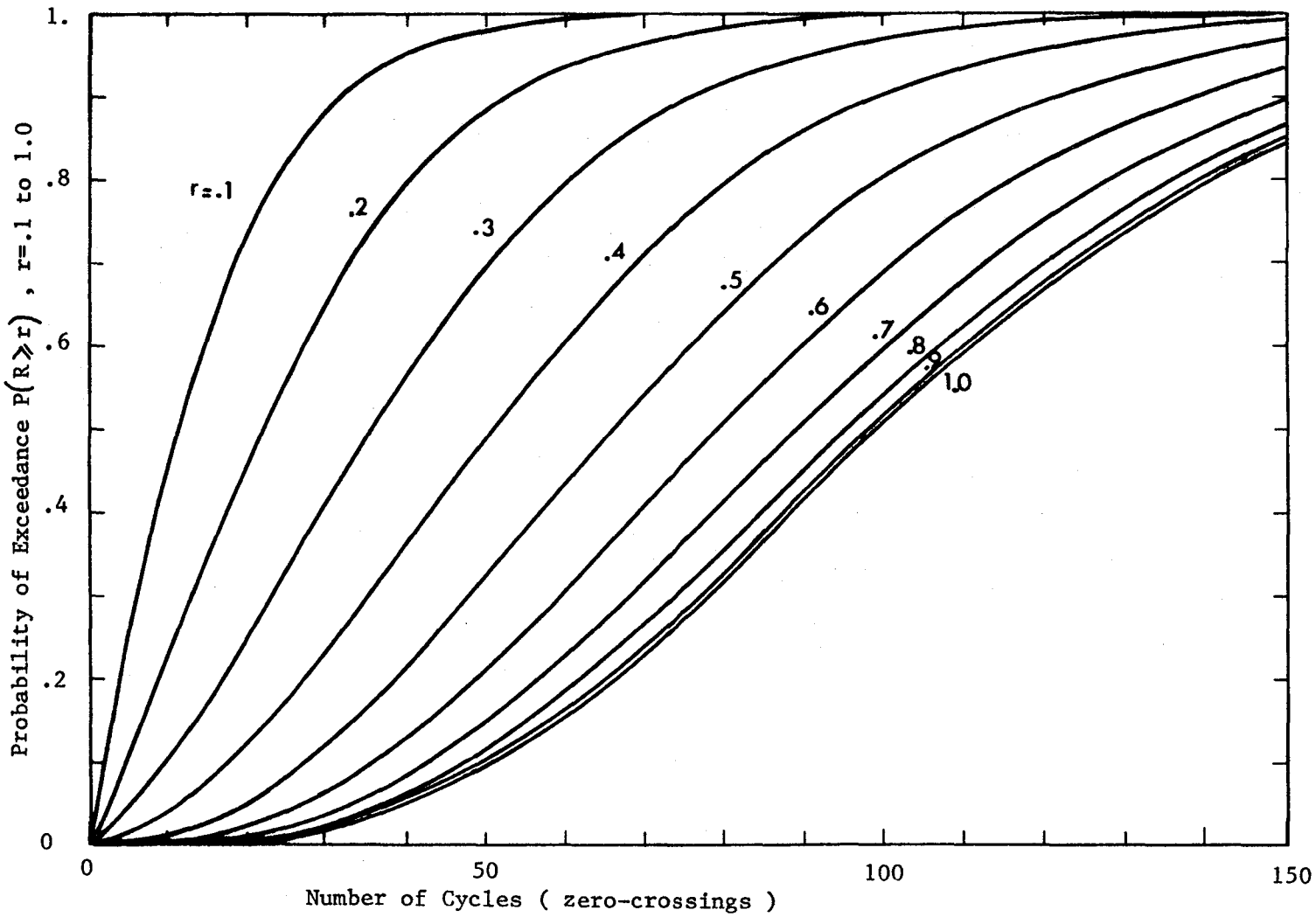

Figure 5.5 Probability Curves - Hypothetical Site - D_r = 54% - $1/\lambda$ = 27 cm/sec^2
No Uncertainty in the Cyclic Strength Curve

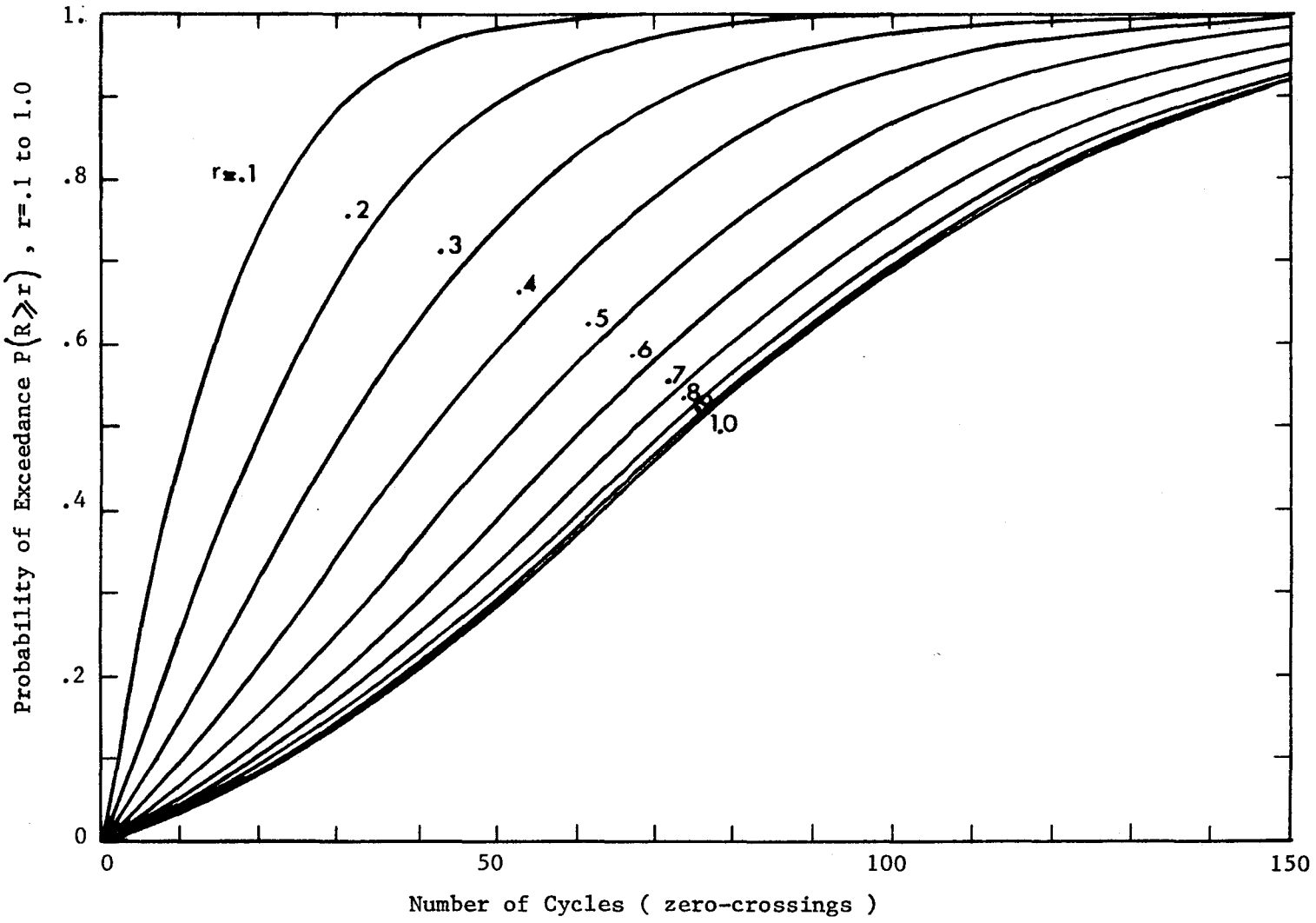

Figure 5.6 Probability Curves - Hypothetical Site - D_r = 54% - $1/\lambda$ = 27 cm/sec^2
Uncertainty of 1.0 in the Cyclic Strength Curve

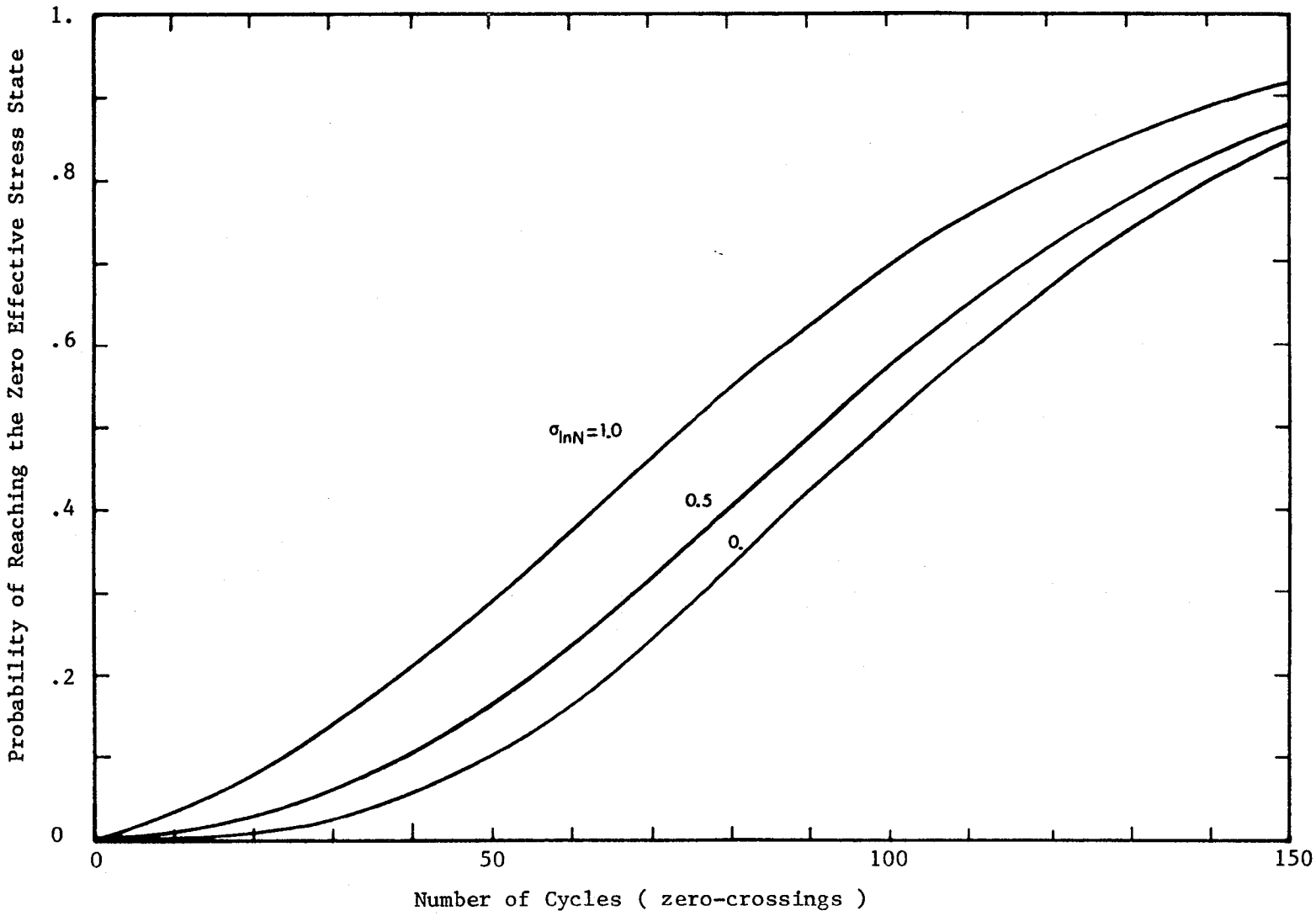

Figure 5.7 Effect of Uncertainty in the Cyclic Strength Curve for a Pore Pressure Ratio of 1.0

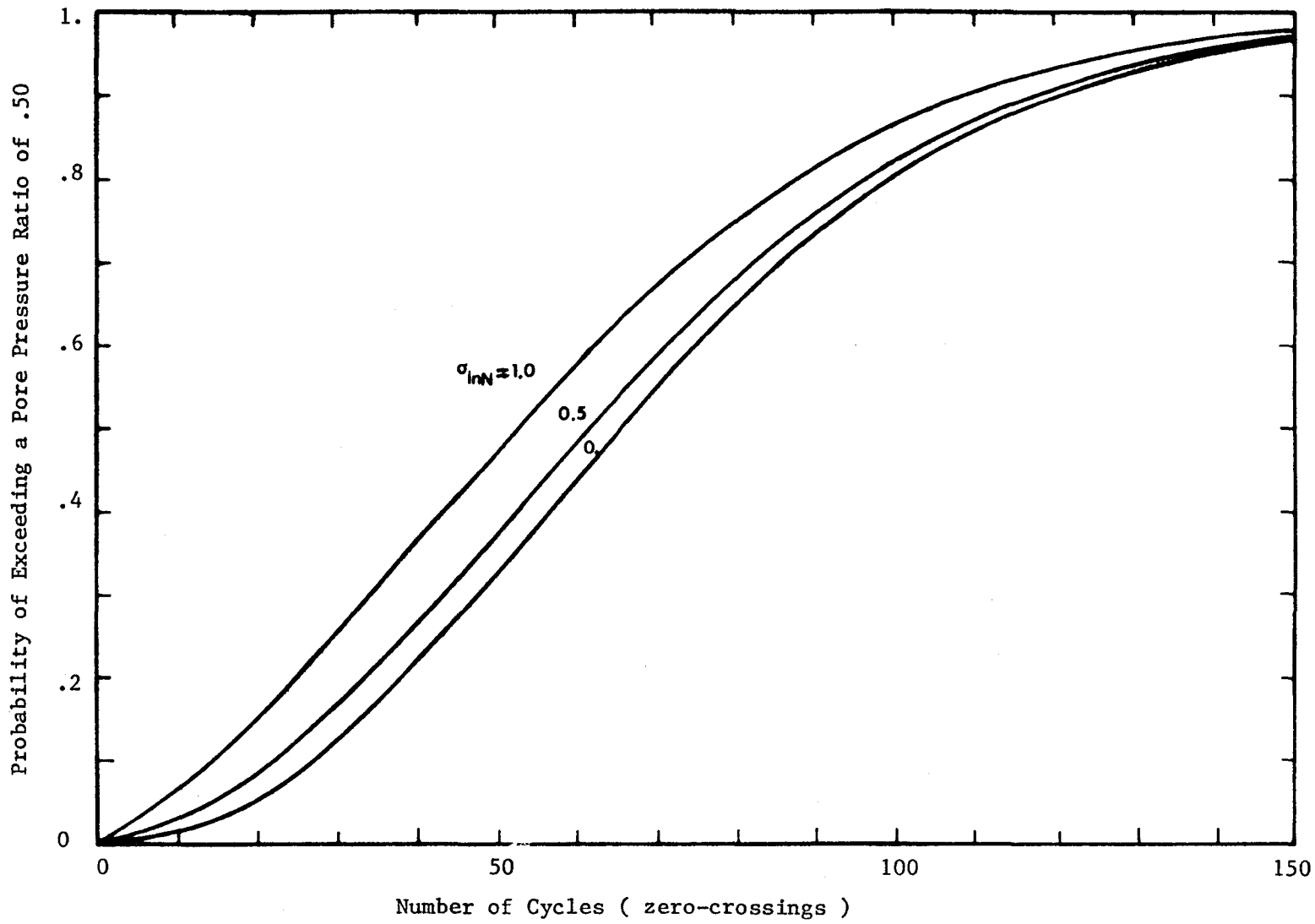

Figure 5.8 Effect of Uncertainty in the Cyclic Strength Curve for a Pore pressure Ratio of 0.50

The probability of reaching the zero effective stress state is almost 1.0 after 100 cycles of loading. Hence the model predicts complete liquefaction during an event with characteristics similar to the El Centro 1940 event. In figure 5.4 the probability of exceeding R = 1.0 after 100 cycles was 7 percent for a parameter $1/\lambda$ = 27 cm/sec^2. The comparison with figure 5.9 shows that increasing the loading parameter $1/\lambda$ by a factor of 2 makes the probability of exceedance jump from 7 percent to 100 percent. A site for which the design parameters are similar to the El Centro characteristics faces a completely different problem than a site located in a less seismic area with reduced design parameters.

5.5.2 Niigata sites

The preceeding examples described how the probabilistic model can be applied to a given site. Several comparisons between site and loading conditions demonstrated the versatility of the model. The next applications will test the ability of the model to predict the behavior of sites for which the field behavior is known.

During the earthquake of June 16, 1964, in Niigata, Japan, extensive damage to engineering structures occurred as a result of liquefaction of sand layers. The earthquake magnitude was about 7.6 and the source of energy release was about 35 miles from Niigata. The sand layers had relative densities ranging from 50 to 70 percent. The soil conditions are not exactly known for each of the liquefied sites, but average soil characteristics have been developed by several investigators (Seed and

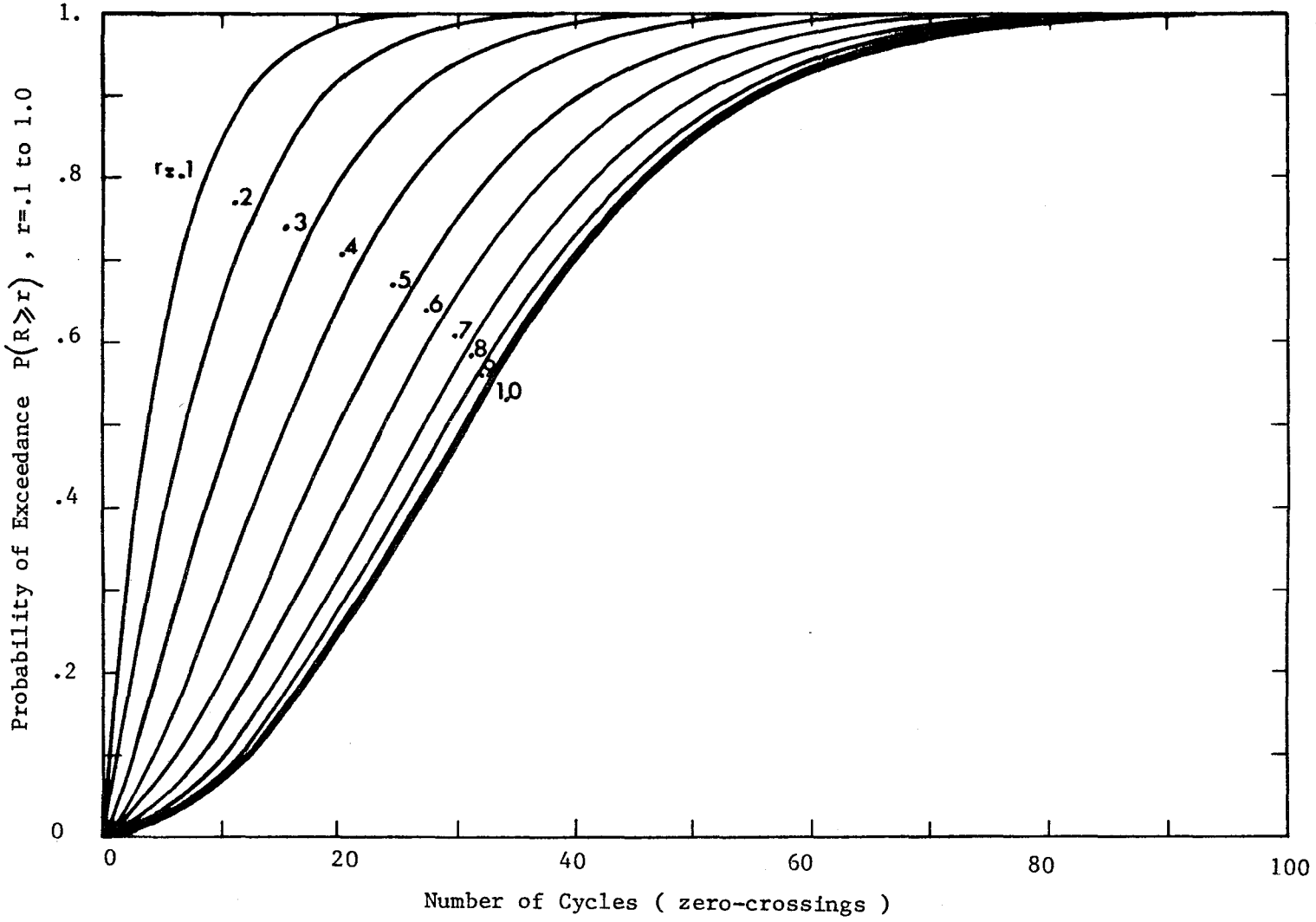

Figure 5.9 Probability Curves - Hypothetical Site - D_r = 68% - $1/\lambda$ = 53 cm/sec^2

Idriss, 1967, Christian and Swiger, 1975, Seed, Martin, and Lysmer, 1976, and Valera, and Donovan, 1977). Cyclic strength curves were defined for Sacramento river sand, a medium sand similar to the Niigata sand. This medium sand has its grain size distribution in the middle range of the liquefied sands in Niigata. The cyclic strength curves at relative densities of 53 and 70 percent are given in figure 5.10. The pore pressure generation curves are not available for this sand. For the purpose of illustration the pore pressure generation curves of the Monterey sand are used in the analysis. This assumption is the best possible with the data available. The Monterey and Sacramento River sands are both fairly uniform and their cyclic strength curves are close to each other.

The other parameters necessary to the analysis are listed in table 5.5. The water table is at a depth of 3.5 feet and the analysis is performed at a depth of 20 feet. The recorded maximum acceleration at the ground surface was 0.16 g. The shear stress density function was assumed to be a Rayleigh distribution. There are two reasons for this choice. First there is no existing statistical study on Japanese earthquakes, and second, previous investigators developed information on the sigma ratio for the Niigata earthquake (Donovan, 1971, Valera and Donovan, 1977). This ratio between the peak ground acceleration and the root mean square of acceleration is assumed to lie between 3 and 4 for the Niigata earthquake. Donovan (1971) used the value 3, while Valera and Donovan (1977) increased the value to 4. The median value of 3.5 is chosen for the present analysis, but it will be demonstrated how the probabilistic model can incorporate the uncertainty in the sigma ratio.

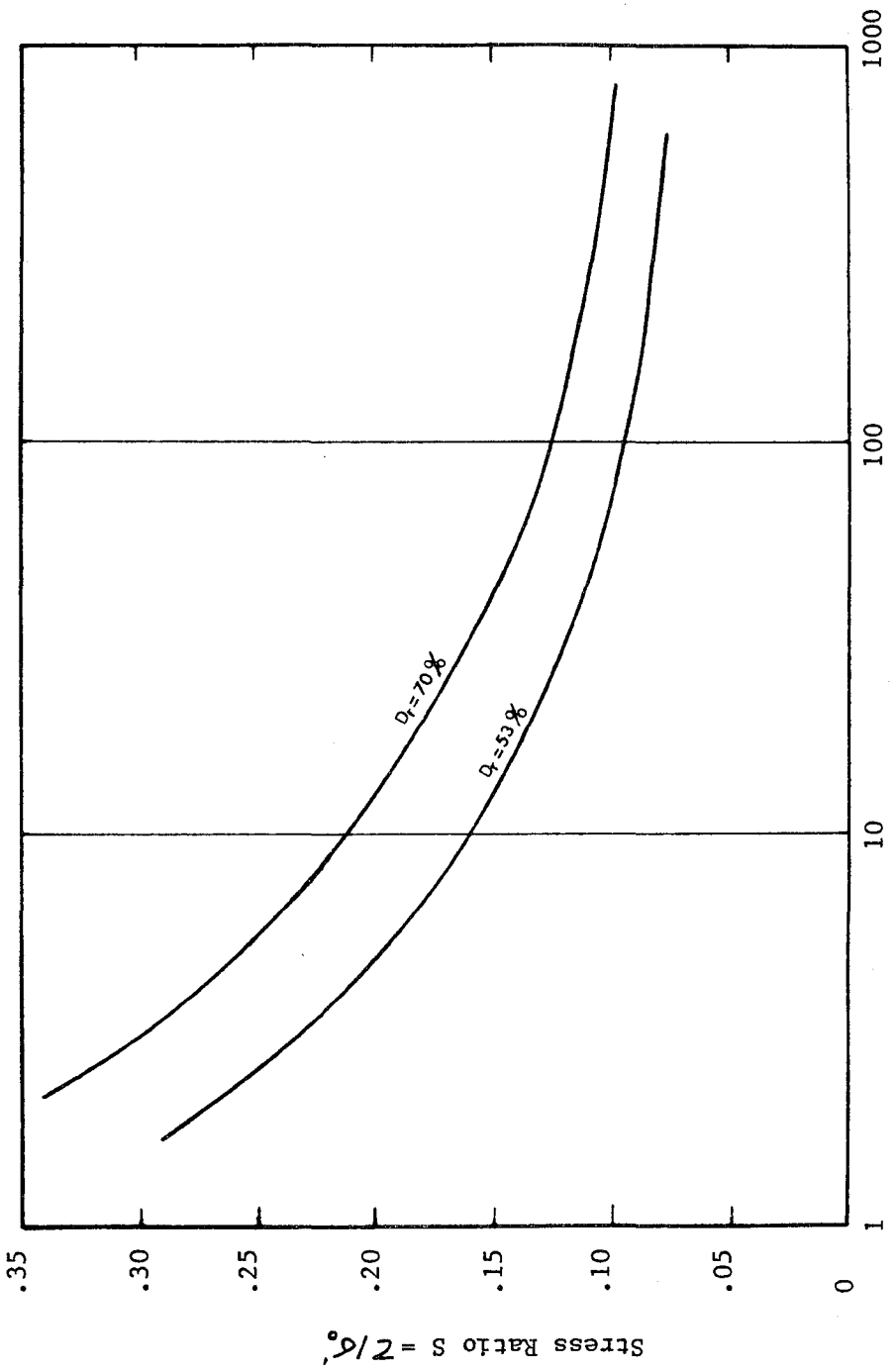

Figure 5.10 Cyclic Strength Curves - Medium Sacramento Sand

Relative Density : 53 and 70 %

Total Unit Weight : 120 pcf

Depth to Water Table : 3.5 feet

Depth of Interest : 20 feet

Effective Stress : 1370 psf

Total Stress : 2400 psf

Flexibility Coefficient r_d : .96

Uncertainty in Cyclic Strength Curve σ_{LnN_1} : .50

Fundamental Period of Deposit : .80 second

Peak Ground Acceleration : .16 g

Duration : 40 seconds

Number of Cycles of Loading : 50

Sigma Ratio : 3 to 4

Table 5.5 Parameters for Niigata sites, Rayleigh Distribution of Shear Stress

(a) Niigata - Case I

Several sand layers which liquefied in Niigata had a relative density of about 53 percent (Seed and Idriss, 1966). Using the cyclic strength curve of the medium sand at a relative density of 53 percent, the probabilistic development of pore pressure is computed. The resulting probability curves are presented in figure 5.11. The probable number of cycles during an earthquake is obtained by dividing the effective duration of the motion by the estimated predominant period. For the Niigata case, this yields a number of cycles of about 50. As a consequence the probability of reaching the zero effective stress state is close to 97 percent. This probability value is in agreement with the fact that liquefaction did occur at those sites with a relative density of 53 percent. It also says that there is a 3 percent chance for a site not to liquefy.

It can be shown that the number of cycles obtained by dividing the duration by the predominant period is slightly less than would be obtained from more complex analysis. This uncertainty in the number of cycles can be easily incorporated :

$$P(R \geq 1.0) = \int_n P(R \geq 1.0/n) f_n(n) dn \qquad (5.19)$$

with :

P(R≥1.0) the probability to reach the zero effective stress state.

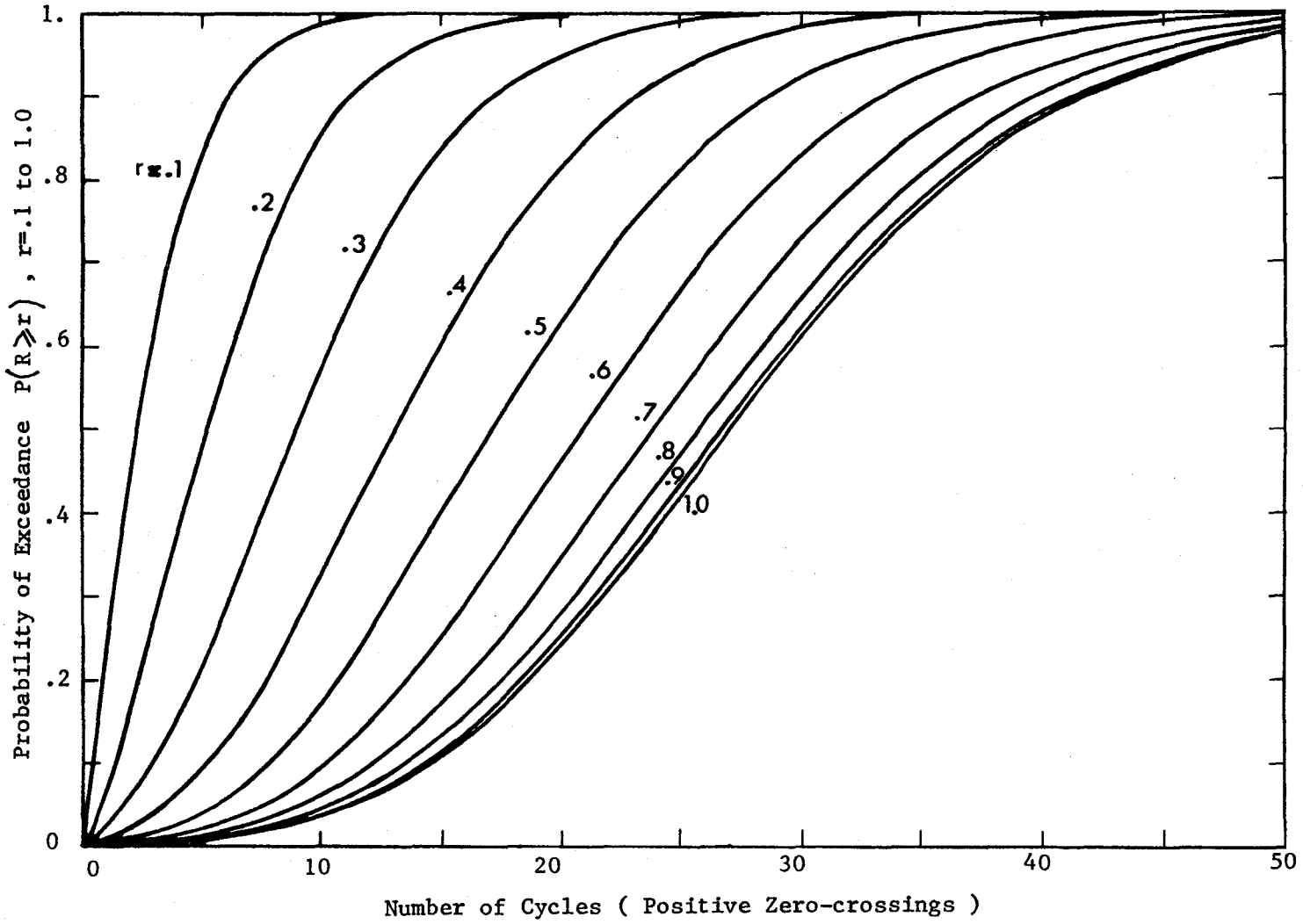

Figure 5.11 Probability Curves - Niigata Sites - D_r = 53%

$P(R \geq 1.0/n)$ the probability to reach the zero effective stress state given n cycles. This is the curve given in figure 5.11.

$f_n(n)$ density function of the number of cycles n.

As an example, if n is assumed equiprobable between 45 and 55, equation 5.18 and figure 5.1 yield a probability of reaching the zero effective stress of 96 percent. This calculation does not change the conclusion reached with a unique value n = 50, but it shows how any new uncertainty can be included in the model.

(b) Uncertainty in the sigma ratio

As demonstrated for the number of cycles, it is possible to incorporate uncertainty in the sigma ratio as follow:

$$P(R \geq r) = \int_{sr} P(R \geq r | sr) f_{sr}(sr) dsr \qquad (5.20)$$

with :

$P(R \geq r)$ the probability to exceed the pore pressure ratio r

$P(R \geq r/sr)$ the probability to exceed the pore pressure ratio r given a value of sigma ratio sr. As example figure 5.11 corresponds to sr = 3.5

$f_{sr}(sr)$ the probability density function of the sigma ratio sr.

In the present case sr ranges between 3 to 4. With no additional information, the best assumption is to make the sigma ratio equiprobable on this interval. Performing the integration in equation 5.15, probabilistic curves are obtained which take into account uncertainty in the sigma ratio (figure 5.12). Considering this uncertainty the probability of reaching the zero effective stress is 0.93 in 50 cycles. This number incorporates uncertainty in the sigma ratio and thus is a better estimate of the probability of liquefaction than the value 0.97 obtained with sr=3.5.

(c) Niigata - Case II

The method is now applied to sites where the relative density of the sand is 70 percent. The cyclic strength curve is given in figure 5.10. The computed probabilities of exceedance are plotted in figure 5.13. The probability of reaching the zero effective stress state is 0.82. As a consequence there is a probability of 18 percent that a site with these characteristics will not completely liquefy. These numbers are in agreement with the fact that several sites with 70 percent relative density liquefied during the Niigata earthquake, and that there is at least one known site which did not liquefy. The probability to exceed pore pressure ratios of 0.5 to 0.6 is greater than 0.95, which means that even if complete liquefaction does not occur, the expected final pore pressure ratio is very high.

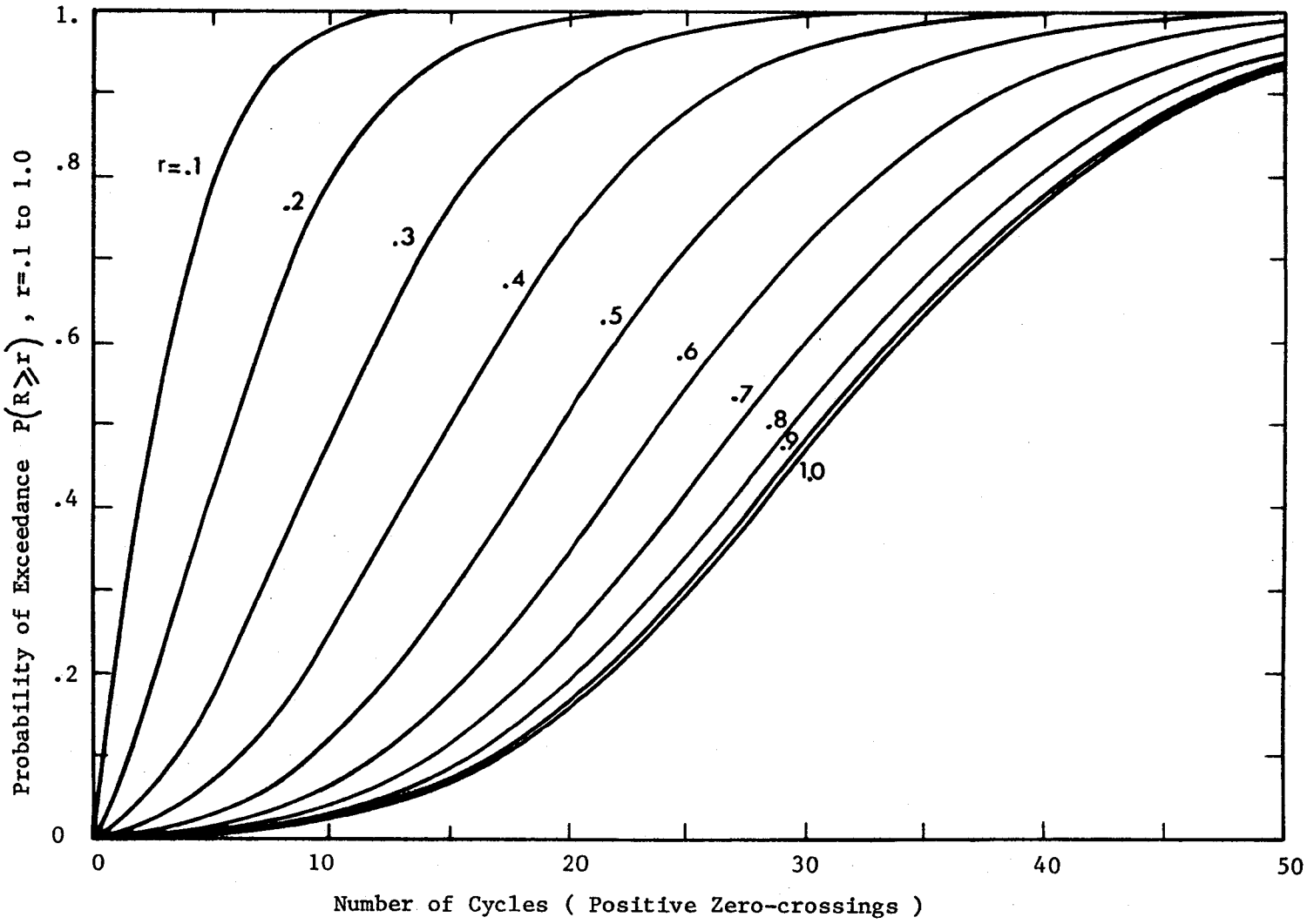

Figure 5.12 Probability Curves - Niigata Sites - D_r = 53% -
Uncertainty in Sigma Ratio Included

5.6 SUMMARY

The different elements which enter the probabilistic pore pressure model have been presented. The shear stress probability density function is modeled as either a Rayleigh or an exponential distribution. The application of stationary random process theory to earthquake ground motion implies the load cycles to be Rayleigh distributed. Statistical procedures show that the exponential distribution fits the distribution of load cycles from available strong-motion time histories reasonably well. The cyclic strength curve is represented by parabolic or piecewise linear expressions. The number of cycles to zero effective stress follows a lognormal distribution around the median cyclic strength curve. Least square regression methods are used to obtain functional relationships between the pore pressure ratio, the stress ratio, and the normalized number of cycles.

Given this information the probabilistic model has been applied to several different soil and loading conditions. These applications demonstrate that, while the mathematical formulation of the model is cumbersome, the results are fairly simple to analyze and well suited to make comparison between site and loading conditions. The model correctly predicts the behavior of sites for which the field behavior during the Niigata earthquake is known. The probabilistic framework of the model makes it possible to include any supplementary uncertainty, such as uncertainties in duration or sigma ratio of the Rayleigh distribution etc. The assumptions made for the practical applications are not critical to the method. The model can easily accommodate any

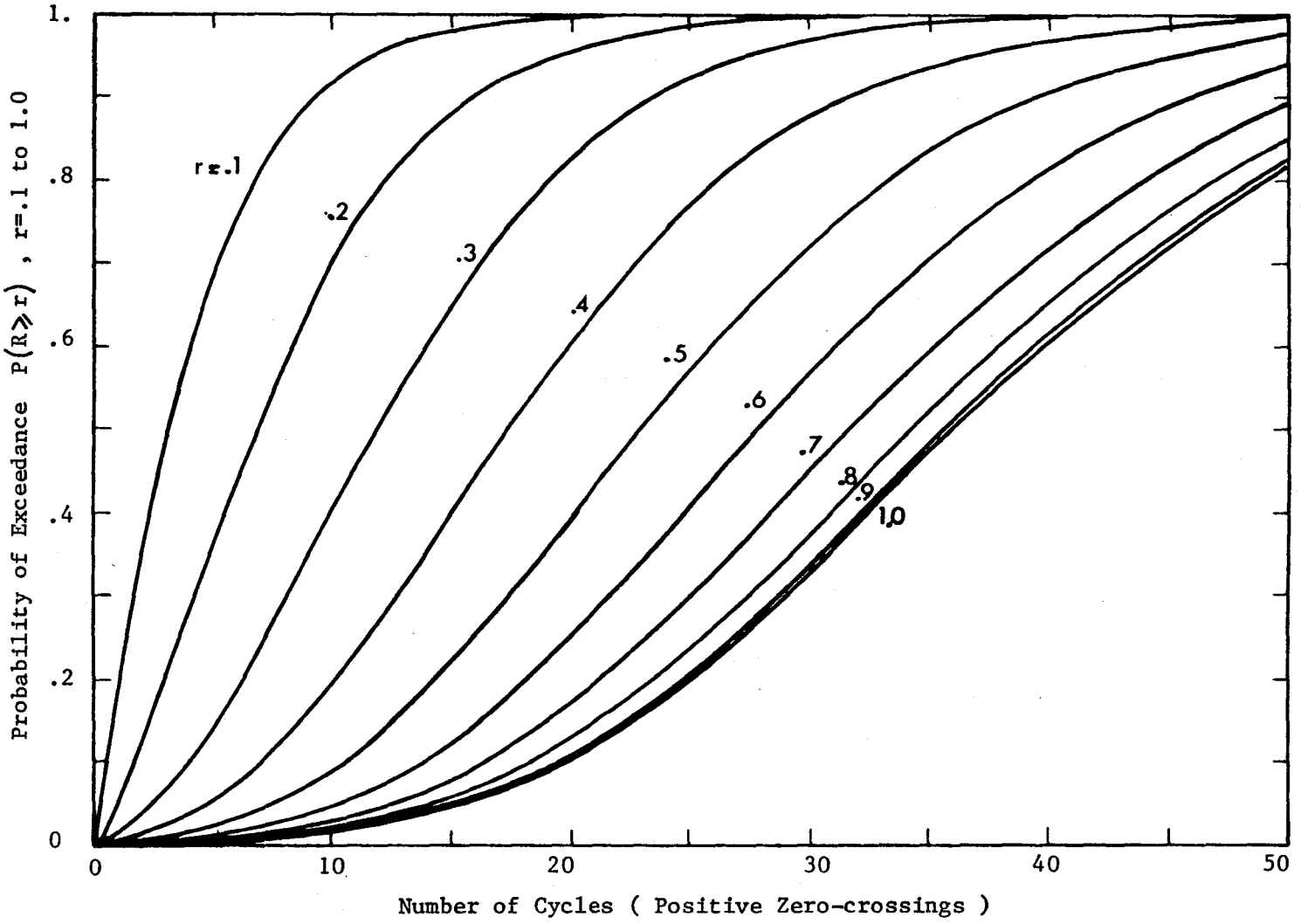

Figure 5.13 Probability Curves - Niigata Sites - D_r = 70%

desired form of the probability density functions of the shear stress and soil parameters.

Chapter VI

PROBABILISTIC DEVELOPMENT OF PORE PRESSURE USING AN EFFECTIVE STRESS MODEL

6.1 INTRODUCTION

Chapters 4 and 5 dealt with the development of a probabilistic pore pressure model based on experimental data. This chapter proposes an alternative method which uses a theoretical effective stress model to probabilistically compute the development of pore pressure during cyclic loading. This second model is developed for several reasons: (1) The effective stress model uses basic soil parameters, such as the coefficient of lateral earth pressure, which can take into account local soil conditions (cementation,overconsolidation etc.); (2) Using an analytical expression for the development of pore pressure greatly improves the mathematical and computer formulation of the probabilistic model; and, (3) A comparison study between different effective stress models is possible.

The following sections make extensive use of concepts and results presented in the previous chapters including the efffective stress model proposed by Finn, Lee and Martin, 1977 (discussed in chapter 3) and the probability concepts of chapter 4. The method developed in this chapter computes the probability of exceedance of any pore pressure ratio as a function of the number of cycles of loading. The applied shear stress is assumed to follow either the Rayleigh or the exponential distribution and the parameters of these distributions are the same as in chapter 5.

The complexity of the effective stress model is such that a direct integration method is not feasible to compute the probabilistic development of pore pressure. As an alternative, simulation techniques are used to generate soil and loading parameters and to estimate the cumulative distribution function of pore pressure.

6.2 SIMULATION TECHNIQUES

The use of simulation techniques was not described in previous chapters. This section briefly discusses the generation of random numbers and simulated observations.

6.2.1 Random number generation

Simulation is essentially a controlled statistical sampling technique which can be used to study complex stochastic systems when analytical and/or numerical techniques do not suffice. A necessary part of any such procedure is an algorithm for random number generation. A random number generator produces sequences that follow a given probability distribution and possess the appearance of randomness. Digital simulations in computer software employ recurrence relations of the form :

$$X_n = a\, X_{n-1} + c \qquad \text{(modulo m)} \tag{6.1}$$

Equation 6.1 says that the number X_n is the remainder when $aX_{n-1}+c$ is divided by m. A number U_n on the interval [0,1] is obtained by dividing X_n by m :

$$U_n = X_n/m \qquad (6.2)$$

A correct choice of the constants a, c and m, and of the starting value X_0 produces uniform random numbers on the interval [0,1]. In general, every computer software system provides the means to generate uniformly distributed random numbers. The SIMSCRIPT II generator is used in this dissertation. It has a multiplier of 630360016 and a modulo of $2^{31} - 1$. The constant c is 0 :

$$X_n = 630360016\ X_{n-1}\ (\text{modulo}\ 2^{31} - 1\ ) \qquad (6.3)$$

This generator has been extensively tested and found to meet the requirements of uniformity, independence, density, efficiency and length of cycle necessary to a good generator. Values for appropriate seeding (changing the sequence) when starting the generator are available in the literature (Fishman, 1978).

The simulation of a sample space of the random variable Un theoretically consists in generating an infinity of numbers U_i, $i=1,2,\ldots,\infty$, such that their cumulative distribution exactly matches the uniform distribution on the interval [0,1]. In practice however, it is impossible to generate an infinity of numbers and the number of sample points is chosen depending on the degree of accuracy required in the analysis.

6.2.2 Inverse transformation method

The inverse transformation method, often called the Monte-Carlo method of simulation, is used to generate a non-uniform random number X. Assume that the cumulative probability function of a random variable X is known and given by :

$$P[X \leq x] = F(x) \tag{6.4}$$

Denoting $F^{-1}(\bullet)$ as the inverse function corresponding to F(x) :

$$y = F(x) \quad \leftrightarrow \quad x = F^{-1}(y) \tag{6.5}$$

If U is uniformly distributed on the interval [0,1] the random variable $X = F^{-1}(U)$ has the distribution function F(x) :

$$\begin{aligned} P[F^{-1}(U) \leq x] &= P[F(F^{-1}(U)) \leq F(x)] \\ &= P[U \leq F(x)] \\ &= F(x) \end{aligned} \tag{6.6}$$

Equation 6.6 provides a way of obtaining non-uniform random numbers. The algorithm is very simple :

1. Generate U uniformly distributed between 0 and 1.

2. Return $X = F^{-1}(U)$

This algorithm assumes that the equation F(X) = U can be solved explicitly. This is the case of the distributions considered in this dissertation. Other distributions can be simulated by direct generation methods such as composition methods and rejection-acceptance methods (Ahrens and Dieter, 1973, and Fishman, 1978).

6.3 CYCLIC STRENGTH CURVE OBTAINED BY SIMULATION

In this section the statistical characteristics of a cyclic strength curve are generated using the simulation technique. As it is demonstrated later in this chapter, this is not a step necessary to the probabilistic pore pressure model, but it clearly illustrates the use of simulation algorithms to generate soil parameters. The effective stress model proposed by Finn, Lee and Martin (1977) predicts the development of pore pressure during cyclic loading by solving the following equations, 3.7 to 3.10 repeated from Chapter 3:

$$\Delta u = E_r \, \Delta \varepsilon_v$$

$$\Delta \varepsilon_v = C_1(\gamma - C_2 \varepsilon_v) + \frac{C_3 \varepsilon_v^2}{\gamma + C_4 \varepsilon_v}$$

$$\tau = \frac{G_{mo}\gamma}{1 + (G_{mo}/\tau_{mo})\gamma} = f(\gamma)$$

$$\frac{\tau - \tau_r}{2} = f\left(\frac{\gamma - \gamma_r}{2}\right)$$

The parameters in these equations have been discussed in detail in chapter 3. For a given set of parameters G_{mo}, τ_{mo}, and E_r and constants C_1 to C_4 the development of pore pressure can be computed for non uniform and uniform loading sequences. This was done in chapter 3 to obtain cyclic strength curves for the crystal silica sand (figures 3.7 and 3.8). The same method is applied in the present section but uncertainties are introduced in the most important parameters of the model; namely G_{mo}, τ_{mo}, E_r and C_1. They are defined by probability density functions. The maximum shear stress τ_{mo} is however not an independent variable. It is related to the coefficient of lateral earth pressure K_0, and the friction angle ϕ' by :

$$\tau_{mo} = \left[\left(\frac{1+K_0}{2}\sin\phi'\right)^2 - \left(\frac{1-K_0}{2}\right)^2\right]^{1/2} \sigma'_{vo} \qquad (6.7)$$

Hence the basic probability density functions for the model are those of K_0, ϕ', G_{mo}, E_r and C_1 The initial effective stress σ'_{vo} is in general a well defined parameter which is considered deterministic. Also, no uncertainty was included in the constants C_2, C_3 and C_4 because a sensitivity study showed that their effects were far less important than the effect of C_1. It should be noted that these two restrictions are not necessary since the computer program developed to implement this method accomodate uncertainties of up to 20 parameters.

Given the probability density functions of the parameters, the simulation algorithm described in table 6.1 computes the statistics of the cyclic strength curve. For a given value of the stress ratio τ/σ'_0,

the algorithm generates a set of parameters K_o, ϕ', G_{mo}, E_r and C_1. For these values the number of cycles to zero effectives stress is computed. The simulation is repeated NS times, which for a given stress ratio yields NS values of the number of cycles N_l.

These NS values are ranged by increasing order, N_{li}, i=1,NS. The mean, median, variance and cumulative distribution function of N_l are estimated as follows :

$$\text{Mean:} \quad (N_l)_{mean} = \frac{1}{NS} \sum_{i=1}^{NS} N_{li} \tag{6.8}$$

$$\text{Median:} \quad (N_l)_{median} = N_{l_{(NS+1)}}/2 \quad \text{if NS odd}$$

$$= \frac{N_{l_{(NS/2)}} + N_{l_{(NS/2+1)}}}{2} \quad \text{if NS even} \tag{6.9}$$

$$\text{Variance:} \quad S^2_{N_l} = \frac{1}{NS-1} \sum_{i=1}^{NS} (N_{li}-(N_l)_{mean})^2 \tag{6.10}$$

$$\text{CDF:} \quad F_{N_l}(N_l) = \frac{1}{NS} \sum_{i=1}^{NS} S_{n_l} \tag{6.11}$$

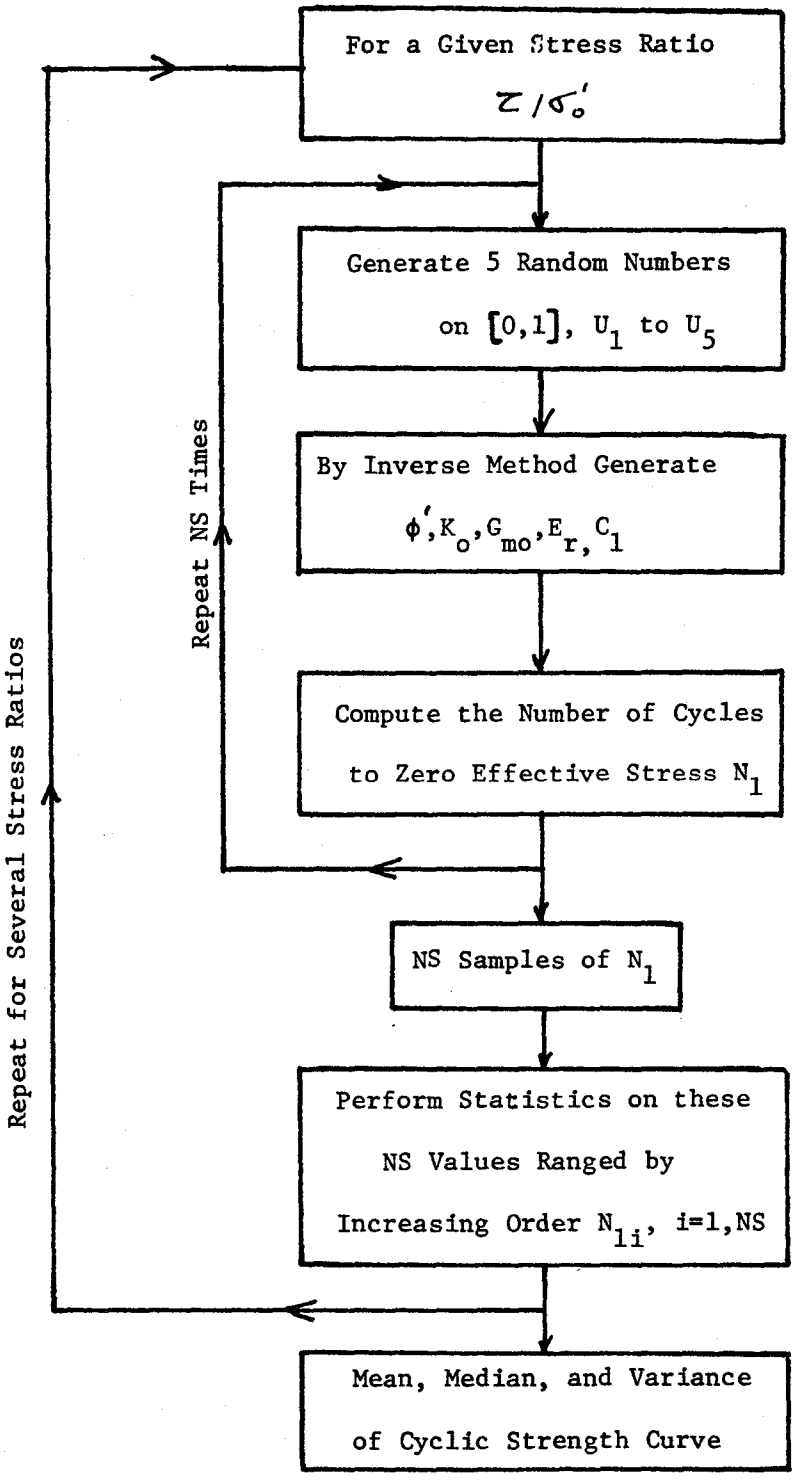

Table 6.1 Simulation Algorithm to obtain a Cyclic Strength Curve

$$\text{with} \qquad S_{n_1}^{N_{1i}} = \begin{cases} 1 & \text{if } N_{1i} < n_1 \\ 0 & \text{if } N_{1i} > n_1 \end{cases} \tag{6.12}$$

The calculations are repeated for a number of stress ratios in order to completely describe the cyclic strength curve.

As an example, the simulation technique is applied to the crystal silica sand at a relative density of 45 percent. The parameters G_{mo}, E_r, ϕ', C_1 and K_0 are assumed to be uniformly distributed with values of G_{mo}, E_r, and C_1 taken to deviate up to 10 percent from their mean values. ϕ' is assumed uniformly distributed between 33 and 37 degrees, and K_0 varies between .4 and .6. These uncertainties are chosen to be in the medium range of what can be expected for most soils. Higher values are possible, especially for the coefficient of earth pressure K_0 and the shear modulus G_{mo}. The uniform distribution used is a simple but fair assumption for soil parameters when confidence in the data is limited. Of course other distributions could be used, such as triangular, normal, lognormal and Beta Distributions. From a physical stand-point, the Beta distribution may be more consistent for observed characteristics of material parameters since it is not necessarily symmetrical and it limits the range of possible values for the variable, as is the case of most soil parameters (Harr,1977). However, for the simplicity of the discussion the uniform distribution is used in this chapter. In order to give the maximum generality to the method, the triangular, normal and Beta distributions are possible alternatives allowed in the computer program.

The application of the simulation technique to crystal silica sand at a relative density of 45 percent leads to the results in figures 6.1 and 6.2. In figure 6.1 the median number of cycles to zero effective stress is plotted as a function of the applied stress ratio. Any point on this median cyclic strength curve has a probability of 50 percent of being exceeded. The simulation technique also provides the cumulative distribution function of the number of cycles to zero effective stress. The corresponding probability density functions are schematically represented in figure 6.1 for stress ratios of 0.15 and 0.10. In figure 6.2 the cumulative distribution function is given for a stress ratio of 0.10. For this stress ratio, the number of cycles to zero effective stress has a median value of about 16, but ranges from 5 up to values greater than 30.

This example demonstrates that, given the probability density functions of basic soil parameters, the simulation technique can provide the statistical characteristics of the cyclic strength curve. It is also interesting to notice that the cumulative distribution function of N_1 is almost perfectly approximated by a lognormal distribution LN (16,.36).This agrees with the choice of the lognormal distribution made in chapter 5.

Work is underway to improve the technique. It consists of (1) compiling data to provide information on the probability density functions of soil parameters and (2) taking into account the possible statistical dependence between parameters. A typical example of the second item is the dependence between the friction angle and the

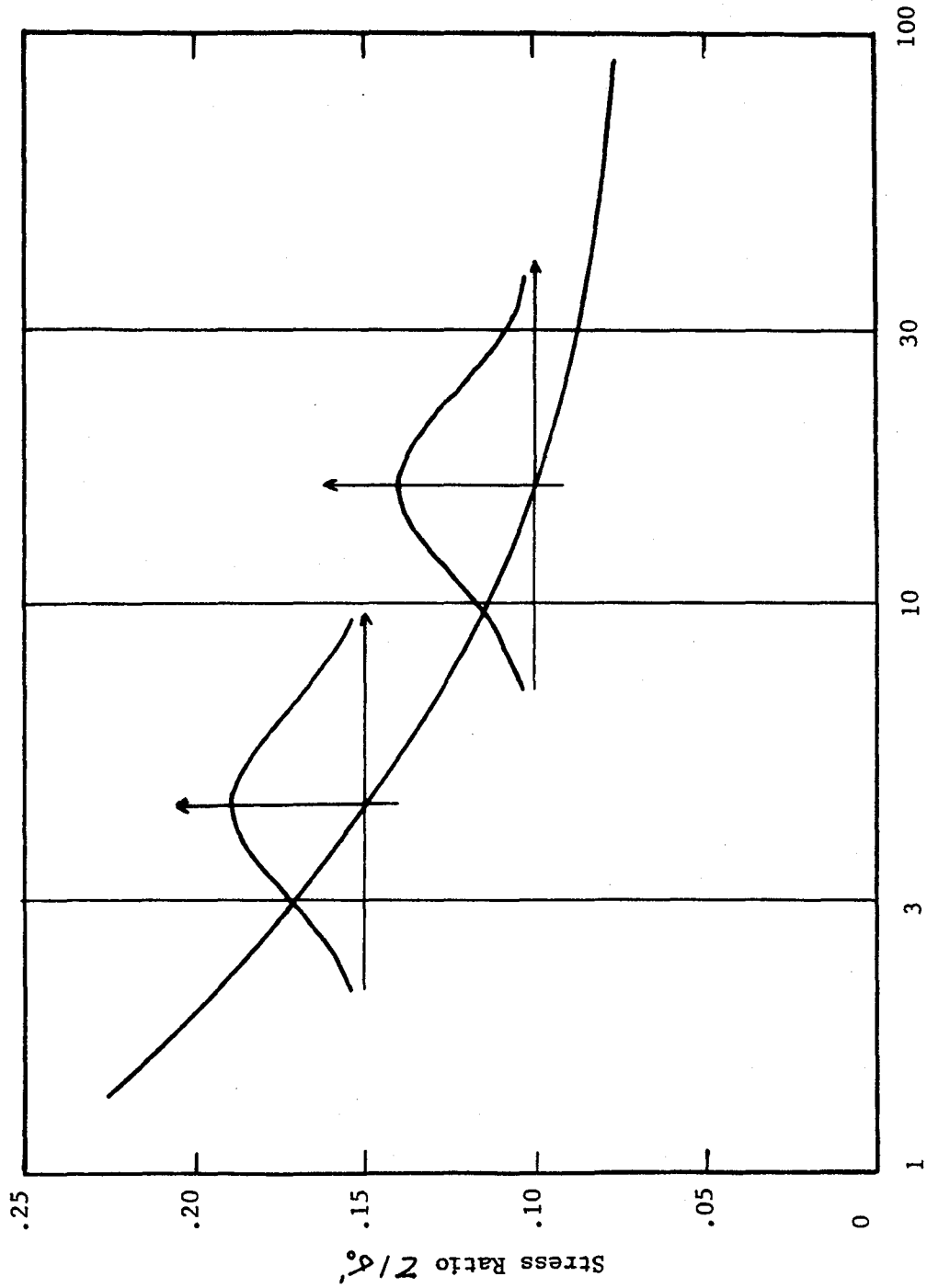

Figure 6.1 Median Cyclic Strength Curve for the Crystal Silica Sand - D_r = 45%

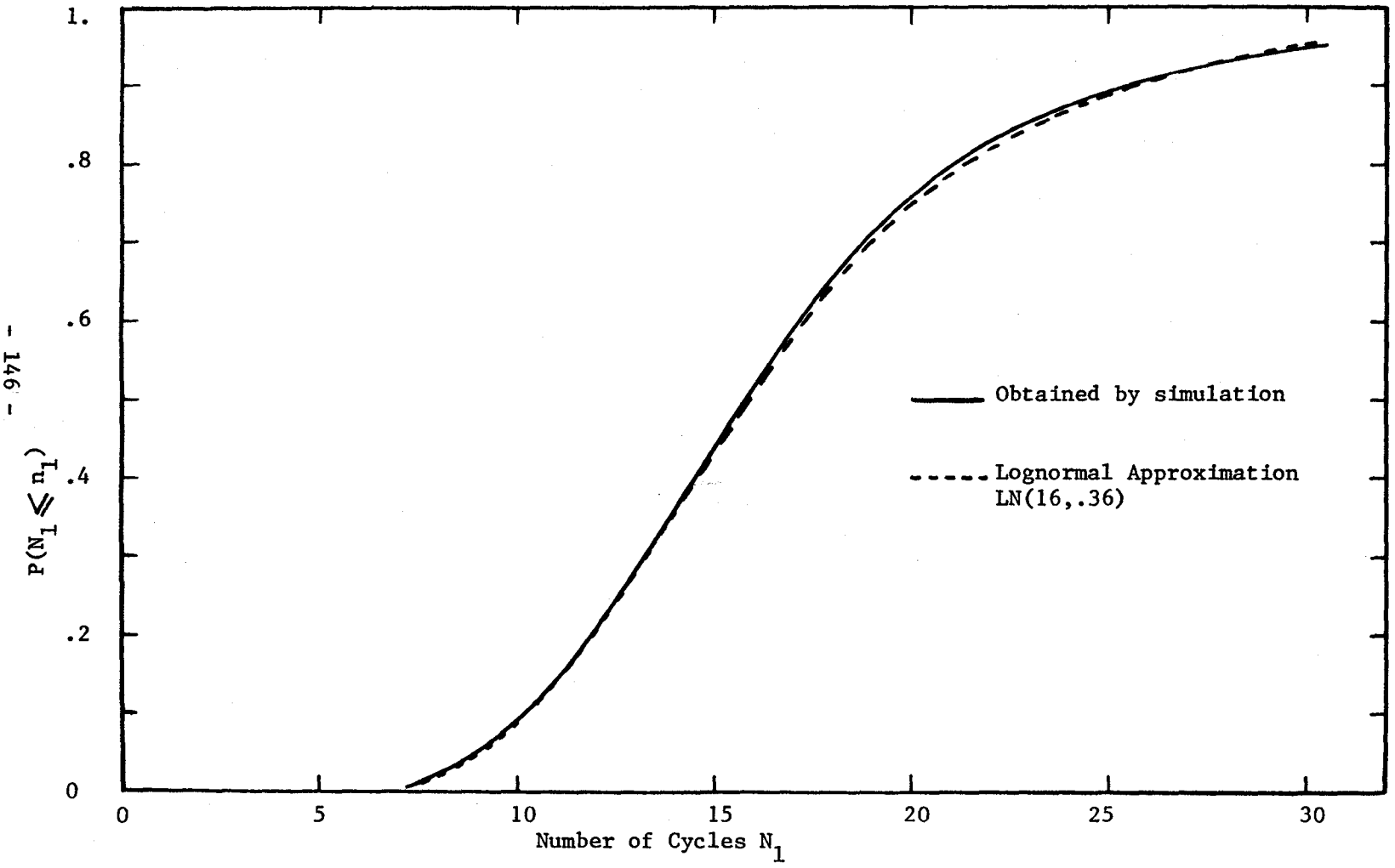

Figure 6.2 Cumulative Distribution Function of the Number of Cycles to Zero Effective Stress ($\tau / \sigma_o' = 0.10$)

coefficient of at rest lateral earth pressure. This can be handled by introducing a joint probability density function of K_0 and ϕ' as a function of the relative density (Lumb,1974 and Harr,1977). The author believes that this method has potential, especially to study the cyclic strength curve and its uncertainty for low stress ratios and accordingly large number of cycles. The problem of low stress ratios and large number of cycles arises in the design of offshore gravity structures (Bjerrum, 1974, Lee and Focht, 1975 and, Hoeg and Tang, 1978).

It should be noted that the simulation of soil parameters is only the first step of the probabilistic pore pressure model. The second step consists in applying the simulation technique to the shear stress distribution in order to generate shear stress time histories. The next sections will describe this second step and show how to deduce the cumulative distribution function of pore pressure from the results of the simulation algorithm.

6.4 SIMULATION OF THE SHEAR STRESS DISTRIBUTION

The inverse transformation technique (section 6.2) provides efficient algorithms to generate random numbers that follow the exponential or the Rayleigh probability density functions.

(a) Exponential distribution

The exponential distribution of shear stress τ is given by (see section 5.2.2) :

$$f_{\tau}(\tau) = \lambda_{\tau} \exp(-\lambda \tau) \tag{6.13}$$

If the random variable U is uniformly distributed between 0 and 1, then $\tau = (-\ln U)/\lambda$ is exponentially distributed. As a consequence, a very simple algorithm to generate sequences of an exponentially distributed shear stress is as follows :

1. Generate U uniformly distributed between 0 and 1

2. Return $\tau = (-L_n U)/\lambda_{\tau}$

The derivation of this algorithm can be found in any textbook on simulation.

(b) Rayleigh distribution

The Rayleigh distribution of shear stress is given by :

$$f_{\tau}(\tau) = (\tau/r)\exp(-\tau^2/2r^2) \tag{6.14}$$

If U is uniformly distributed between 0 and 1, then $\tau=(-2r^2 L_n U)^{1/2}$ is Rayleigh distributed :

$$\begin{aligned} F(\tau) &= 1 - P[\sqrt{-2r^2 L_n U} > \tau] \\ &= 1 - P[U < \exp(-\tau^2/2r^2)] \\ &= 1 - \exp(-\tau^2/2r^2) \end{aligned} \tag{6.15}$$

$$\text{and } f_{\tau}(\tau) = dF_{\tau}(\tau)/d\tau = \tau/r^2 \exp(-\tau^2/2r^2) \quad (6.16)$$

The following algorithm generates sequences of a Rayleigh distributed shear stress :

1. Generate U uniformly distributed between 0 and 1

2. Return $\tau=(-2r^2 L_n U)^{1/2}$

In figures 6.3.a and 6.3.b the exponential and Rayleigh density functions are compared to frequency histograms obtained by simulation. The simulated frequencies compare very well with the exact frequencies. In terms of cumulative distribution function , the fit between exact and simulated function is almost perfect.

6.5 PROBABILISTIC DEVELOPMENT OF PORE PRESSURE FROM SIMULATION TECHNIQUE

In order to compute the probabilistic development of pore pressure, the only step to add to the algorithm of table 6.1 is the generation of shear stress time histories. Table 6.2 describes the resulting algorithm. Using the inverse transformation method the soil parameters and the shear stress time history are simulated. For each set of soil parameters and each shear stress time history the development of pore pressure is computed and the pore pressure values obtained at the end of any cycle of loading are recorded. The simulation is repeated NS times. In the following applications NS is equal to 1,000.

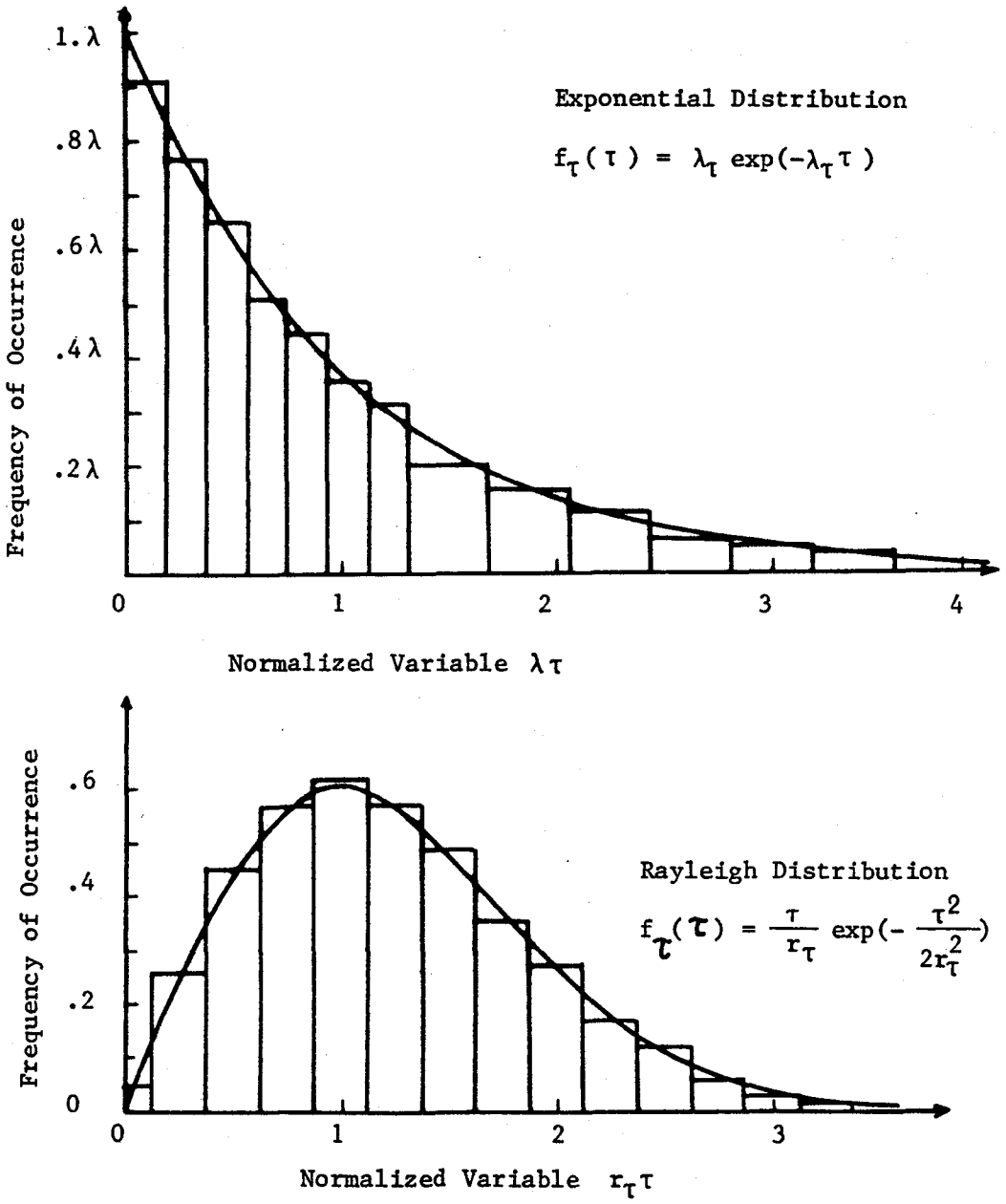

Figure 6.3 Comparison Between Theoretical Probability Density Functions and Simulated Histograms

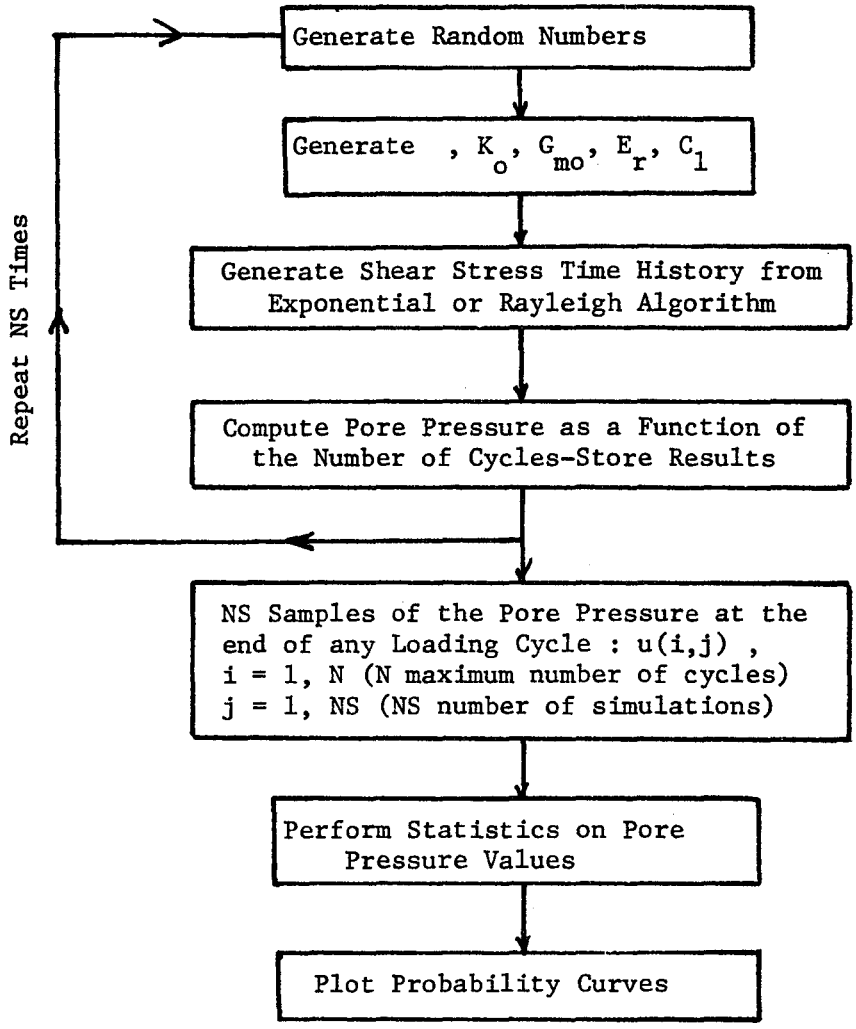

Table 6.2 Simulation Algorithm to Obtain the Probability Curves of Pore Pressure Development

At the end of the simulation procedure the mean, median, variance and cumulative distribution function of the pore pressure are computed as a function of the number of cycles. The equations to do so are exactly similar to those used for the cyclic strength curve. The following cases demonstrate that this method results in probability curves comparable to the curves derived by direct integration in chapter 5.

(a) Case I

In this first case the performance of the crystal silica sand at a relative density of 45 percent is investigated under loading conditions similar to the Taft, Hollister, First, and Figueroa St records (see table 5.1). Similarly to the examples in chapter 5, the water table is assumed at a depth of 2 feet and the pore pressure development is studied at a depth of 25 feet. The soil parameters have been discussed in section 6.3. The shear stress is assumed to be exponentially distributed. The parameter $1/\lambda$ of the acceleration density function is equal to 27 cm/sec^2 which corresponds to a root mean square of shear stress r_c of 110 psf. Using the simulation technique the probability of exceeding a given level of excess pore pressure is computed at the end of each cycle. The results of this analysis are presented in figure 6.4 where the probability of exceeding pore pressure ratios of 0.1, 0.5 and 1.0 is plotted versus the number of cycles of motion. The interpretation of these curves is similar to the one made in chapter 5.

- After 50 cycles the probabilities of exceeding pore pressure ratios of 0.1, 0.5 and 1.0 are 1.0, 0.85 and 0.67, respectively.

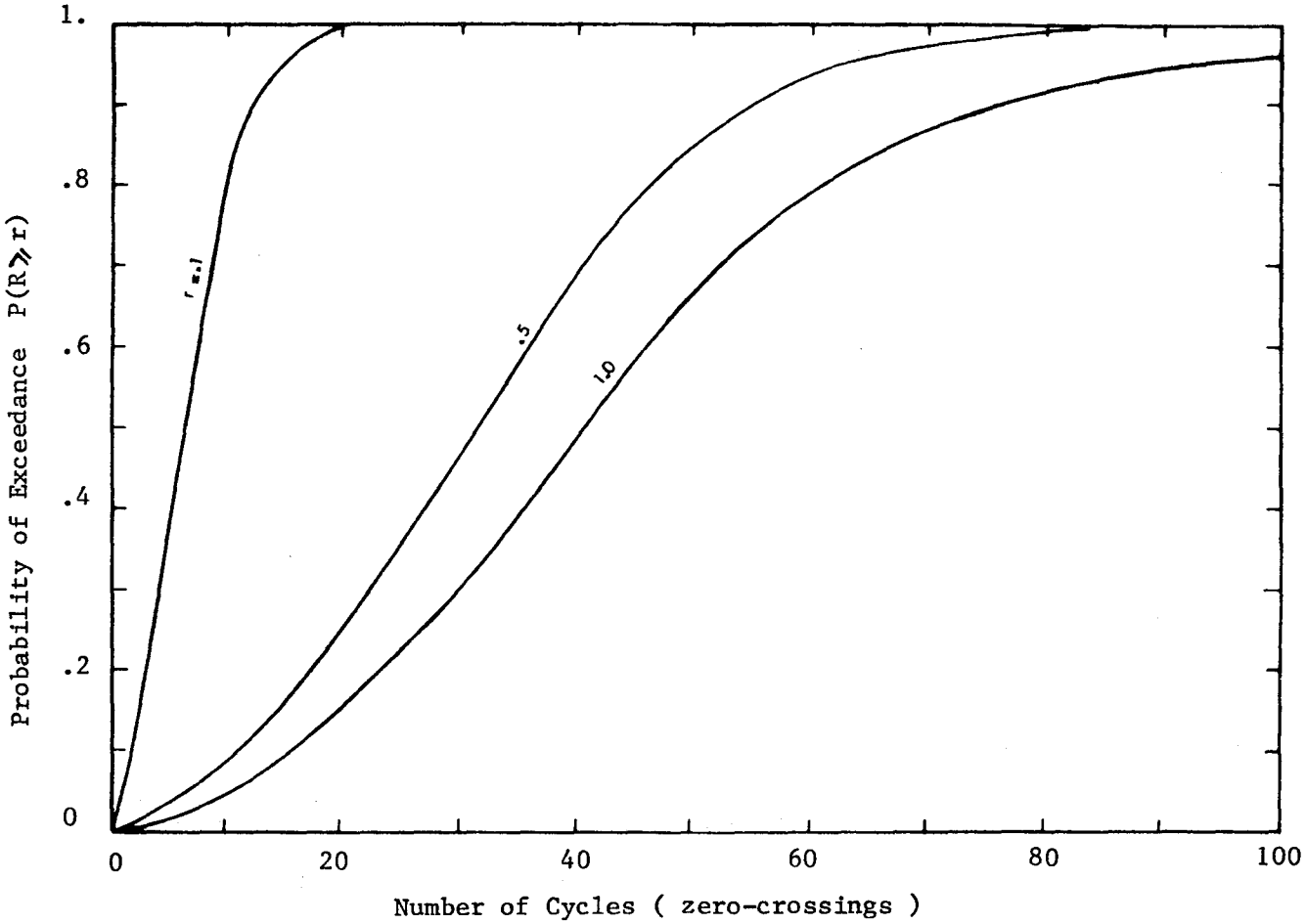

Figure 6.4 Probability Curves Obtained by Simulation - Crystal Silica Sand (D_r = 45%)

- After 100 cycles these probabilities are 1.0, 0.995 and 0.97, respectively.

The probability of reaching the zero effective stress state during an event having characteristics similar to the Figueroa St record is 91 percent, corresponding to 82 cycles. This probability is 100 percent for the Taft record, corresponding to 320 zero-crossings.

(b) Case II

The loading conditions are kept the same, but the crystal silica sand is now considered to have a relative density of 55 percent.The resulting probability curves are given in figure 6.5 for pore pressure ratios of 0.1, 0.5 and 1.0. As expected the probabilities of exceedance are reduced relative to the first case with a looser sand. After 50 cycles the probability of exceeding the zero effective stress state is 0.34, which is half the value obtained for a relative density of 45 percent. After 100 cycles this probability is 0.81, as compared to 0.97 for a relative density of 45 percent. In other words there is a 19 percent chance of not reaching the zero effective stress state if the relative density is 55 percent. At a relative density of 45 percent it is reduced to a 3 percent chance.

(c) Case III

To facilitate direct comparison with results obtained in chapter 5, the simulation technique was applied to Monterey sand at a relative

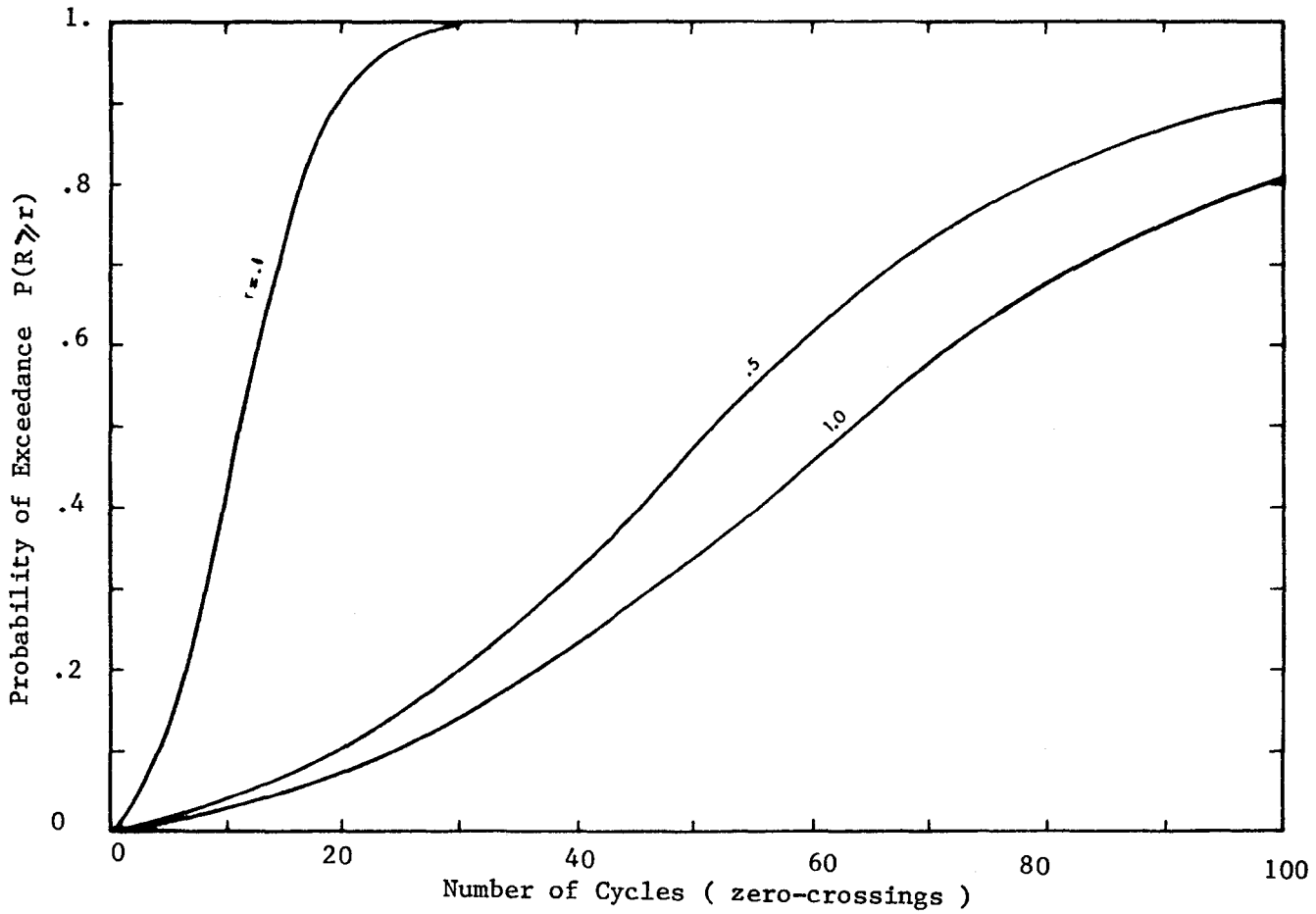

Figure 6.5 Probabbilty Curves Obtained by Simulation - Crystal Silica Sand (D_r = 55%)

density of 54 percent. The loading condition is kept the same as in case 1 of section 5.5.1, with the parameter $1/\lambda$ of the accleration density function equal to 27 cm/sec^2. The Monterey sand is less resistant to liquefaction than the crystal silica sand and consequently the probabilities of exceedance in this case (figure 6.6) are lower than those obtained in the preceeding case (crystal silica sand at a relative density of 55 percent, figure 6.5).

The results in figure 6.6 compare very well with those obtained in figure 5.3 :

- After 50 cycles of loading the probabilities of exceeding pore pressure ratios of 0.1, 0.5 and 1.0 are 1.0, 0.36 and 0.20, respectively. The direct integration method gave probabilities of 0.98, 0.37 and 0.16, respectively.

- After 150 cycles the probabilities of exceeding the same pore pressure ratios are 1.0, 0.96 and 0.87, respectively. Almost identical values were obtained in chapter 5, 1.0, 0.97 and 0.87, respectively.

It is encouraging to note that when applied to similar conditions the experimentally and theoretically based probabilistic models give close results. As a consequence, the discussion given in chapter 5 concerning the behavior of the Monterey sand under different loading conditions also applies to the present model.

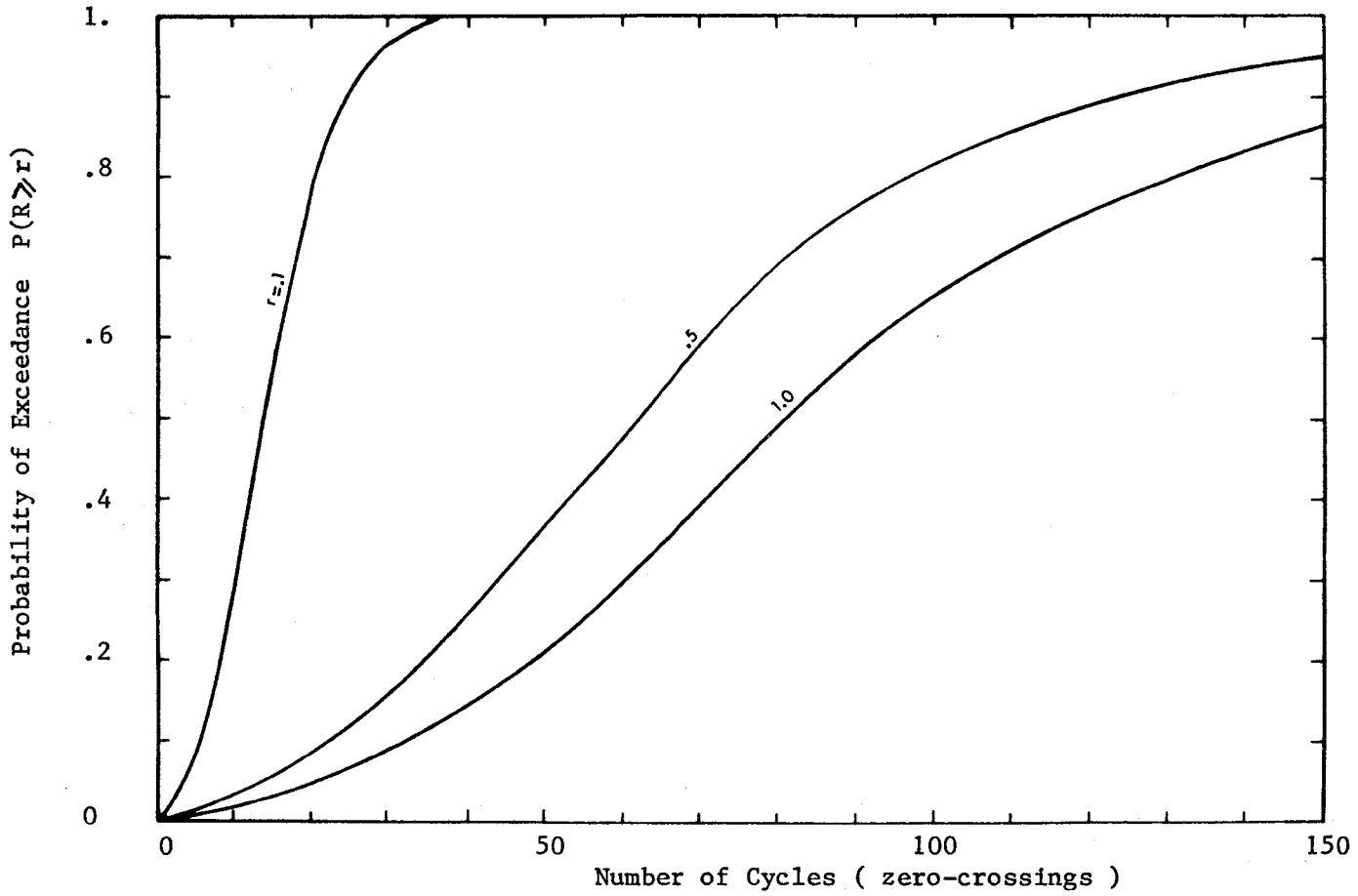

Figure 6.6 Probability Curves Obtained by Simulation - Monterey Sand
(D_r = 54%)

(d) Case IV

The simulation technique is not limited to the exponential distribution of shear stress. This application uses the Rayleigh distribution. The conditions are identical to the Niigata example of chapter 5. The peak ground acceleration of the earthquake is 0.16 g with a sigma ratio of 3.5. The study is performed at a depth of 20 feet with the water table at a depth of 3.5 feet. The parameters necessary to the effective stress model are not available for the medium sand of the Niigata sites. For the purpose of illustration the properties of the Monterey sand at a relative density of 54 percent are used in the analysis. The resulting probability curves are presented in figure 6.7. The probability of exceeding the zero effective stress state is 99 percent after 50 cycles of loading corresponding to the duration of the Niigata earthquake. This is consistent with the results obtained in chapter 5 for the medium sand at a relative density of 53 percent. The Niigata medium sand and the Monterey sand have similar characteristics in terms of cyclic strength curve and it is expected that they exhibit similar behavior under cyclic loading.

The effective stress model and the simulation technique of this chapter yield results similar to those obtained with the probabilistic model based on laboratory data and the direct integration technique. When applied to identical loading conditions and similar soil charateristics the two models give close results. It should be noted that the comparative studies of chapter 5 can also be performed with the simulation model. Similarly, additional uncertainties such as

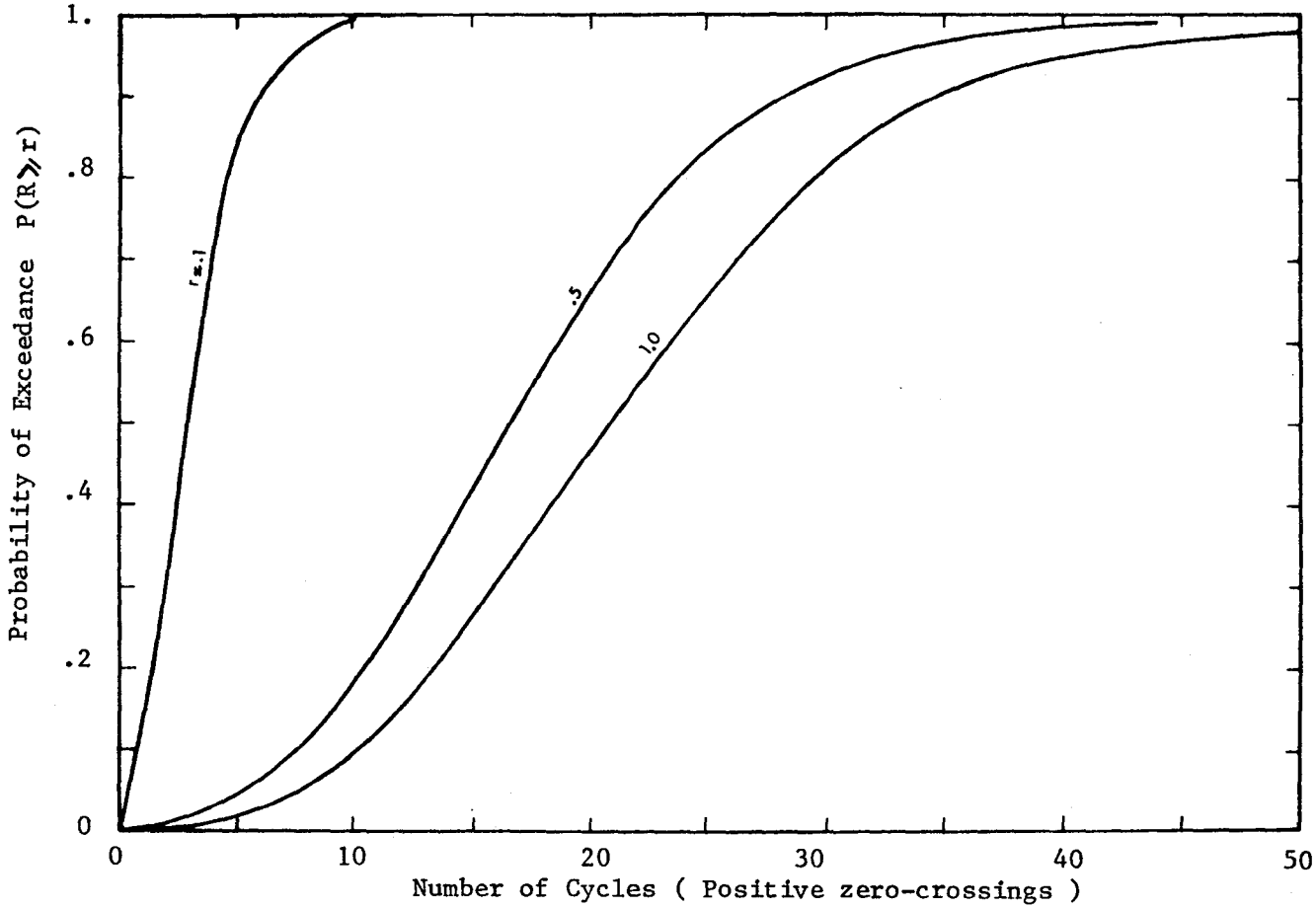

Figure 6.7 Probability Curves Obtained by Simulation - Monterey Sand
(Niigata Conditions)

uncertainty in the number of cycles or in the sigma ratio can be included. In fact it is easier to include these additional uncertainties with the simulation technique. One must only simulate additional parameters rather than perform the new integration required with the integration model of chapters 4 and 5.

6.6 APPLICATION TO OTHER PORE PRESSURE MODELS

The Finn, Lee, and Martin model was used in the preceeding sections for two reasons. First, it is the most comprehensive pore pressure model presently available and it has been extensively tested. Second, the complexity of the model is such that if the simulation technique can be successfully applied to it, it can certainly be applied to simpler pore pressure models. As an example, the following section describes the application of the simulation methodology to the pore pressure model proposed by Sherif and Ishibashi (1979).

The fundamental idea of this model is that the increment of pore pressure during a cycle of loading is function of both the amplitude of the stress cycle and of the previous pore pressure history. This premise is exactly the same as for the non-linear accumulation of pore pressure described in chapter 3. The development of pore pressure under uniform cyclic simple shear loading is defined by :

$$\Delta U_n = (\sigma'_0 - U_{N-1}) \left[\frac{C_1 N}{N^{2-C_3}}\right] \left[\frac{\tau}{\sigma'_{-1}}\right]^{\alpha} \qquad (6.17)$$

where ΔU is the increase in pore pressure during the Nth cycle, U_{-1} the accumulated pore pressure at the end of the (N-1)th cycle, $\sigma'_{-1}(=\sigma'_0-U_{-1})$ the vertical effective stress at the beginning of the Nth cycle and τ the amplitude of the stress cycles. The four constants α, C_1, C_2 and C_3 are obtained from the results of a series of uniform cyclic loading tests performed in a torsional simple shear device. A similar equation is used for the case of non uniform loading :

$$\Delta U_n = (\sigma'_0 - U_{N-1}) \left(\frac{C_1 N'}{N'^2 - C_3}\right) \left(\frac{\tau}{\sigma'_{-1}}\right)^{\alpha} \qquad (6.18)$$

with

$$N' = \sum_{i}^{N} \left(\frac{\tau_i}{\tau}\right)^{\alpha} \qquad (6.19)$$

where τ and τ_i are the shear stress amplitudes during cycles N and i, respectively.

This model and equations are based on the results of fundamental studies and of regression analysis performed on torsional simple shear test data (Sherif and Ishibashi, 1979). Preliminary results indicate that the constants C_1, C_2, C_3 and α are function of soil type and density. The constants C_2, C_3 and α are less soil-dependent than the constant C_1

The above equations can be used in the simulation methodology as an alternative to the Finn, Lee, and Martin model. The techniques to

simulate cyclic strength curves and/or obtain probabilistic pore pressure curves remain the same. The application of this model is described herein for Ottawa sand at a relative density of about 65 percent. The results are given in figures 6.8 to 6.10. The constants C_1, C_2, C_3 and α have mean values equal to 6.13, 1.77, 0.46 and 2.4, respectively (Sherif and Ishibashi, 1979). Since information on the Sherif and Ishibashi model is still very limited, there is no published data available to assess the variability of these constants. It is arbitrarily assumed that they can deviate up to 10 percent from their mean values. This assumption does not seem unreasonable and in any case does not affect the purpose of this section; namely, to illustrate the application of the simulation technique to pore pressure models other than the Finn, Lee, and Martin model. Figure 6.8 presents the median cyclic strength curve obtained with these parameters. The cumulative distribution function of the number of cycles to zero effective stress is given in figure 6.9 for two stress ratios, 0.20 and 0.175. The cumulative distribution functions of pore pressure ratios can also be computed with this model. As an example figure 6.10 presents the results obtained under the loading conditions of the Niigata earthquake. The results in figures 6.8 to 6.10 are not intended to provide definitive probability statements using the Sherif and Ishibashi model. More rigorous analysis can be performed when additional data enable assessment of the uncertainty in the model parameters. But these results demonstrate that the probabilistic methodology can be applied to pore pressure models which differ from the Finn, Lee, and Martin model.

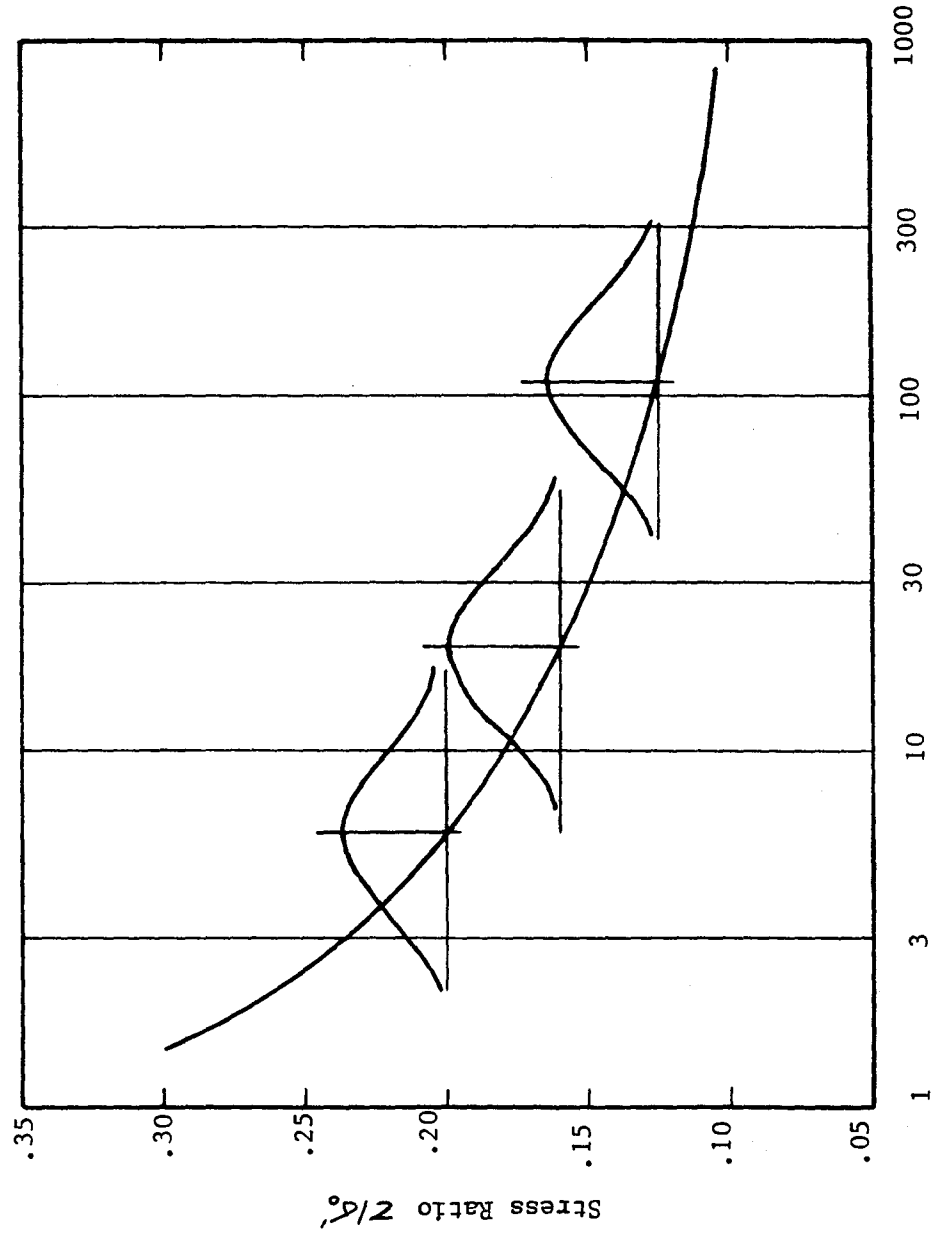

Figure 6.8 Median Cyclic Strength Curve for Ottawa Sand
Obtained with Sherif's Model

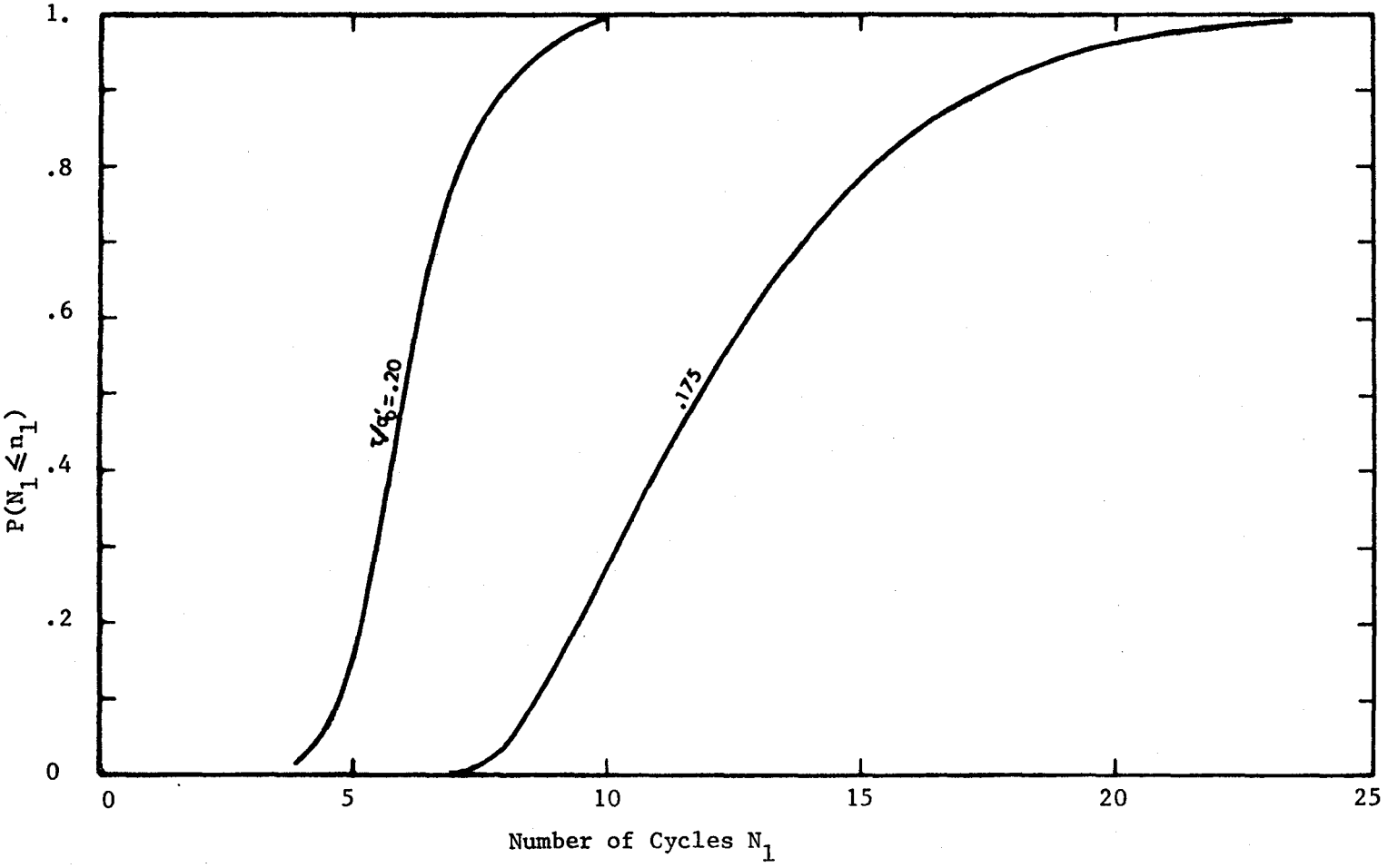

Figure 6.9 Cumulative Distribution Function of the Number of Cycles to Zero Effective Stress - Sherif's Model

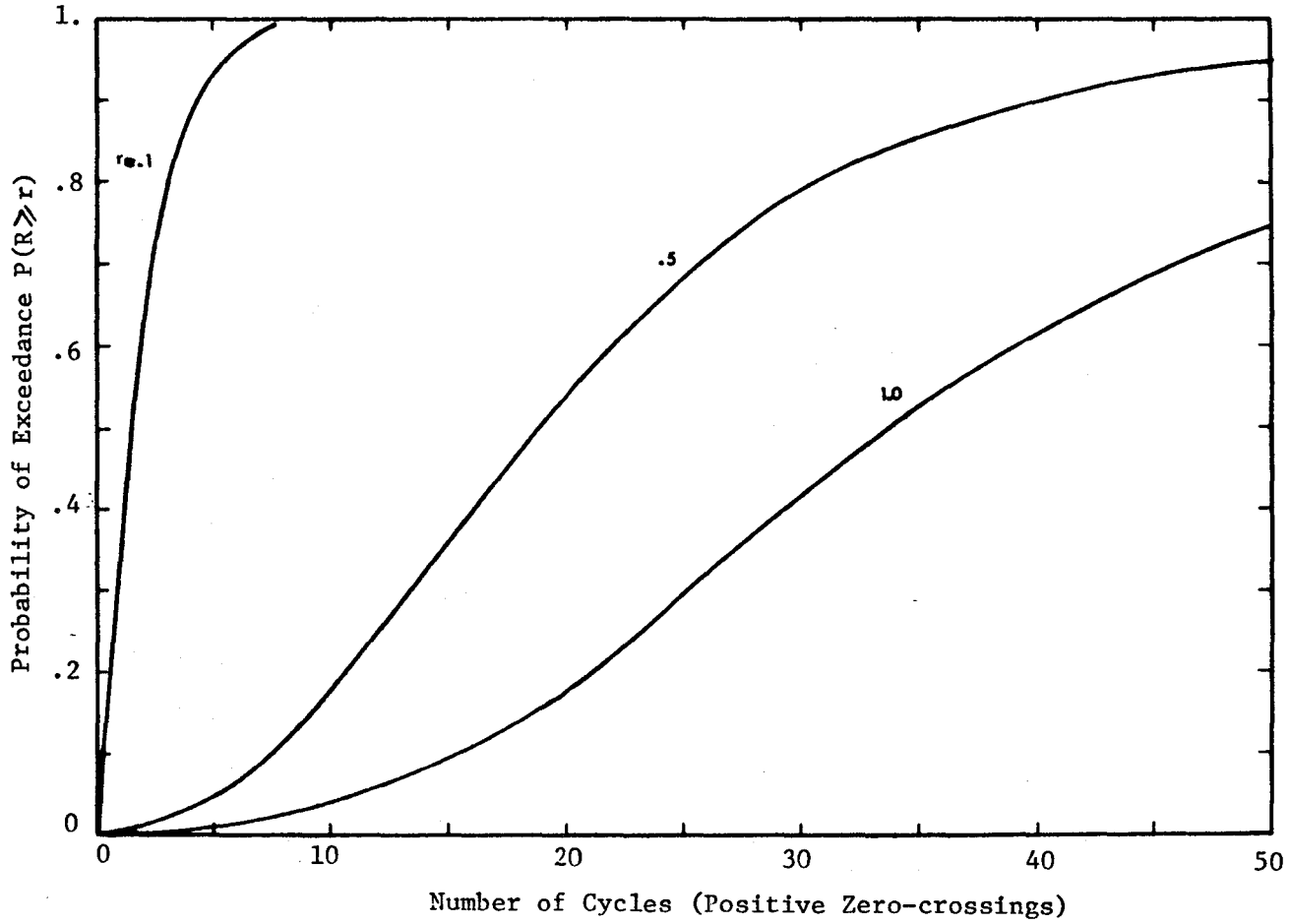

Figure 6.10 Probability Curves - Sherif's Model

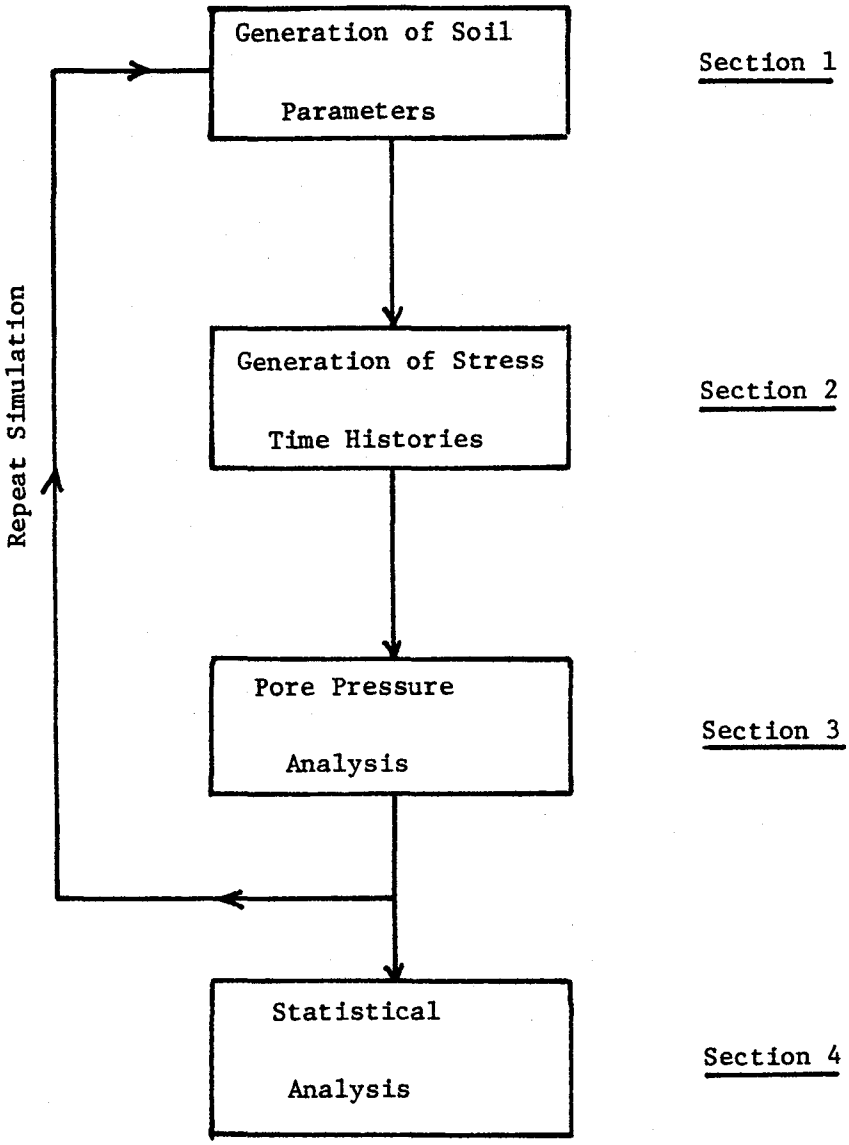

Table 6.3 Organization of Computer Program

The computer program developed to implement this methodology is ordered in four different sections. The simulation and statistical computations (sections 1, 2 and 4 in table 6.3) are performed independently of the pore pressure analysis (section 3). The introduction of a new pore pressure model is done simply by transforming section 3 so that it performs the computations prescribed by the new model. As a consequence very limited effort is necessary to incorporate a new pore pressure model in the computer program.

6.7 SUMMARY

In this chapter an effective stress model has been used to probabilistically study the development of pore pressure under random loading. A simulation algorithm generates samples of the soil parameters and of the shear stress time histories. The development of pore pressure is then computed using an effective stress model. At the end of the simulation procedure the statistical characteristics of the pore pressure are computed as a function of the number of cycles of loading.

The effective stress model and the simulation technique provide results similar to those obtained by the model based on laboratory data and direct integration technique. When applied to identical loading conditions and similar soil characteristics the two models give close results. This indicates that one can reliably use either one of the models, depending upon which kind of data are available. The computer program developed to implement the model can easily be transformed to incorporate any desired pore pressure generation model.

Chapter VII

PROBABILISTIC PORE PRESSURE ANALYSIS AND SEISMIC HAZARD EVALUATION

7.1 INTRODUCTION

This chapter demonstrates how the probabilistic pore pressure analyses developed in the preceding chapters can be incorporated into a methodology for seismic hazard evaluation. First a theoretical formulation is presented which shows that existing seismic hazard analysis procedures can be formally extended to assess the hazard in terms of a soil related parameter, the level of pore pressure. In this formulation the seismic hazard evaluation for root mean square of acceleration becomes the input to the seismic hazard evaluation for pore pressure. The hazard methodology applied to pore pressure necessitates the knowledge of the statistical relation between root mean square of acceleration and duration of the earthquake. Since this relation is not completely known at present, reasonable assumptions are required to enable the development of a practical formulation of the methodology. Finally several applications of this seismic hazard methodology for pore pressure are presented.

7.2 HAZARD ANALYSIS. THEORETICAL FORMULATION

The overall methodology for performing seismic hazard assessments has been presented and discussed by several investigators (Cornell, 1968,

Cornell and Merz, 1975, Mc Guire, 1974 and 1976, Shah, Mortgat, Kiremidjian and Zsutty, 1975, Mortgat, 1976). The seismic hazard is usually expressed in terms of peak ground acceleration, root mean square of acceleration or response spectrum. The purpose of the present section is to show that the seismic hazard methodology can be taken one step further to express the hazard in terms of a soil related parameter, the level of pore pressure.

7.2.1 Summary of existing seismic hazard methodologies

In general a given site is surrounded by a number of independent seismic sources. For design purposes, the probabilistic loading at the site is obtained by combining the effect of all the sources. In order to do so the following steps are necessary :

- The seismic sources that can affect the site under consideration are located.

- The seismicity of each source is determined. The seismicity is considered homogeneous over the entire source. A Poisson model is used to estimate earthquake occurrence. It implies : (1) Earthquakes are spatially and temporally independent; and, (2) The probability that two seismic events will occur at the same time and at the same location approaches zero. With these assumptions the seismicity can be described by $P_t(i,M)$, the probability of having i occurrences of events of magnitude M for a given period of time t.

- An attenuation law is used to transfer information from the sources to the site. The historical earthquake record and local attenuation data are combined to produce the functional relationships applicable to the area under consideration. Typically the attenuation law has the form :

$$r_a \text{ or } PGA = \frac{b_1 \exp(b_2 M)}{(D+b_4)^{\,3}} \qquad (7.1)$$

where D is the significant distance from the site to the source and b_1, b_2, b_3 and b_4 are regression constants. A probability density function is chosen to express the uncertainty in the attenuation law. This density function is usually a lognormal distribution (Mc Guire, 1977).

- The seismic sources are divided into point sources made of small segments or small areas. The total probable activity of a point source is evaluated in terms of magnitude and occurrences of each magnitude. Using the transfer function from the source to the site, the total effect of the activity of the point source is calculated at the site. Assuming independence between events, the cumulative effect of additional segments and areas is obtained until all the seismic sources modeled in the region have been covered.

This methodology results in the probabilities of exceeding discrete values of the peak ground acceleration, or of the root mean square of acceleration for a given time period. Usually the results are expressed

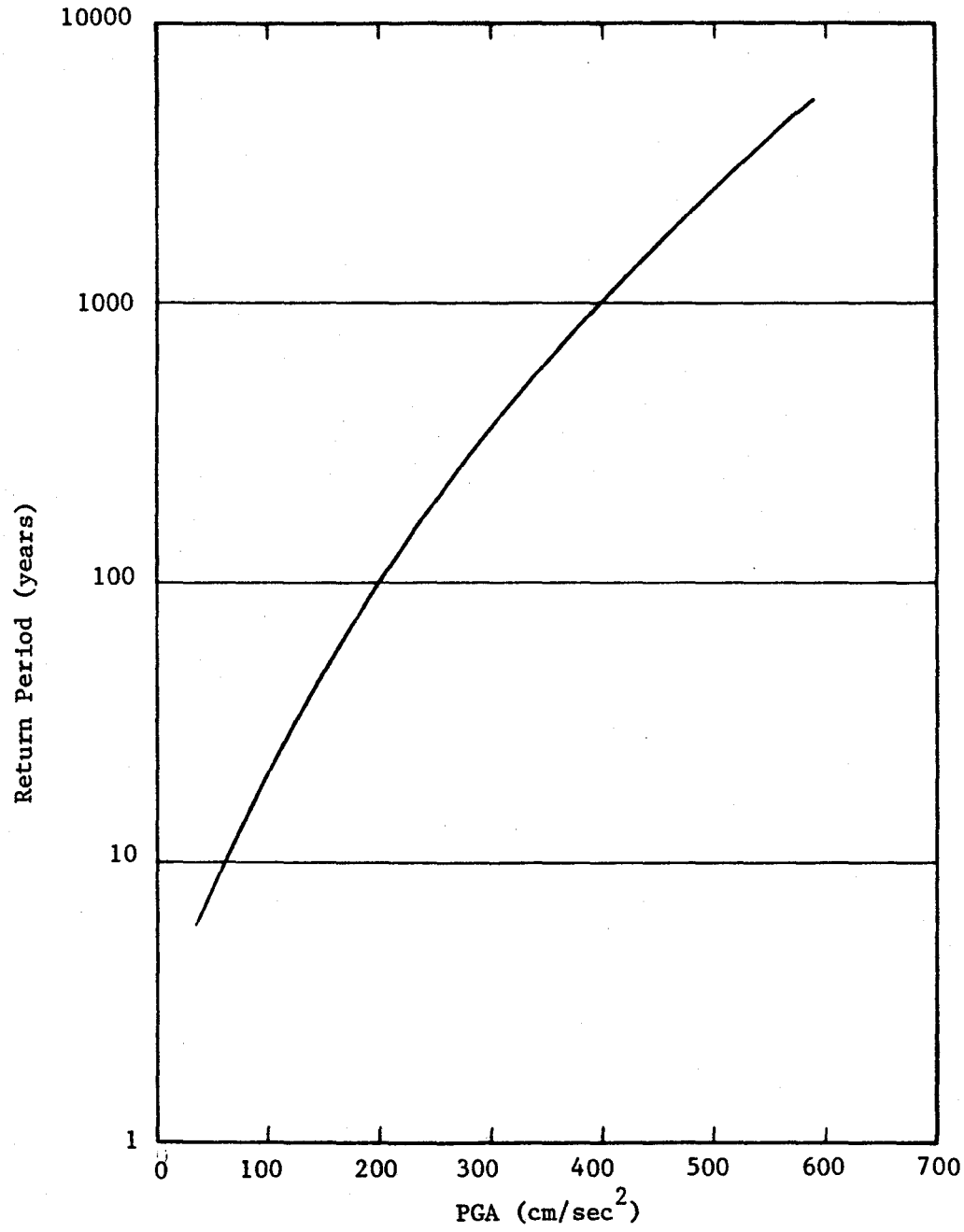

Figure 7.1 PGA versus Return Period

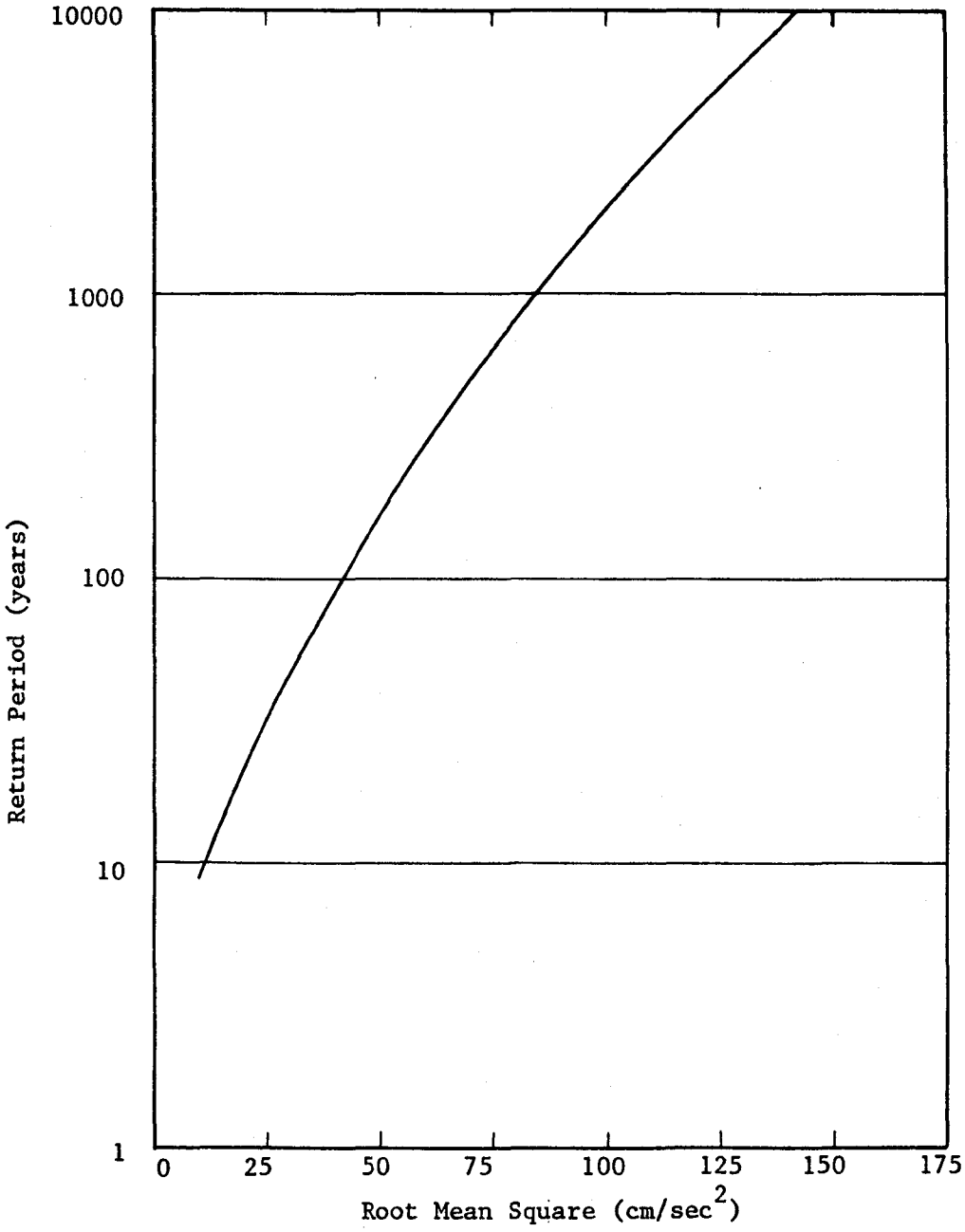

Figure 7.2 Root Mean Square of Acceleration Versus Return Period

by graphs which relate the peak ground acceleration or the root mean square to a given return period. Typical examples of these graphs are given in figures 7.1 and 7.2. The return period is the inverse of the annual probability of exceedance of the PGA or r_a to which it corresponds.

Similar concepts can be applied to obtain the probability of exceeding a certain level of pore pressure at a site, for a given seismic environment and a given time period. This is done by first defining the contribution of a point seismic source and then summing the contribution of all sources.

7.2.2 Contribution of a point source

Consider a point seismic source at a distance D from the site. Since the distance from the source to the site is known, the parameters of the attenuation relationship and of its uncertainty are known.The probability of exceeding a root mean square value greater than or equal to r_a given an event M is :

$$P = \int_{r_a}^{+\infty} f_{R_a|M}(r_a,M)\, dr_a \qquad (7.2)$$

where $f_{R_a|M}(r_a,M)$ is the density function which expresses the uncertainty in the attenuation law. The contribution to root mean square values greater than or equal to r_a of all events M occurring at the point source is written as :

$$P(\text{root mean square} \geq r_a | M) = \sum_{i=1}^{\infty} (1-q^i) P_t(i,M) \qquad (7.3)$$

where :

$P(\text{root mean square} \geq r_a/M)$ is the probability of obtaining a root mean square greater than or equal to r_a.

$P_t(i,M)$ is the probability of i occurrences of events M during the time period t.

and q is equal to 1-p; p is given by equation 7.2.

The above expression can be differentiated to obtain :

$$f_{r_a|M}(r_a,M) = \frac{d[1-P(\text{root mean square} \geq r_a|M)]}{dr_a} \qquad (7.4)$$

which is the conditional probability density function of the root mean square r_a given the magnitude M. The joint probability density function of r_a and N the number of cycles (zero-crosings) is expressed as :

$$f_{(N,r_a)|M}(N,r_a,M) = f_{N|r_a|M}(N,r_a,M) f_{r_a|M}(r_a,M) \qquad (7.5)$$

In this expression it is assumed that information exists on the statistical relation between root mean square, duration and magnitude (formally expressed by $f_{N|r_a|M}[\cdot]$). The joint distribution of r_a and N

represents the seismic input to the hazard methodology for pore pressure build-up. It has now to be combined with the probabilistic pore pressure analysis developed in the previous chapters, which produced the probability of exceeding a certain pore pressure ratio r as a function of the number of cycles (zero-crossings) of loading. This probability was expressed by pore pressure probability curves in chapters 5 and 6 which represent :

$$P(R \geq r | r_a, N) \quad \text{for } 0 \leq r \leq 1 \tag{7.6}$$

where $P[R>r/r_a,N]$ is the probability that the pore pressure ratio R will be greater than or equal to r given the root mean square r_a and the number of cycles N. Combining equations 7.5 and 7.6 yields :

$$P(r \geq r | M) = \int_N \int_{r_a} P[R \geq r | r_a, N] \, f_{(N, r_a) | M}(N, r_a, M) \, dr_a \, dN \tag{7.7}$$

which is the probability of exceeding a pore pressure ratio r given the magnitude M. Assuming independence between events the dependence on M is removed :

$$P(R \geq r) = 1 - \prod_M [1 - P(r \geq r | M)] \tag{7.8}$$

where the product sign π integrates the contribution of all magnitudes. $P[R \geq r]$ is the probability of exceeding the pore pressure ratio r at least once during the time period t due to events occurring at the point source.

7.2.3 Contribution of all sources

A seismic source is divided in several point sources, made of small segments or small areas. As the events are assumed independent from point source to point source, the contribution of a source is obtained as :

$$P(R \geq r)_{\text{one source}} = 1 - \prod_{\text{all sources}} [1 - P(R \geq r)_{\text{one point source}}] \qquad (7.9)$$

When several sources are considered, the same principle is applied for each source :

$$P(R \geq r) = 1 - \prod_{\text{all sources}} [1 - P(R \geq r)_{\text{one source}}] \qquad (7.10)$$

This expression gives the probability of at least one occurrence at the site of a pore pressure ratio greater than or equal to the level r.

7.2.4 Discussion of the theoretical formulation

The derivation in sections 7.2.2 and 7.2.3 demonstrates that seismic hazard evaluation concepts can be applied to a soil related parameter such as pore pressure. The formulation is very similar to previous formulations for PGA and root mean square of acceleration (Cornell, 1968, Mc Guire, 1976, Mortgat, 1976) but it incorporates one more step in which the seimic analysis is combined with the pore pressure analysis (equation 7.7). Existing hazard analysis computer programs could theoretically be transformed to accomodate this supplementary step and

express the hazard in terms of pore pressure. However an important problem lies in the fact that information is needed on the statistical relation between root mean square, duration, and magnitude expressed by $f_{NRaM}[\cdot]$ in equation 7.5. Available studies and results to assess this relation are very sparse. Duration was not an essential parameter of previous hazard analysis studies and very little attention was devoted to it. Seismic hazard analysis investigations were initially performed for peak ground acceleration without any specific regard to duration. More recent analyses based on root mean square of acceleration used implicitly a duration expressed in terms of number of cycles. But these studies were concerned with the definition of an effective acceleration which is fairly insensitive to the duration (Mortgat, 1979). The lack of information on duration is further explained by the limited data available. There have been relatively few large magnitude events and the data from them are biased by the few well instrumented earthquakes such as the 1971 San Fernando event. The preceeding remarks show why relatively little is known about duration and its relation to r_a and M. However, under the impulse of seismic investigations for nuclear power plants, research studies on this subject are under way in several institutions and consulting companies. Until further results become available, certain assumptions must be made in order to perform a seismic hazard analysis using duration as a parameter. This is the subject of the next section which presents a practical hazard formulation for pore pressure.

7.3 HAZARD ANALYSIS. PRACTICAL FORMULATION

Figure 7.2 describes typical results of a seismic hazard analysis based on root mean square of acceleration. Each value of r_a is associated with a return period T. The annual probability of exceedance of the root mean square is 1/T and the cumulative distribution function of r_a is :

$$F_{r_a}(r_a) = 1 - 1/T \qquad (7.11)$$

By differentiation the probability density function of r_a is obtained as :

$$f_{r_a}(r_a) = \frac{1}{T^2}\frac{dT}{dr_a} \qquad (7.12)$$

where dT/dr_a is the slope of the curve in figure 7.2. Given this function the joint probability density of r_a, the root mean square, and N, the number of cycles is expressed by :

$$f_{r_a,N}(r_a,N) = f_{N|r_a}\, f_{r_a}(r_a) \qquad (7.13)$$

where $f_{N|r_a}(\bullet)$ is the conditional probability density function of the number of cycles N given the root mean square r_a. Assumptions will be necessary to define this function.

Equation 7.13 can be combined with the pore pressure analysis to obtain the annual probability of exceedance of the pore pressure ratio R :

$$P(R \geq r) = \int_N \int_{r_a} P(R \geq r | r_a, N) f_{r_a, N}(r_a, N) dr_a dN \qquad (7.14)$$

With the preceeding equations the seismic hazard analysis for pore pressure involves the following steps :

1) Perform a seismic hazard analysis in terms of root mean square and obtain a root mean square versus return period graph.

2) From this graph develop the density function of the root mean square (equation 7.12).

3) Make assumptions on the conditional function $f_{a}(\bullet)$.

4) Numerically perform the integration over all possible values of root mean sqare r_a and number of cycles N (equation 7.14).

The assumptions used to express the statistical relation between the number of cycles N and the root mean square r_a are based upon a review of the work by Vanmarcke and Lai (1977), Hanks (1979), Mortgat (1979), Shah and Mc Cann (1979), and Zsutty and De Herrera (1979 and 1980). At present two assumptions can be made :

- Assumption 1 : The root mean square r_a and duration N are considered to be statistically independent. This approach was used by Mortgat (1979) and is substantiated by previous work on PGA and

duration (Lee and Chan, 1972, Yegian, 1976). The physical reasoning behind it is that earthquake source mechanisms, travel paths and local conditions are so complex that earthquakes having same PGA or root mean square can be associated with completely different duration.

With this assumption equation 7.14 reduces to :

$$P(R \geq r) = \int_N \int_{r_a} P[R \geq r | r_a, N] f_N(n) f_{r_a}(r_a) dr_a dN \qquad (7.15)$$

where f (N) is the probability density function of N, the number of zero-crossings. N can be assumed to be uniformly distributed between a minimum and a maximum value. Based upon the limited data available the minimum and maximum values are about 50 and 350, respectively. Other distributions could also be considered such as the Chi-square distribution (Hanks, 1979 and Shah, 1980).

- Assumption 2 : A weak dependence between number of cycles and root mean square is assumed. Considering available results (Vanmarcke and Lai, 1977, and Zsutty, and De Herrera, 1979 and 1980) there is a slight trend to indicate that the range of N values increases with r_a. As an example small r_a values are generally associated with N values between 50 and 150, while large r_a are associated with N between 125 and 350. As a consequence the number of cycles N can be made weakly dependent on r_a and the conditional probability density function $f_{N|r_a}(N, r_a)$ is built as described in figure 7.3.

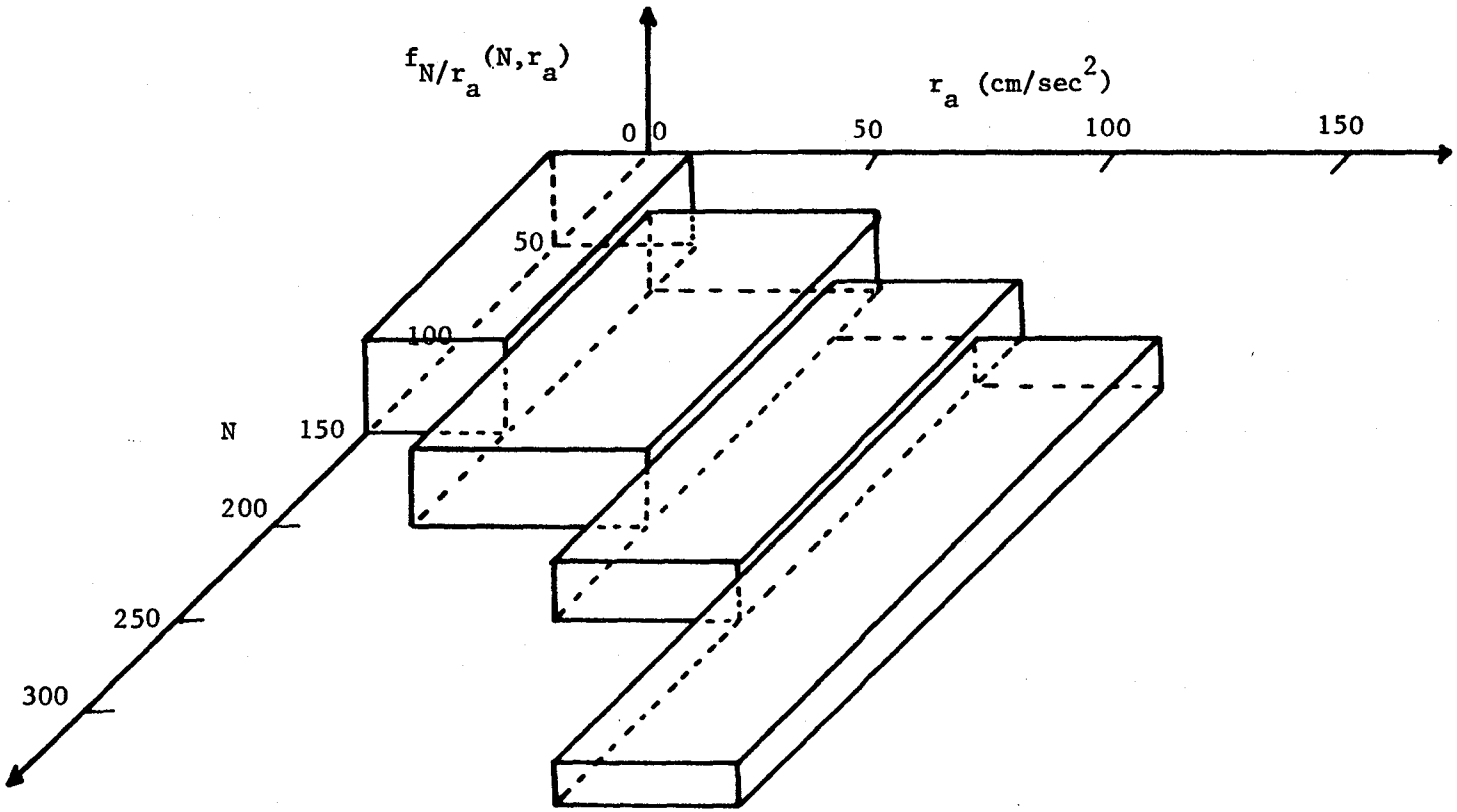

Figure 7.3 Conditional Probability Density Function of the Number of Zero-crossings N Given the Root Mean Square of Acceleration r_a (Weak Dependence)

The r_a axis is decomposed in several ranges and within each range the N values are equiprobable between a minimum and a maximum value. These values are the author's best estimates based upon the available data. Recognizing that the data are very limited, an actual hazard analysis should include a sensitivity study on these minimum and maximum values. An example of such a sensitivity study is described in the next section.

The pore pressure hazard analysis methodology is completely defined by equations 7.11 to 7.15. Typical applications and results are presented in the next section.

7.4 APPLICATIONS OF THE SEISMIC HAZARD METHODOLOGY

In order to assure consistency with the preceeding chapters these applications use examples with site conditions the same as those employed in chapters 5 and 6. The soil is assumed to consist of sand having the characteristics of Monterey sand with the water table at a depth of two feet. Two relative densities are considered, 68 and 54 percent, for which the development of pore pressure at a depth of 25 feet has been studied in details in chapters 5 and 6.

(a) Case I

The hazard analysis is performed for a relative density of 68 percent and a pore pressure ratio of 1.0 (liquefaction). The root mean square versus return period curve in figure 7.2 describes the seismic hazard at

the site in terms root mean square of acceleration. This curve approximatively represents the conditions expected for a site located in the Bay area close to the San Andreas fault, such as Stanford.In this application it is assumed that the root mean square r_a and the number of cycles N are independent (assumption 1). The results of the analysis are given in figure 7.4. The probability of exceeding the pore pressure ratio R = 1.0 is expressed as a function of the time period under consideration. This probability is 0.43 for a 50 year time period and 0.68 for a 100 year time period. Such high numbers are to be expected for a site close to the San Andreas fault.

(b) Case II

The data for this case are kept the same, except that the assumption of weak dependence between root mean square and number of cycles (assumption 2) is used in the analysis. Figure 7.5 presents the computed probabilities of exceedance for this case. The probability of exceeding R = 1.0 is 0.36 for a 50 year time period and 0.59 for a 100 year time period. These results are about 20 percent lower than those obtained with assumption 1. Assumption 2 restricts the range of possible N values and as a consequence yields lower probabilities of exceedance.

(c) Case III

The two preceding cases present different estimates of the hazard, depending upon the assumption used. Even if it is not uncommon for engineering analyses to provide several answers corresponding to several

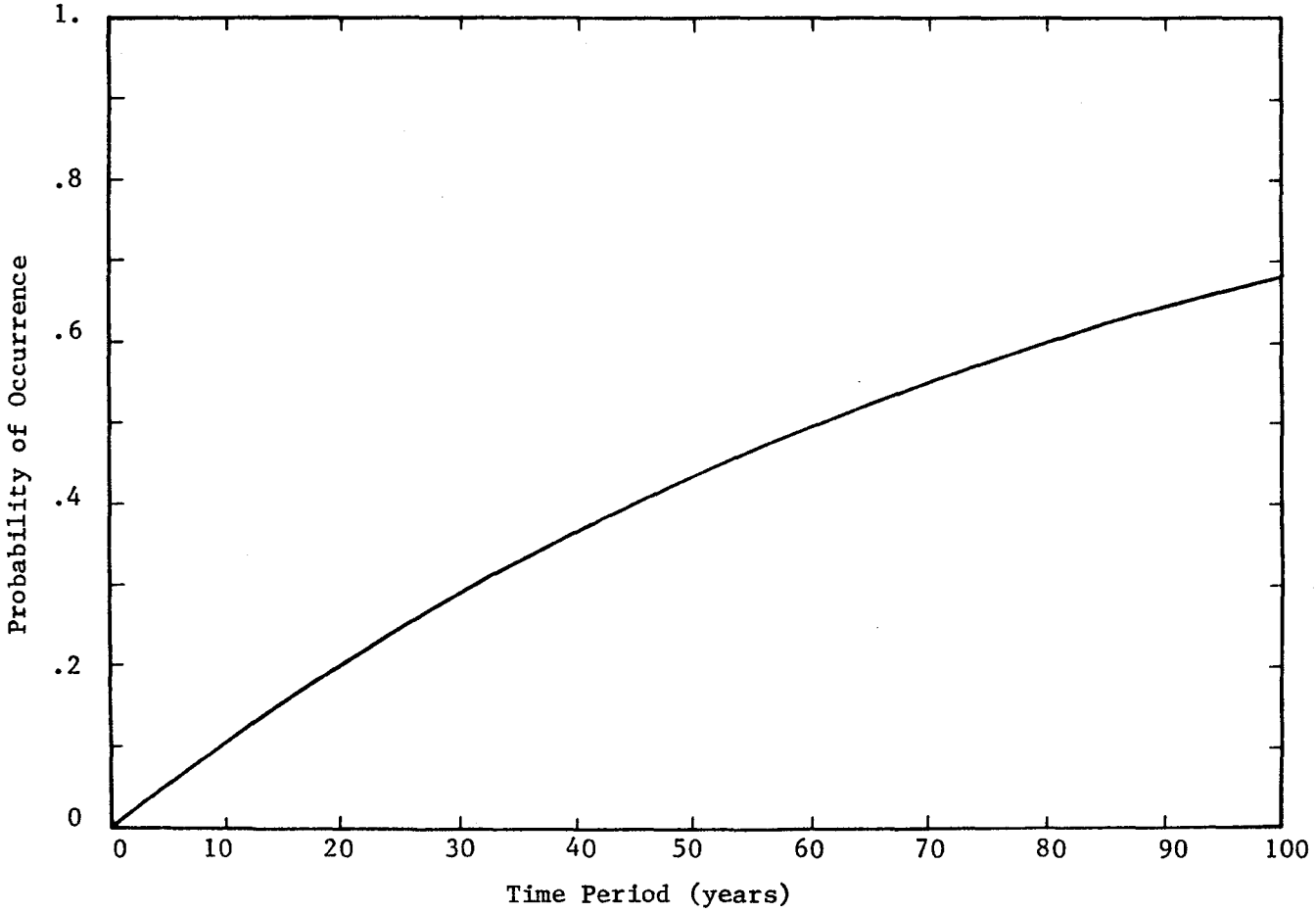

Figure 7.4 Seismic Hazard Evaluation for a Pore Pressure Ratio of 1.0
(D_r = 68%, assumption 1)

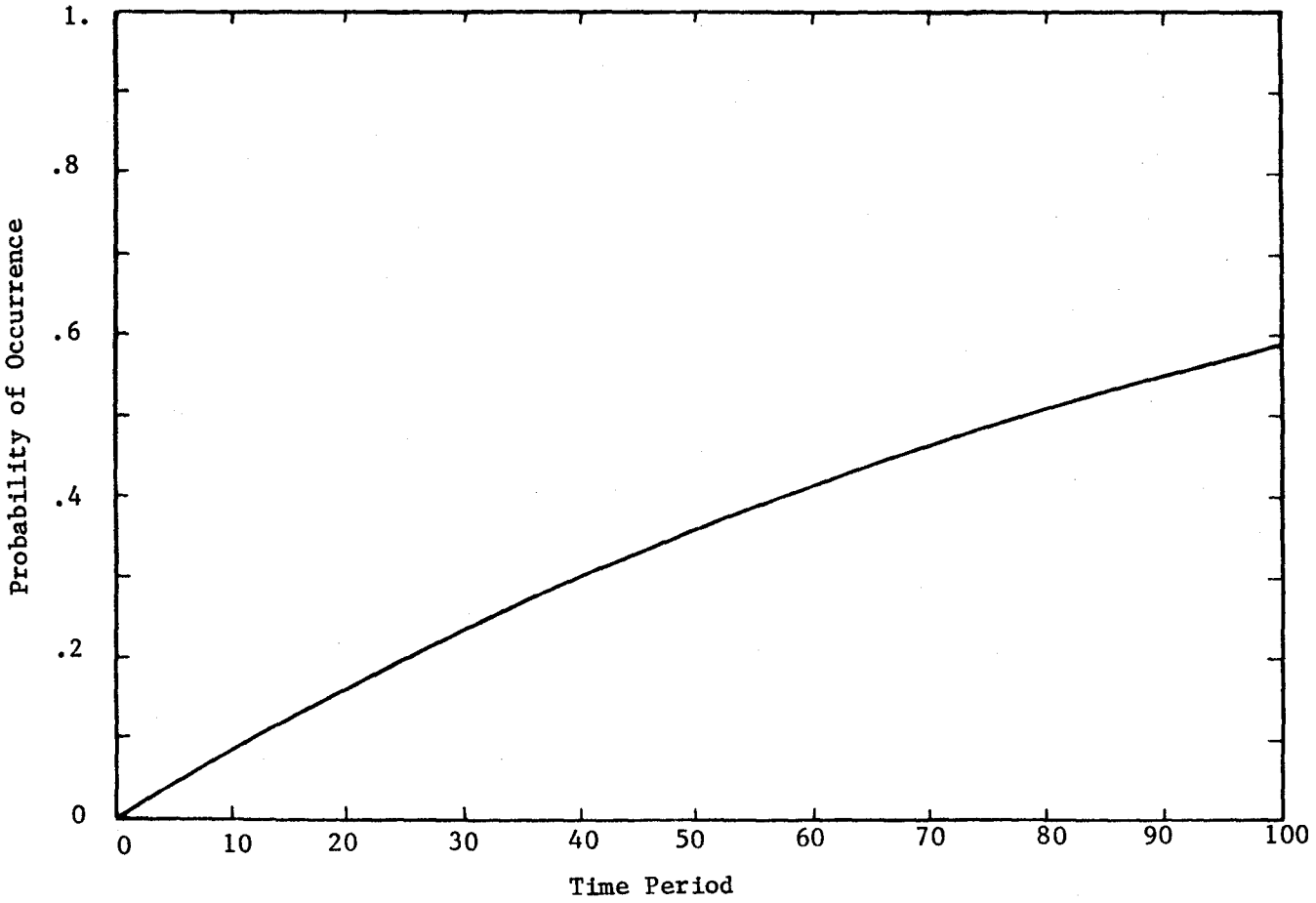

Figure 7.5 Seismic Hazard Evaluation for a Pore Pressure Ratio of 1.0
(D_r = 68%, assumption 2)

assumptions, it is in general more efficient to provide a unique answer. This can be done by a weighted or Bayesian analysis of the results. The estimate of the hazard can be computed as the weighted results from m individual calculations :

$$P[R \geq r] = \sum_{i=1}^{m} P_i(R \geq r)\, w_i \qquad (7.16)$$

where $P_i[R>r]$ is the probability that R is greater than or equal to r using analysis i, and w_i is the subjective weight given to the sensitivity analysis i. In the present study, the sensitivity analyses represent : (1) The inability to make a definitive choice between assumptions 1 and 2 and (2) The uncertainties in the limits of the number of cycles N values within each assumption. To illustrate the use of equation 7.16 the author performed 4 sensitivity analyses :

- Sensitivity analysis 1 : Assumption 1 with N uniformly distributed between 50 and 350 (identical to case I)

- Sensitivity analysis 2 : Assumption 2 and $f_{N|r_a}(N,r_a)$ given in figure 7.3 (identical to case II)

- Sensitivity analysis 3 : Assumption 1 with N uniformly distributed between 50 and 300

- Sensitivity analysis 4 : Same as analysis 2 but minimum and maximum N values reduced by 25 and 50, respectively.

A weight of 1/3 was assigned to each of analyses 1 and 2. Analyses 3 and 4 were each given a weight of 1/6. The weights represent the author's subjective judgement. They mean that assumptions 1 and 2 are considered 50 percent probable and that within each assumption one sensitivity analysis has twice more weight than the other. The results obtained from the weighted average of these four analyses (equation 7.16) are presented in figure 7.6. This figure shows the best estimate, together with an estimate of the lower and upper limits. These limits can be roughly taken as the one standard deviation with respect to the best estimate. According to the best estimate curve, the probability of exceeding R = 1.0 is 38 percent in a time period of 50 years and 62 percent in 100 years.

(d) Case IV

The hazard analysis methodology can be applied to pore pressure ratios other than 1.0. Figure 7.7 presents the results obtained for a pore pressure ratio R = 0.50. The conditions of this analysis were identical to the conditions of case I. The probabilities of exceedance are 0.57 and 0.81 for time periods of 50 and 100 years, respectively. These values are about 30 percent higher than those obtained for a pore pressure ratio of 1.0.

(e) Case V

The probability of exceedance of a pore pressure ratio for a given time period depends upon the seismic hazard conditions expressed in

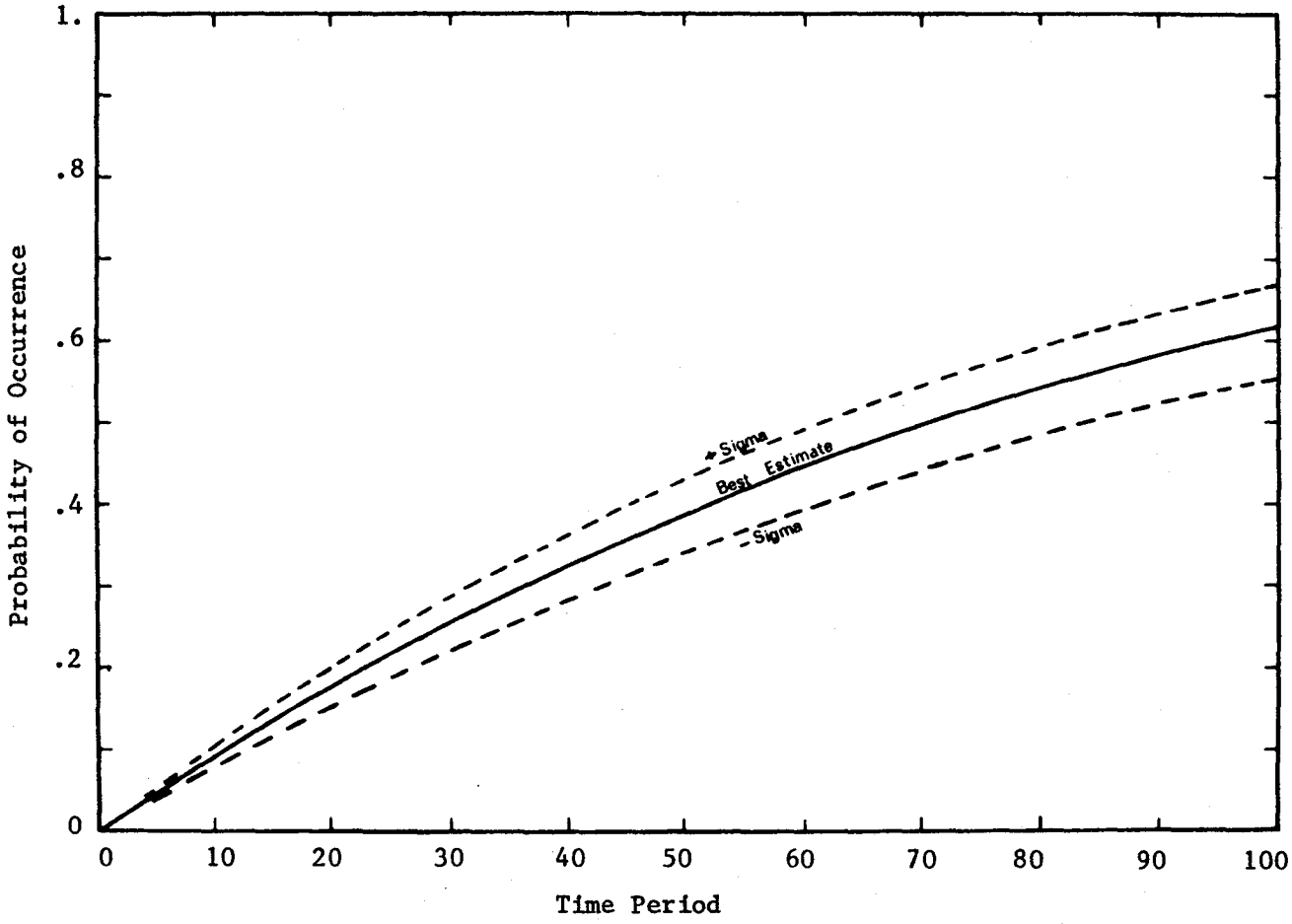

Figure 7.6 Seismic Hazard Evaluation for a Pore Pressure Ratio of 1.0
(D_r = 68%, weighted Analysis)

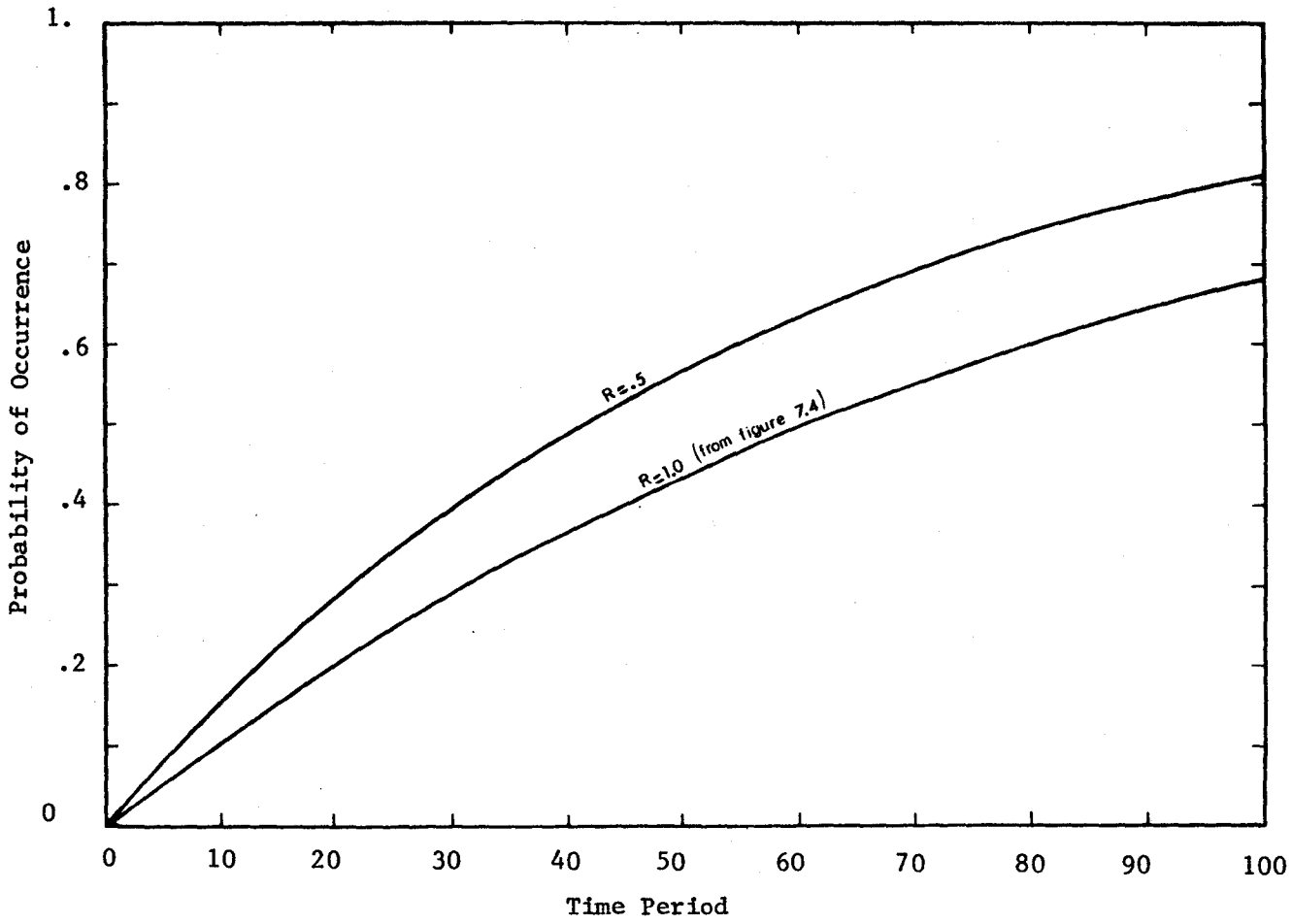

Figure 7.7 Seismic Hazard Evaluation for a Pore Pressure Ratio of 0.50
(D_r = 68%, assumption 1)

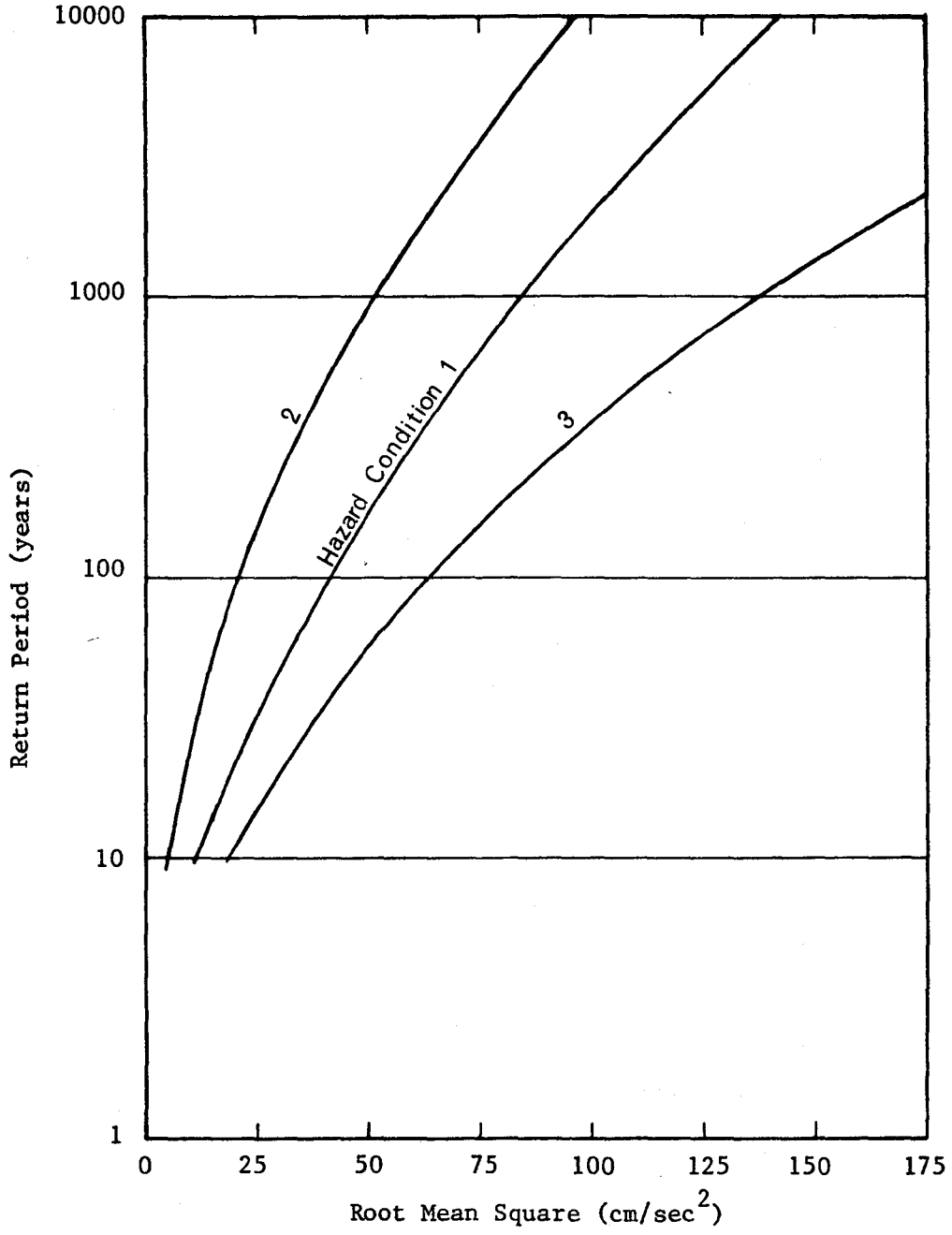

Figure 7.8 Root Mean Square of Acceleration
Versus Return Period Curves

terms of root mean square of acceleration. Figure 7.8 presents three root mean square versus return period curves corresponding to three different seismic hazard conditions. Curve 1 is the curve previously used in cases I and II (figure 7.2). For a given return period curve 2 yields a smaller root mean square than does curve 1, thus representing a less severe condition. Physically it means that the site to which curve 2 applies is located farther from the main seismic sources or in an area of lower seismic activity. On the contrary curve 3 corresponds to a more severe condition (higher root mean square values). The case I analysis is repeated for hazard conditions 2 and 3. The computed results are plotted in figure 7.9 together with the results obtained in case I. The probability of exceeding R = 1.0 under the condition 1 is 68 percent in 100 years. This probability is reduced to 18 percent under condition 2, and increased to 94 percent under condition 3. It has to be recognized that even curve 2 represents a relatively severe condition. Much lower seismic hazard conditions would apply to a site located in a less seismic area, such as the Eastern United States.

(f) Case VI

The effect of soil resistance is demonstrated by comparing figure 7.10 to figures 7.4 and 7.7. The results in figure 7.10 were obtained under the conditions of case I but for a relative density of 54 percent. The reduction in relative density increases significantly the probability of at least one occurrence of a given pore pressure ratio during a given time period. The probability of at least one occurrence of the ratio R = 1.0 increases from 68 percent to 85 percent for a time

period of 100 years. Similar remarks apply for other time periods and for a pore pressure ratio of 0.5.

7.5 SUMMARY

The probabilistic pore pressure analysis has been incorporated into a seismic hazard analysis framework. The conditional probability of exceeding a given pore pressure ratio is combined with the joint distribution of root mean square and number of cycles. This results in the probability of exceeding at least once a certain pore pressure ratio for a given seismic environment and a given time period. In order to perform such an analysis assumptions are made on the statistical relationship between root mean square and duration. Sensitivity studies are performed to take into account the uncertainties underlying these assumptions. Typical applications described how the assumptions, seismic environment, and site resistance affect the hazard assessment at a given site.

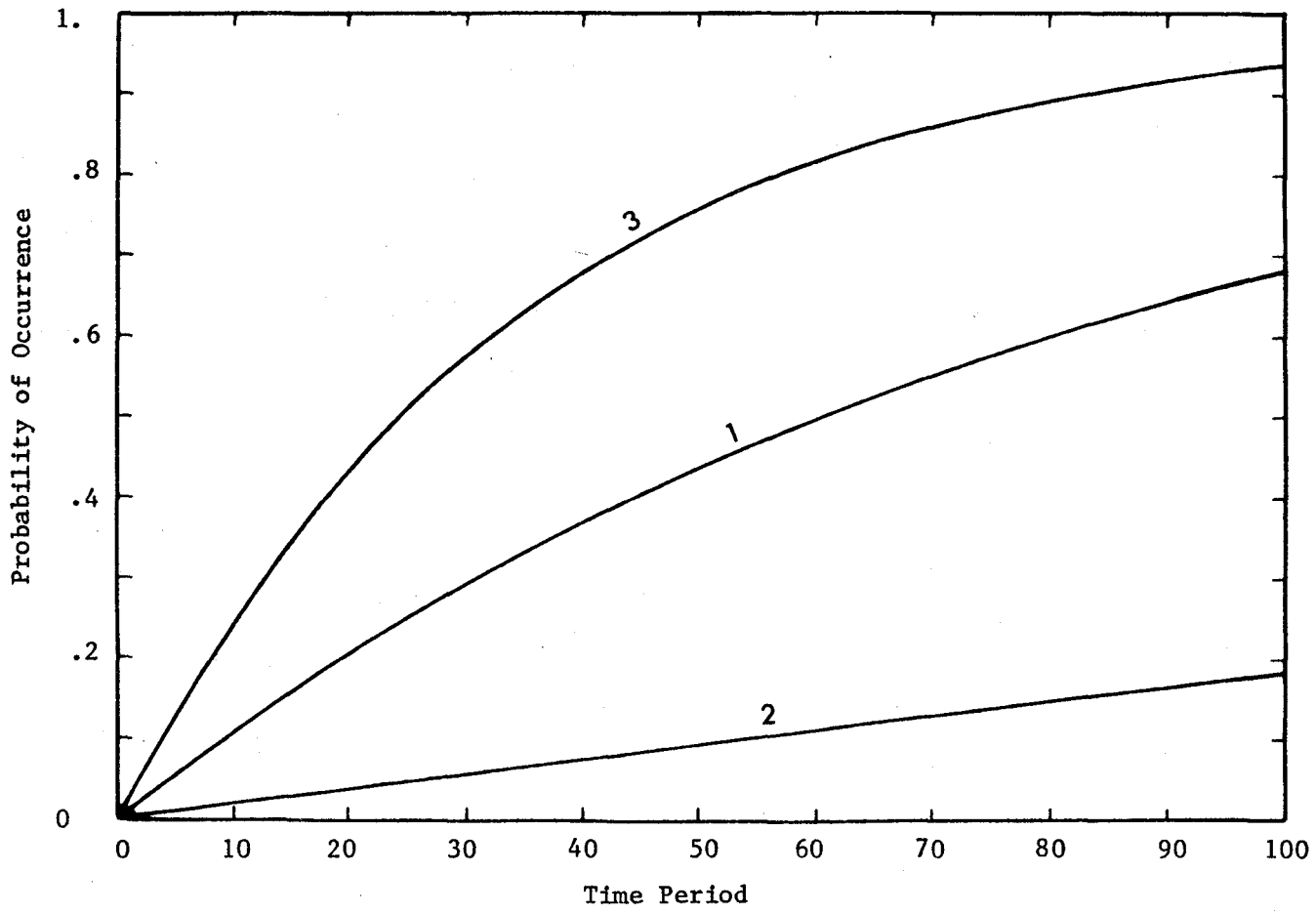

Figure 7.9 Seismic Hazard Evaluation for a Pore Pressure Ratio of 1.0
(D_r=68%, Hazard Conditions 1,2, and 3)

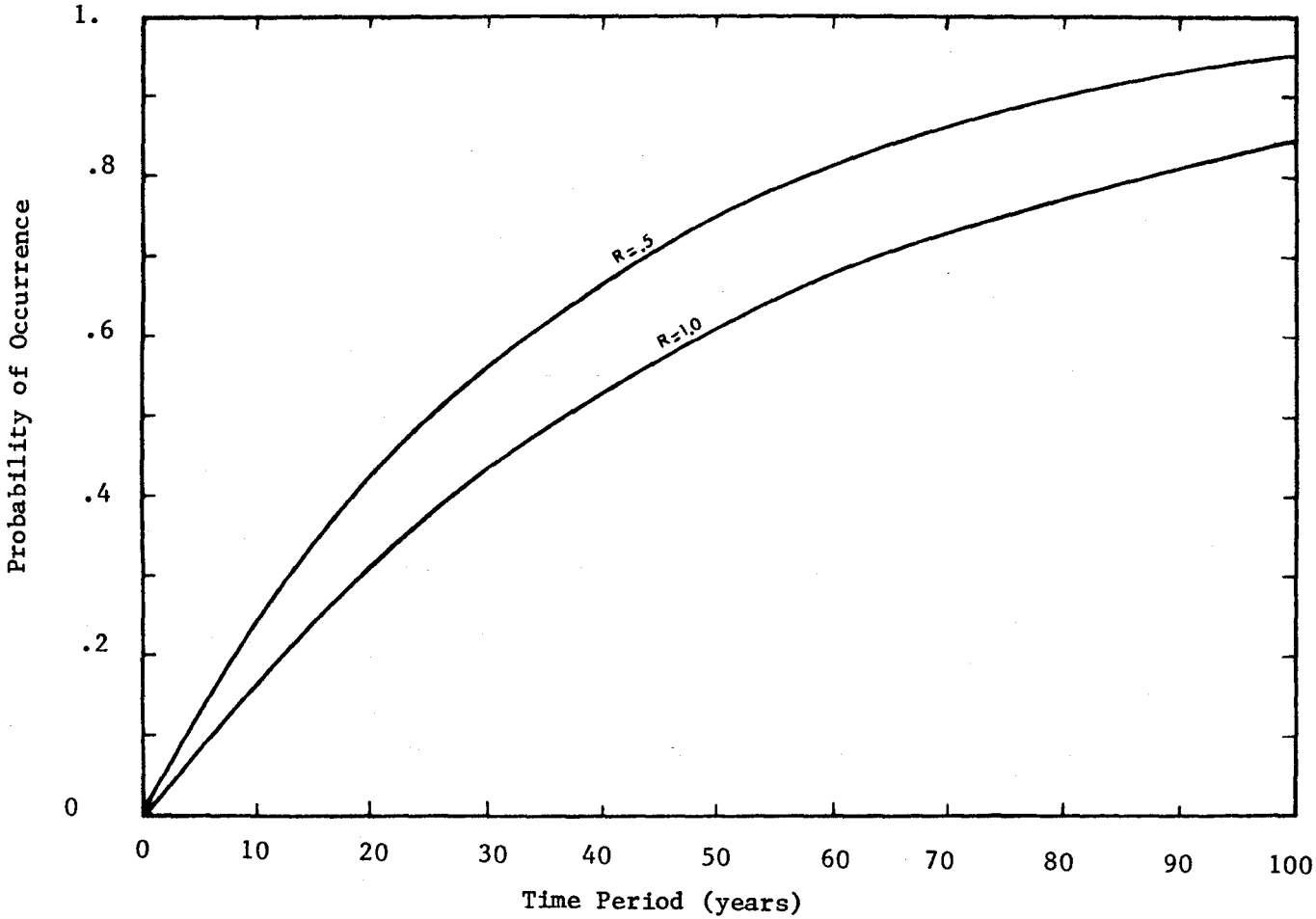

Figure 7.10 Seismic Hazard Evaluation for Pore Pressure Ratios of 0.50 and 1.0 (D_r = 54%, Assumption 1)

Chapter VIII

GENERALIZED METHODOLOGY AND RECOMMENDATIONS

8.1 INTRODUCTION

The last aspect of this dissertation is to propose a generalized methodology to assess the risk and damage associated with the development of pore water pressure in cohesionless soils during seismic loading.

This chapter describes the general methodology. The probabilistic pore pressure models and seismic hazard evaluation concepts developed in the preceeding chapters are the first steps towards achievement of the program proposed in the methodology.

Specific recommendations for future research are discussed. They follow along two lines : (1) Improvement and application of the models presented in this dissertation and, (2) Completion of the final steps of the methodology.

8.2 GENERALIZED METHODOLOGY

A recent study of the behavior of the San Francisco waterfront under seismic loading (Clough and Chameau, 1979) showed that :

- Similar sites can experience liquefaction (zero effective stress state) but be affected by completely different ground movements due to subtle differences in site characteristics.

- It is possible to have significant ground deformations caused by significant excess pore pressure, prior to liquefaction.

- The development of pore water pressure does not necessarily lead to damage, and the level of damage depends upon the type of supported structures.

Following this study the authors felt that there was a need for further research to develop a fundamental approach directed towards predicting the likelihood of pore pressure build-up and ground deformations, and the resultant damage potential as consequences.

The study of an engineering problem can generally be decomposed in three phases : an initial phase provides a theoretical understanding of the phenomenon, a second phase defines and quantifies the resulting effects of this phenomenon, and a third phase characterizes the economics of the problem. This general framework can be applied to pore pressure build-up as illustrated in figure 8.1.

The study of the basic problem of pore pressure build-up during earthquake loading is done in phase 1; Phase 2 provides a quantitative description of the effects of pore pressure increase on foundations and structures; Phase 3 uses the information obtained in phases 1 and 2 to

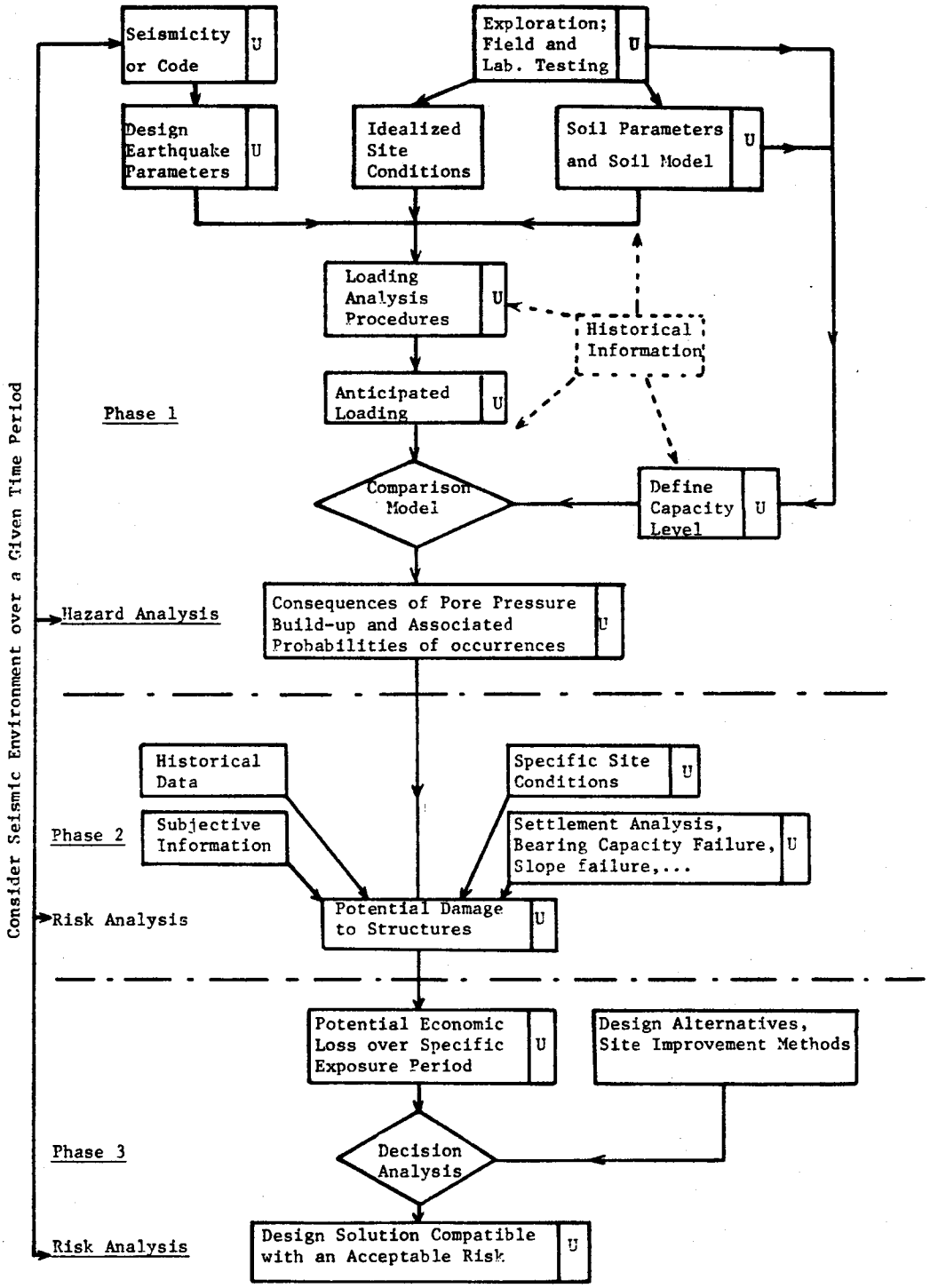

Figure 8.1 Generalized Methodology

complete the economic analysis. Furthermore risk analysis studies are performed to compute the risk associated with pore pressure build-up for a given time period and a given seismic environment.

The relatively complex phase 1 portion of the flow-chart shows the interactions between the parameters and analytical models required for the liquefaction analysis of a given site. A review of present methods of liquefaction analysis shows them all to fit the general format of the phase 1 portion. Design earthquake parameters are obtained from a seismicity study or the use of a code, and are generally expressed in terms of a "punch" parameter, such as magnitude or seismic moment, and a site parameter, such as acceleration time history, peak ground acceleration or root mean square of acceleration. A site exploration and testing program provides a set of soil parameters and idealized site conditions. The earthquake and soil parameters are then input to a loading analysis which yields as output an anticipated loading at the site; one of the most common expressions of the loading is the shear stress level. Laboratory data and a soil model are used to define the capacity level, or strength parameters, at the site. The comparison between anticipated loading and strength provides the assessment of pore pressure build-up and liquefaction potential.

The procedure previously described assumes perfect parameters and models. In fact, a comprehensive analysis should incorporate the uncertainties regarding earthquake, soil, and model parameters. When the analysis incorporates these uncertainties, it becomes probabilistic in nature. The distribution functions of the anticipated loading and

capacity are derived and the probability of occurrence associated with any consequence of pore pressure build-up is computed.

The potential for pore pressure build-up and liquefaction represents a computed, theoretical assessment of the problem, but is not sufficient to describe the actual potential damage. Phase 2 should provide the link between the potential for pore pressure build-up and the actual damage to soils and soil-supported structures. Historical data show that damage to structures is related to the level and extent of the pore pressures, the soil density and geologic history, the type of foundation system, and the general topography. Given the pore pressure levels from phase 1, settlement analyses, bearing capacity analyses or slope stability analyses may be used in phase 2 to obtain the potential damage to structures. Historical data can be used to input some subjective information to the analysis, and uncertainties in the results are computed as previously done in phase 1.

Phase 3 is formally straight forward, but its implementation is certainly as difficult as the two other phases. It involves three parts : obtain a potential economic loss from the knowledge of potential structural damage; study the technical and economic feasibility of site improvement methods; and obtain a design solution compatible with an acceptable risk through decision analysis. The fundamental aspect of this phase lies in determining the relationship between structural damage and economic damage; there is no exact relationship between the two, and empirical relations cannot include special economic aspects such as social loss.

Phases 2 and 3 show the desirability in performing risk analysis studies over a specific investment period. A comprehensive analysis for a given site should provide this kind of "return period" study along with the means of deducing the seismic risk from the seismic hazard evaluated at the end of phase 1.

The probabilistic developments presented in this dissertation mainly addressed the phase 1 analysis and the hazard analysis methodology. The proposed methods probabilistically evaluate the generation of pore pressure due to earthquake loading. The evaluation is done using experimental data or pore pressure generation models. Allowance is made for the non linear development of pore pressure as a function of the relative intensities of stress cycles and their positions in the stress history. The soil and loading parameters are not deterministic but defined by probability density functions. The uncertainty levels are assumed from existing data and subjective judgement when necessary. All these different aspects are combined into a probabilistic framework which yields a complete description of the pore pressure build-up. This description is expressed by probability curves which relate the probability of exceeding a certain level of pore pressure to the number of cycles (zero-crossings) of loading. Furthermore the probabilistic pore pressure analysis can be incorporated in a hazard analysis methodology. Given a seismic environment and a time period, this methodology assesses the hazard in terms of a soil related parameter, the pore pressure.

The preceeding remarks briefly summarize the work described in the previous chapters. This work was primarily concerned with the evaluation of the likelihood of pore pressure build-up during an earthquake and only represents the first step towards the complete achievement of the program of figure 8.1.

8.3 RECOMMENDATIONS FOR FUTURE WORK

The author believes that future work should follow along two lines. The first one is to improve a few characteristics of the probabilistic pore presssure models developed in this dissertation and to apply those models to actual sites. The general idea of this line of work is to show that the proposed methods are operational and can provide reliable and practical results for engineering purposes. The second line of work is concerned with the development of ideas and tools necessary to the realization of the last two steps of the generalized methodology.

8.3.1 Improvement and application of the probabilistic models

The immediate work to follow this dissertation should be to apply the probabilistic models to sites where past behavior during earthquakes has been observed. An effort has to be made to gather information on three types of sites :

- sites where evidence of liquefaction and important related damage were observed;

- sites with evidence of liquefaction but no significant damage;

- sites with no evidence of liquefaction during an earthquake.

The purpose of this work is to check the validity of the models and to define the "probabilistic difference" between a site where high pore pressures occur and a site where they do not occur. Given this information, seismic hazard evaluations, such as those presented in chapter 7, could be performed for typical site conditions and seismic environment. They could be presented in the form of charts which, for several relative densities, relate the probability of at least one occurrence of a given pore pressure ratio to the time period of interest.

For a better utilization of the models, several parameters and ideas presented in this dissertation can be improved by :

- Performing statistical analyses of simple shear test data in order to provide better guidelines for the estimation of the uncertainty level in cyclic strength curves.

- Compiling data on soil parameters, such as the friction angle ϕ' and the coefficient of lateral earth pressure K_0, in order to better assess the uncertainty in the parameters required in effective stress models.

- Investigating the effects of specific site characteristics such as previous strain history and the geologic age of the deposit on

pore pressure generation. One should try to account for these types of influences by transforming the probability density functions of soil parameters so that they take into consideration the specific characteristics of the site.

Of these three points, only the last one should require significant research. The author believes that these improvements and the application to actual sites will further demonstrate the value of the probabilistic models. Two other developments would be perfect complements to this dissertation. First, pore pressure generation models other than the ones used in this work could be incorporated in the method. As demonstrated in chapter 6, once the probabilistic framework is built, it is very simple to add a new model. This would involve very limited effort and permit comparisons between available models. A second and very fruitful development would be to conduct non-uniform cyclic loading experiments to verify and further assess the characteristics of the non-linear development of pore pressure under cyclic loading. An ideal testing program would be to perform such tests for a series of different stress time histories, compute the statistics of the results, and compare them to the results of the probabilistic analysis. It is evident that, while being very promising, such a testing program necessitates a significant amount of time and research funds.

8.3.2 Research tasks for completion of the generalized methodology

The methodology presented in figure 8.1 distinguishes between damage and liquefaction (or more generally, damage and pore pressure build-up). This emphasizes that a theoretical analysis and assessment of pore pressure is not sufficient to describe the real damage, if any, to the soil and supported structures. As a consequence future work is needed in the following areas of research :

- Investigation of the problems of slope instabilities, bearing capacity and settlement failures, given the characteristics of pore pressure build-up. It is suggested to first study the relatively simple problem of foundation failure given that a certain level of pore pressure has developed in a soil profile. This could be evaluated by employing current analysis techniques for foundation stability modified for use in a probabilistic model. It is recommended to attack the more complex problem of slope failures by analyzing the seismic stability of geometrically well defined cases. As an example, preliminary work has been undertaken to assess the seismic stability of a bluff composed of cohesive soil interlaced by a thin horizontal seam of liquefiable sand (similar to the Government Hill slide in Alaska, 1964). Once these simple problems have been solved, the methodology could be applied to more complex geometric and loading conditions.

- Once the probability of foundation or slope failure can be estimated, it could be incorporated into a risk analysis

methodology similar to the hazard methodology proposed in this dissertation for pore pressure. An important effort should be devoted to provide practical guidelines to deduce the likelihood of foundation failure from the seismic hazard assessed in phase 1 (pore pressure levels). This is necessary to avoid cumbersome computer formulations which increase in size every time a step is added to a risk or hazard analysis methodology.

- The last of the research tasks would be to study the geotechnical methods available to improve a site against the effects of pore pressure build-up during seismic loading. Their applicability should be assessed, depending upon specific site conditions, and their costs should be compared to the reduction in potential economic loss that they procure.

It is hoped that the probabilistic ideas presented in this dissertation can be used to complete the above suggested work. These ideas can certainly be implemented to solve the problem of foundation and slope failures, which should be the first one to be considered in future research.

8.4 SUMMARY

The probabilistic models developed in this dissertation represent the first step towards the achievement of a more complete program. A generalized methodology is proposed to study the liquefaction potential

of a given site. It is directed towards predicting the likelihood of pore pressure build-up and associated ground deformations, and assessing the resultant damage potential. It is recommended that future work be devoted to : (1) The application of the probabilistic models to actual cases and, (2) Specific research on the methods to assess the probability that a given pore pressure increase will cause ground deformation. The first line of work can make direct use of this dissertation and the second can be inspired by the concepts and ideas developed for pore pressure.

Chapter IX

CONCLUSION

9.1 SUMMARY

This study represents an initial part of a project undertaken at Stanford to assess the damage potential associated with pore pressure increases in cohesionless soils under seismic loading. The specific objectives of this project are : (1) Developing procedures to evaluate the likelihood of pore pressure build-up during an earthquake; (2) Assessing the probability of ground deformation and damage caused by the pore pressure build-up; and, (3) Evaluating the resulting potential for economic loss. This dissertation was oriented towards casting the phenomenon of pore pressure build-up into a probabilistic and hazard analysis framework.

One task of this work is to document and investigate the behavior of cohesionless soils under cyclic loading. A review of previous studies indicates that the Palmgren-Miner rule of linear accumulation of damage is currently applied to sand materials subjected to undrained cyclic loading. However it is shown in this dissertation that the accumulation of pore pressure does not follow the Palmgren-Miner rule. The increase in pore pressure during a stress cycle depends on the stress intensity and on the pore pressure accumulated during the previous stress cycles. This behavior is demonstrated to be valid for uniform and non-uniform cyclic loading.

In a second part of the dissertation, a probabilistic model is proposed to study the development of pore pressure in sands under random loading. This model incorporates uncertainties in the soil and loading characteristics and makes allowance for the non-linear accumulation of pore pressure. The pore pressure development characteristics of sand are defined by a cyclic strength curve and a set of pore pressure generation curves, both to be obtained in laboratory experiments. The loading shear stress is characterized by a probability density function describing the amplitude of the peaks. The model computes the cumulative distribution function of pore pressure at the end of any cycle of loading.

Several applications of the probabilistic pore pressure model are presented. The first series of applications considers a hypothetical level ground site. Different soil and loading conditions are used to assess the versatility of the model. The second series of applications tests the ability of the model to predict the behavior of sites for which the field behavior is known.

As an alternative to the probabilistic model based on laboratory data, a second approach is developed which uses an analytically based effective stress technique to probabilistically compute the development of pore pressure during cyclic loading. In this approach uncertainty in soil parameters is included by defining a probability density function for each parameter. This function describes the variations of the parameter between given limits and a simulation algorithm is used to generate soil parameters within those limits. The probability density

function of the shear stress amplitude is used to generate shear stress time histories. The development of pore pressure is computed for each simulation and the statistical characteristics of the pore pressure are determined at the end of the simulation procedure. This model is applied to several hypothetical and actual cases. Two different effective stress models are used in these analyses.

The results of the applications performed with the two probabilistic models can be compared to those obtained with conventional liquefaction analysis. For example, a site is analyzed under loading conditions corresponding to the Taft, Hollister, First St., and Figueroa records, for which the PGA, root mean square of acceleration and duration are known. Under these conditions the probabilistic models lead to a probability of liquefaction of 1.0, 0.52, 0.67, and 0.42 for the four records, respectively, while the Seed and Idriss simplified method predicts liquefaction in all for cases.

The probabilistic pore pressure model based on an effective stress model has several advantages over the first model, based on experimental data : (1) The basic soil parameters can account for local soil conditions; (2) The mathematical formulation is simplified; and, (3) It can be easily transformed to incorporate any desired pore pressure model, and thus make comparisons between models. Its main disadvantage is that the soil parameters necessary to it are more difficult to obtain than the cyclic strength curve and pore pressure generation curves required by the first model. When applied to identical loading conditions and similar soil characteristics the two models give close

results. This indicates that one can reliably use either one of the models, depending upon which kind of data are available.

The two probabilistic models are incorporated into a hazard analysis methodology. In this methodology the probability of exceeding a given pore pressure ratio is combined with the joint distribution of root mean square of acceleration and number of cycles of the earthquake. This results in the probability of exceeding at least once a certain pore pressure ratio for a given seismic environment and a given time period.

Finally the author proposes a generalized approach to cast the pore pressure hazard evaluation into a methodology to evaluate the seismic risk due to pore pressure buid-up. In order to do so, several recommendations are presented. They follow along two lines : (1) Application and improvement of the probabilistic models developed in this dissertation; and, (2) Research on the methods to assess the likelihood of damage associated with pore pressure build-up.

9.2 RESULTS AND CONCLUSIONS

The most important results and conclusions of this study are :

- The probabilistic pore pressure models developed in this dissertation are advantageous over conventional methods for several reasons. First, they are not restricted to the question of liquefaction per se, but provide a complete description of pore pressure, for any pore pressure ratio between 0. and 1.0. Second, they include uncertainty in both soil and loading conditions. And,

third, they make a distinction between cases where liquefaction is certain and cases where it is not 100 percent probable.

- The probability curves reflect the effect of earthquake duration, showing that for the same PGA or root mean square of acceleration substantialy different levels of pore pressure are likely to develop.

- The models are well suited to make comparisons between site and loading conditions. The probability of exceedance of a given pore pressure level or of liquefaction represents a quantitative measure of the effect of design parameters and local soil conditions on the potential for pore pressure build-up.

- The effect of uncertainty in the soil parameters is important for moderate intensity loading and short duration events which lead to a probability of liquefaction less than 1.0. For very high intensity events the probability of liquefaction is close to 1.0, and the effect of soil uncertainty is very limited.

- The models correctly predict the behavior of sites for which the field behavior during the Niigata earthquake is known. For example, a probability of liquefaction of 97 percent is obtained for sites with a relative density of 53 percent which are known to have liquefied during the earthquake.

- The probabilistic framework of the models makes it possible to include any supplementary uncertainty, such as uncertainty in the number of cycles (zero-crossings) of the earthquake records.

- The hazard analysis methodology demonstrates that the hazard at a given site can be described in terms of a soil related parameter, the level of pore pressure. This methodology is well suited to compare the hazard potential of sites with different soil resistance and seismic environment.

The author hopes that the ideas presented in this dissertation can improve the analysis of pore pressure build-up in soils due to seismic loading, and that the proposed hazard and risk analysis methodology will allow assessment of the potential damage which results.

Appendix A

REFERENCES

1. A-Grivas, D., Howland, J., and Tolcser, P., "A Probabilistic Model for Seismic Slope Analysis", Report 78-5, Dept. of Civil Engineering, Rensselaer Polytechnic Institute, June 1979.

2. Ahrens, J., and Dieter, U., "Non-uniform Random Numbers", Institut fur Mathematische Statistick Technische Hochschule in Graz, Graz, Austria, 1973.

3. Bazant, Z.P., and Krizek, R.J., "Endochronic Constitutive Law for Liquefaction of Sand", Jour. of the Eng. Mech. Div., ASCE, Vol. 102, No. EM2, April 1976.

4. Bjerrum, l., "Geotechnical Problems involved in Foundations of Structures in the North Sea", Norwegian Geotechnical Institute, Publ. No. 100, Oslo, 1974.

5. Casagrande, A., "Characteristics of Cohesionless Soils Affecting the Stability of Earth Fills", Jour. of the Boston Society of Civil Engineers, Jan., 1936. (reprinted in "Contributions to Soil Mechanics, 1925-1940", Boston Society of Civil Engineers, Oct., 1940).

6. Casagrande, A., "liquefaction and Cyclic Deformation of Sands, a Critical Review", Harvard Soil Mechanics Series No. 88, Harvard U., 1976.

7. Castro, G.,"Liquefaction and Cyclic Mobility of Saturated Sands", Jour. of the Geot. Eng. Div., ASCE, Vol. 101, No. GT6, 1975.

8. Castro, G., "Liquefaction of Sands", Harvard Soil Mechanics Series No. 81, Harvar U., 1969.

9. Castro, G., and, Poulos, S.J., "Factors Affecting Liquefaction and Cyclic Mobility", Jour. of the Geot. Eng. Div., ASCE, Vol. 103, No. GT6, June, 1977.

10. Cho, Y., Rizzo, P.C., and Humphries, W.K., "Saturated Sand and Cyclic Dynamic Tests", presented at the 1976 ASCE Annual Convention and Exposition, held at Philadelphia, Pa.

11. Christian, J.T., and Swiger, W.F., "Statistics of Liquefaction and SPT Results", Jour. of the Geot. Eng. Div., ASCE, Vol. 101, No. GT11, No.v., 1975.

12. Clough, G.W., and Chameau, J.l.,"A Study of the Behavior of the San Francisco Waterfront Fills under Seismic Loading", Report No. 35, The John A. Blume Earthquake Engineering Center, Stanford, February, 1979.

13. Cornell, C.A., "Engineering Seismic Risk Analysis", BSSA 58(5), 1968.

14. Cornell, C.A., and Merz, H.A., "A Seismic Risk Analysis of Boston", Jour. of the Str. Div., ASCE, Vol.110, No. ST10, 1975.

15. De Alba, P., Seed, H.B., and Chan, C.K., "Sand Liquefaction in Large Scale Simple Shear Tests", Jour. of the Geot. Eng. Div., ASCE, Vol. 102, No. GT9, Sept., 1976.

16. Donovan, N.C., "A Stochastic Approach to the Seismic Liquefaction Problem", First National Conference on Applications of Statistics and Probability to Soil and Structural Engineering, Hong Kong, Sept., 1971.

17. Donovan, N.C., and Singh, S., "Development and Application of Liquefaction Criteria for the Trans-Alaska Pipeline", ASCE Annual Convention and Exposition, Philadelphia, Pa., 1976.

18. Faccioli, E., "A Stochastic Model for Predicting Seismic Failure in a Soil Deposit", Earthquake Engineering and Structural Dynamics, Vol. 1, 1973.

19. Faccioli, E., and Resendiz, D., "Soil Dynamics: Behavior Including Liquefaction", Seismic Risk and Engineering Decisions, Elsevier, Amsterdam, 1975.

20. Fardis, M.W., and Veneziano, D., "Probabilistic Liquefaction of Sands during Earthquakes", Report R79-14, Massachusetts Institute of Technology, March, 1979.

21. Ferrito, J.M., Forrest, J.B., and Wu, G., "A Compilation of Cyclic Triaxial Liquefaction Test Data", Geotechnical Testing Journal, Vol.2, No. 2, June, 1979.

22. Finn, W.D.L., "Critical Review of Dynamic Effective Stress Analysis", Proceedings of the 2nd National Conf. on Earthquake Engineering, Stanford, 1979.

23. Finn, W.D.L., Lee, K.W., and Martin, G.R., "Stress Strain Relations for Sand in Simple Shear", presented at the ASCE Annual Convention and Exposition, Denver, Colorado, No.v., 1975.

24. Finn, W.D.L., Lee, K.W., and Martin, G.R., "An Effective Stress Model for Liquefaction", Jour. of the Geot. Eng. Div., ASCE, Vol. 103, No. GT6, June, 1977.

25. Finn, W.D.L., Lee, K.W., and Martin, G.R.,"Comparison of Dynamic Analyses for Saturated Sands", Earthquake and Soil Dynamics Conference, Pasadena, 1978.

26. Finn, W.D.L., Lee, K.W., and Vaid, Y., "Experimental and Analytical Study of Stress-Strain Relations in Simple Shear", Dept. of Civil Eng., Soil Mechanics Series No. 30, U. of British Columbia, 1976.

27. Finn, W.D.L, Pickering, D.J., and Bransby, P.L., "Sand Liquefaction in Triaxial and Simple Shear Tests", Jour. of the Soil Mech. and Found. Div., ASCE, Vol. 97, No. SM4., April, 1971.

28. Finn, W.D.L., Byrne, P.M., and Martin, G.R., "Seismic Response and Liquefaction of Sands", Jour. of the Geot. Eng. Div., ASCE, Vol. 102, No. GT8, Aug., 1976.

29. Fishman, G.S., "Principles of Discrete Event Simulation", Wiley, New York, 1978.

30. Ghaboussi, J., and Dikmen, U.S., "Liquefaction Analysis of Horizontally Layered Sands", Jour. of the Geot. Eng. Div., ASCE, Vol. 104, No. GT3, March, 1978.

31. Gibbs, H.J., and Holtz, W.G., "Research on Determining the Density of Sands by Spoon Penetration Testing", Proceedings, Fourth International Conference on Soil Mechanics and Foundation Engineering, London, 1957.

32. Haldar, A., and Tang, W.H., "Probabilistic Evaluation of Liquefaction Potential", Journal of the Geotechnical Engineering Division, ASCE, Vol. 105, No. GT2, Feb. 1979.

33. Hanks, T.C., "Seismological Aspects of Strong Motion Seismology", Proceedings of the 2nd National Conference on Earthquake Engineering, Stanford, Aug., 1979.

34. Harr, M.E., "Mechanics of Particulate Media, a Probabilistic Approach", Mc Graw Hill, 1977.

35. Hoeg, K., and Tang, W.H., "Probabilistic Considerations in the Foundation Engineering of Offshore Structures", Norwegian Geotechnical Institute, Publication No. 120, Oslo, 1978.

36. Ishibashi, I., and Sherif, M.A., "Soil Liquefaction by Torsional Simple Shear Device", Jour. of the Geot. Eng. Div., ASCE, Vol. 100, No. GT8, Aug., 1974.

37. Ishihara, K., Tatsuoka, F., and Yasuda, S., "Undrained Deformation and Liquefaction of Sand under Cyclic Stresses", Soils and Foundations, Vol. 15, No. 1, March, 1975.

38. Ishihara, K., and Yasuda, S., "Sand Liquefaction in Hollow Cylinder Torsion Under Irregular Excitation", Soils and Foundations, Vol. 15, No. 1, March, 1975.

39. Ishihara, K., and Yasuda, S., "Sand Liquefaction under Random Earthquake Loadind Conditions", Proceedings of the 5th World Conference on Earthquake Engineering, Rome, 1973.

40. Kishida, H., "Characteristics of Liquified Sands during Mino-Owari, Tohnarkai, and Pukui Earthquakes", Soils and Foundations, Vol. 9, No. 1, 1969.

41. Kishida, H., "Damage to reinforced concrete buildings in Niigata City with Special Reference to Foundation Engineering", Soils and Foundations, Vol. 7, No. 1, 1966.

42. Lee, K.W., and Chan, K., "Number of Equivalent Significant Cycles in Strong Motion Earthquakes", Proceedings of the International Conference on Microzonation, Seattle, Oct., 1972.

43. Lee, K.L., and Focht, J.A., "Liquefaction Potential at Ekofisk Tank in North Sea", Jour. of the Geot. Eng. Div., ASCE, Vol. 100, No. GT1, January, 1975.

44. Lin, Y.K., "Probabilistic Theory of Structural Dynamics", Mc Graw-hill, New York, 1967.

45. Liou, C.P., Streeter, V.L., and Richart, F.E., "Numerical Model for Liquefaction", Jour. of the Geot. Eng. Div., ASCE, Vol. 103, No. GT6, June, 1977.

46. Lumb, P., "Application of Statistics in Soil Mechanics", in "Soil Mechanics-New Horizons", Elsevier, New York, 1974.

47. Lysmer, J., Takekazu, T., and Tsai, C.F., "FLUSH, a Computer Program for Approximate 3-D Analysis of Soil-Structure Interaction", Report EERC 75-30, U. of California, Berkeley, No.v., 1975.

48. Martin, P.P., "Non Linear Methods for Dynamic Analysis of Ground Response", Thesis Presented to the U. of California at Berkeley, in 1975, for Partial Fulfillment of the Requirements for the Degree of Doctor of Philosophy in Engineering.

49. Martin, G.R., Finn, W.D.L., and Seed, H.B., "Fundamentals of Liquefaction under Cyclic Loading", Jour. of the Geot. Eng. Div., ASCE, Vol. 101, No. GT5, May, 1975.

50. Masing, G., "Eigenspannungen und Verfestigung beim Messing", Proceedings 2nd International Congress of Applied Mechanics, Zurick, 1926.

51. Miner, M.A., "Cumulative Damage in Fatigue", Transactions of the American Society of Mechanical Engineers, Vol. 67, 1945.

52. Mortgat, C.P., and Shah, H.C., "A Bayesian Approach to Seismic Hazard Mapping; Development of Stable Design Parameters", The J.A. Blume Earthquake Engineering Center, Report No. 28, Stanford, 1978.

53. Mortgat, C.P., "A probabilistic Definition of Effective Acceleration", Proceedings of the 2nd National Conference on Earthquake Engineering, Stanford, Aug., 1979.

54. Newland, D.E., "An Introduction to Random Vibrations and Spectral Analysis", Longman, London and New York, 1975.

55. Ohsaki, Y., "Effects of Sand Compaction on Liquefaction during the Tokachioki Earthquake", Soils and Foundations, Vol. 10, No. 2, June, 1970.

56. Palmgren, A., "Die Lebensdauer von Kugellagern", Ver. Deut. Ingr., Vol. 68, 1924.

57. Peacock, W.H., and Seed, H.B., "Sand Liquefaction under Cyclic Loading Simple Shear Conditions", Jour. of the Soil Mech. and Found. Div., ASCE, Vol. 94, No. SM3, May, 1968.

58. Poncelet, "Memoires d'un officier du Genie", Tome III, 1839. Also "Introduction a la mecanique industrielle", 1870.

59. Pyke, R., Chan, C.K., and Seed, H.B., "Settlement and Liquefaction of sands under Multidirectional Shaking", Report EERC 74-2, Earthquake Engineering Research Center, U. of California, Berkeley, Feb., 1974.

60. Romo-Organista, M.P., Chen, J.-H., Lysmer, J., and Seed, H.B., "PLUSH a Computer Program for Probabilistic Finite Element Analysis of Seismic Soil-Structure Interaction", Report EERC 77-01, Earthquake Engineering Research Center, U. of California, Berkeley, June, 1977.

61. Schnabel, P.B., Lysmer, J., and Seed, H.B., "SHAKE a Computer Program for Earthquake Response Analysis of Horizontally Layered Sites", Report EERC 72-12, Earthquake Engineering Research Center, U. of California, Berkeley, Dec., 1972.

62. Seed, H.B., and Idriss, I.M., "Simplified Procedure for Evaluating Soil Liquefaction Potential", Jour. of the Soil Mech. and Found. Div., ASCE, Vol. 97, No. SM9, Sept., 1971.

63. Seed, H.B., Idriss, I.M., Makdisi, F., and Banerjee, N., "Representation of Irregular Stress Time Histories by Equivalent Uniform Stress Series in Liquefaction Analyses", Report EERC 75-29, Earthquake Engineering Research Center, U. of California, Berkeley, Oct., 1975.

64. Seed, H.B., and Lee, K.L., "Liquefaction of Saturated Sands During Cyclic Loading", Jour. of the Soil Mech. and Found. Div., ASCE, Vol. 92, No. SM6, No.v., 1966.

65. Seed, H.B., Lee, K.L., and Idriss, I.M., "Analysis of the Sheffield Dam Failure", Jour. of the Soil Mech. and Found. Div., ASCE, Vol. 95, No. SM6, No.v.,1969.

66. Seed, H.B., Martin, P.P., and Lysmer, J., "The Generation and Dissipation of Pore Presures during Soil Liquefaction", Report EERC 75-26, Earthquake Engineering Research Center, U. of California, Berkeley, Aug., 1975.

67. Seed, H.B., Martin, P.P., and Lysmer, J., "Pore Water Pressures during Soil Liquefaction", Jour. of the Geot. Eng. Div., ASCE, Vol. 102, No. GT4, April, 1976.

68. Seed, H.B., and Idriss, I.M., "Analysis of Soil Liquefaction : Niigata Earthquake", Jour. of the Soil Mech. and Found. Div., ASCE, Vol. 93, No. SM3, May, 1967.

69. Seed, H.B., Mori, K., and Chan, C.K., "Influence of Seismic History on the Liquefaction Characteristics of Sands", Report EERC 75-25, Earthquake Engineering Research Center, U. of California, Berkeley, Aug., 1975.

70. Seed, H.B., and Peacock, W.H., "Test Procedures for Measuring Soil Liquefaction Characteristics", Jour. of the Soil Mech. and Found. Div., ASCE, Vol. 97, No. SM8, Aug., 1971.

71. Seed, H.B, Pyke, R., and Martin, G.R., "Analysis of the Effect of Multi-directional Shaking on the Liquefaction Characteristics of Sands", Report EERC 75-41, Earthquake

Engineering Research Center, U. of California, Berkeley, Dec., 1975.

72. Seed, H.B., "Soil Liquefaction and Cyclic Mobility Evaluation for Level Ground during Earthquakes", Jour. of the Geot. Eng. Div., ASCE, Vol. 105, No. GT2, Feb., 1979.

73. Shah, H.C., Personal Communication, 1980.

74. Sherif, M.A., Seminar Presented at Stanford University, March, 1980.

75. Sherif, M.A., and Ishibashi, I., "Prediction of Soil Liquefaction Potential during Earthquakes", Proceedings of the 2nd National Conference on Earthquake Engineering, Stanford, Aug., 1979.

76. Silver, M.L., "Laboratory Triaxial Testing Procedures to Determine the Cyclic Strength of Soils", Report NUREG-31, April, 1976.

77. Valera, J.E, and Donovan, N.C., "Soil Liquefaction Procedures - A Review", Jour. of the Geot. Eng. Div., ASCE, Vol. 101, No. GT6, June, 1975.

78. Vanmarcke, E.H., "Structural Response to Earthquakes", Chapter 8 in "Seismic Risk and Engineering Decisions", C. Lomnitz, and E. Rosenblueth, Elsevier, 1976.

79. Veneziano, D., and Antoniano, J., "Reliability of Slopes : Frequency Domain Method", Jour. of the Geot. Eng. Div., ASCE, Vol. 105, No. GT2, Feb.,1979.

80. Wohler, A., "Z. Bauwesen", Volumes 8, 10, 13, 16, and 20, 1850-70. An account of his work in English is given in Engineering, Vol.11, 1871.

81. Yegian, M.K., and Whitman, R.V., "Risk Analysis for Ground Failure by Liquefaction", Jour. of the Geot. Eng. Div., ASCE, Vol. 104, No. GT7, July, 1978.

82. Zienkiewicz, O.C., Chang, C.T., and Hinton, E., "Non-linear Seismic Response and Liquefaction", Int. Jour. for Num. and Anal. Meth. in Geom., Vol. 2, 1978.

83. Zsutty, T., and De Herrera, H., "A Statistical Analysis of Accelerogram Based upon the Exponential Distribution Model", Proceedings of the 2nd National Conference on Earthquake Engineering, Stanford, Aug., 1979.

Appendix B

HARDENING EFFECT IN THE FINN, LEE, AND MARTIN EFFECTIVE STRESS MODEL

Several mathematical relations, which are not explicitely derived in the paper by Finn, Lee and Martin (1977), are presented in this appendix.

In a study on the fundamental behavior of sands under cyclic loading, Martin, Finn and Seed suggested that the stress-strain relation in simple shear might be represented in the form:

$$\tau = \frac{\gamma\sqrt{\sigma'_v}}{a + b\gamma} \tag{B.1}$$

in which τ and γ are the horizontal shear stress and shear strain respectively, and σ'_v the effective vertical stress. The parameters a and b were found to be functions of the accumulated volumetric strain ε_v:

$$a = A_1 \frac{\varepsilon_v}{A_2 + A_3\varepsilon_v} \tag{B.2}$$

$$b = B_1 \frac{\varepsilon_v}{B_2 + B_3\varepsilon_v} \tag{B.3}$$

The maximum value of the shear modulus, G_{mn}, in any cycle of loading n is given by:

$$G_m = (d\tau/d\gamma) \text{ at } \gamma = 0 \qquad = \frac{\sqrt{\sigma'_v}}{a} \tag{B.4}$$

$$= \frac{\sqrt{\sigma'_v}}{A_1} \cdot \frac{A_1}{A_1 - \varepsilon_v/(A_2+A_3\varepsilon_v)} \tag{B.5}$$

By making a few substitutions, it follows:

$$G_{mn} = G_{mo}\left(1 + \frac{\varepsilon_v}{H_1 + H_2\varepsilon_v}\right) \tag{B.6}$$

where G_{mo} is the initial shear modulus at $\sigma'_v = \sigma'_{vo}$, and H_1 and H_2 are constants:

$$H_1 = A_1A_2 \tag{B.7}$$

$$H_2 = A_1A_3 - 1 \tag{B.8}$$

The maximum shear stress, τ_{mn}, in the nth cycle of loading is the limit as $\gamma \to \infty$ of the shear stress τ in equation B.1:

$$\tau_{mn} = \sqrt{\sigma'_v}/b \tag{B.9}$$

It can be easily deduced that:

$$\tau_{mn} = \tau_{mo}\left(1 + \frac{\varepsilon_v}{H_3 + H_4\varepsilon_v}\right) \qquad (B.10)$$

where τ_{mo} is the maximum initial shear stress, and H_3 and H_4 are constants:

$$H_3 = B_1B_2 \qquad (B.11)$$

$$H_4 = B_1B_3 - 1 \qquad (B.12)$$

The four constants H_1, H_2, H_3 and H_4 can be obtained by fitting equations B.5 and B.9 to the results of constant strain cyclic loading tests.

In the pore pressure model it is assumed that most of the hardening occurs also in undrained shear and for undrained sands, therefore, the maximum shear moduli and maximum shear stresses for the nth cycle are related to the initial value by:

$$G_{mn} = G_{mo}\left(1 + \frac{\varepsilon_v}{H_1 + H_2\varepsilon_v}\right)\left(\frac{\sigma'_v}{\sigma'_{v0}}\right)^{1/2} \qquad (B.13)$$

and

$$\tau_{mn} = \tau_{mo}\left(1 + \frac{\varepsilon_v}{H_3 + H_4\varepsilon_v}\right)\left(\frac{\sigma'_v}{\sigma'_{v0}}\right) \qquad (B.14)$$

in which σ'_{v0} is the initial vertical effective stress, and σ'_{v} the vertical effective stress at the beginning of the nth cycle. These values of τ_{mn} and G_{mn} are used in the constitutive relations during the nth cycle of loading.

Appendix C

NON-LINEAR NUMBER OF EQUIVALENT UNIFORM CYCLES

A formulation can be derived which leads to an number of equivalent uniform cycles, taking into account the non-linearity of the pore pressure development.

In figure C.1 the normalized pore pressure ratio $R = u/\sigma'_0$ is plotted versus the number of cycles N for uniform cyclic loading and two stress ratios S_1 and S_2 Similar results have been previously given in figure 3.13. The non-linearity of these curves is evident: starting from a pore pressure ratio R_1, ΔN_1 cycles are required to get an increase ΔR in pore pressure ratio, while only $\Delta N'_1$ cycles ($\Delta N'_1 < \Delta N_1$) are required to produce the same increase ΔR if the initial ratio is R'_1. The functional relationship between R,N and S can be formally expressed by:

$$N_1 = f_{S_1}(R) \tag{C.1}$$

$$N_2 = f_{S_2}(R) \tag{C.2}$$

where the subscripts S_1 and S_2 indicate that the curves are function of the stress ratios.

Considering the generation curves for the ratios S_1 and S_2, it is apparent that the pore pressure paths ab and cd are equivalent: from the same initial pore pressure ratio R, ΔN_2 cycles at a stress ratio S_2 causes the same increase ΔR as ΔN_1 cycles at a stress ratio S_1. ΔN_1 and ΔN_2 can be approximated by:

$$\Delta N_1 \simeq f'_{S_1}(R) \cdot \Delta R \qquad (C.3)$$

$$\Delta N_2 \simeq f'_{S_2}(R) \cdot \Delta R \qquad (C.4)$$

where $f'_{S_1}(R)$ and $f'_{S_2}(R)$ are the first derivatives of the functions f and f respectively. ΔR being the same in equations C.3 and C.4, it follows that:

$$\Delta N_1 = \Delta N_2 \frac{f'_{S_1}(R)}{f'_{S_2}(R)} \qquad (C.5)$$

This relation can be generalized to :

$$\Delta N = f'_{S_{eq}}(R) / f'_{S}(R) \qquad (C.6)$$

which means that 1 cycle at a stress ratio S is equivalent to ΔN cycles at a stress ratio S_{eq}, where S_{eq} is an arbitrary reference level. As a consequence, a sequence of N cycles with different amplitudes S is equivalent to N_{eq} cycles with amplitude S_{eq} if:

$$N_{eq} = \sum_{i=1}^{N} f'_{S_{eq}}(R_{i-1}) / f_{S_i}(R_{i-1}) \qquad (C.7)$$

where S_i is the amplitude of cycle i and R_{i-1} the pore pressure ratio at the end of cycle i-1. N_{eq} is a "non-linear number of equivalent uniform cycles" which can be computed from any loading sequence, if the results of uniform cyclic loading tests are available for a given sand and expressed in a form similar to figure C.1. Equation C.7 is powerful to find N_{eq} values for a large number of stress sequences; For a unique sequence it would be easier to directly compute the pore pressure path as described in figure 3.14.

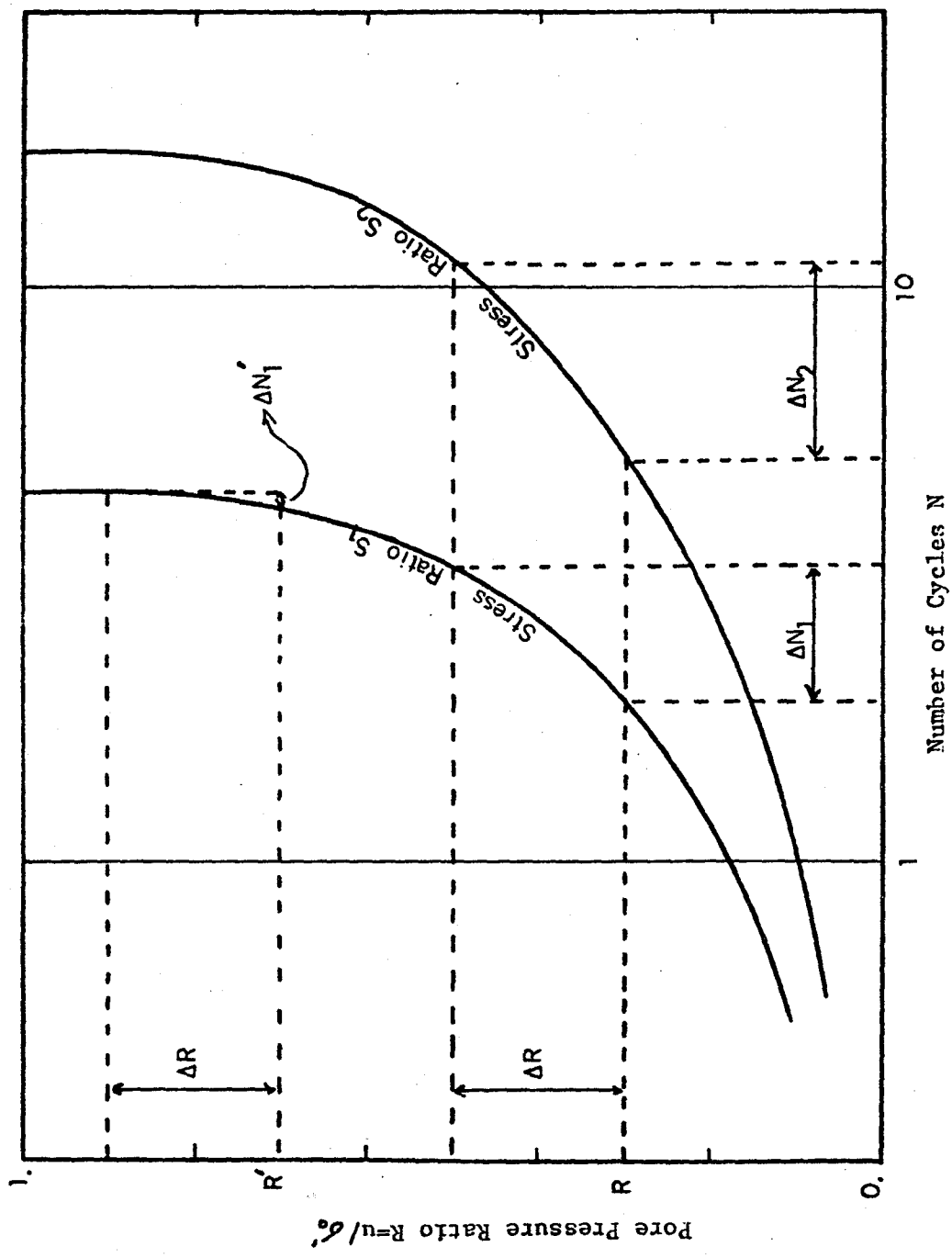

Figure C.1 Schematic Representation of the Non-Linear Equivalent Number of Uniform Cycles Concept